(20)

A TRIDENT SCHOLAR PROJECT REPORT

NO. 208

INVESTIGATION OF BUBBLE DOSIMETER SUITABILITY FOR TREATY VERIFICATION APPLICATIONS

UNITED STATES NAVAL ACADEMY
ANNAPOLIS, MARYLAND

U.S.N.A.— Trident Scholar project report; no. 208 (1993)

INVESTIGATION OF BUBBLE DOSIMETER SUITABILITY FOR TREATY VERIFICATION APPLICATIONS

by
Midshipman Jeremy C. Rich, Class of 1993
United States Naval Academy
Annapolis, Maryland

Advisors: Professor Martin E. Nelson
Naval Architecture, Ocean and Marine Engineering Department

Assistant Professor Mark J. Harper
Naval Architecture, Ocean and Marine Engineering Department

Accepted for Trident Scholar Committee

Chair

May 17, 1993
Date

USNA-1531-2

REPORT DOCUMENTATION PAGE

Form Approved
OMB no. 0704-0188

1. AGENCY USE ONLY (Leave blank)	2. REPORT DATE	3. REPORT TYPE AND DATES COVERED
	May 17, 1993	

4. TITLE AND SUBTITLE

Investigation of bubble dosimeter suitability for treaty verification applications

5. FUNDING NUMBERS

6. AUTHOR(S)

Jeremy Christopher Rich

7. PERFORMING ORGANIZATIONS NAME(S) AND ADDRESS(ES)

U.S. Naval Academy, Annapolis, MD

8. PERFORMING ORGANIZATION REPORT NUMBER

U.S.N.A. - Trident scholar project report ; no. 208

9. SPONSORING/MONITORING AGENCY NAME(S) AND ADDRESS(ES)

10. SPONSORING/MONITORING AGENCY REPORT NUMBER

11. SUPPLEMENTARY NOTES

Accepted by the U.S. Trident Scholar Committee

12a. DISTRIBUTION/AVAILABILITY STATEMENT

This document has been approved for public release; its distribution is UNLIMITED.

12b. DISTRIBUTION CODE

13. ABSTRACT (Maximum 200 words)

The objective of this project was to investigate the feasibility of using the bubble dosimeter as an alternative to the present methods used to verify nuclear arms treaties. Because of the draw-downs of nuclear forces associated with the end of the cold-war, demand has increased for an unobtrusive technology that could be used in the field by inspectors to measure whether the nuclear weapons inspected meet the guidelines of the treaties. The Defense Nuclear Agency (DNA) sponsored the project, believing that the bubble dosimeter could fulfill this need.

Although the bubble dosimeter is a rugged device, idealy suited for field work, three problems must be tackled and overcome before use of the dosimeter can be considered feasible. This project focussed upon evaluating and solving the problems of temperature dependence, bubble growth rate and accurate statistical analysis of the data. Extensive theoretical and experimental work was undertaken to design new detectors which would have a response which remained consistent with temperature. Furthermore, extensive experimentation was conducted at USNA's Neutron Generator Facility, with the purpose of evaluating the neutron detection characteristics of the bubble dosimeter.

14. SUBJECT TERMS

bubble dosimeter, nuclear arms treaties, verfication of treaties, neutron detection

15. NUMBER OF PAGES

112

16. PRICE CODE

17. SECURITY CLASSIFICATION OF REPORT	18. SECURITY CLASSIFICATION OF THIS PAGE	19. SECURITY CLASSIFICATION OF ABSTRACT	20. LIMITATATION OF ABSTRACT
UNCLASSIFIED	UNCLASSIFIED	UNCLASSIFIED	UNCLASSIFIED

ABSTRACT

The objective of this project was to investigate the feasibility of using the bubble dosimeter as an alternative to the present methods used to verify nuclear arms treaties. Because of the draw-downs of nuclear forces associated with the end of the cold-war, demand has increased for an unobtrusive technology that could be used in the field by inspectors to measure whether the nuclear weapons inspected meet the guidelines of the treaties. The Defense Nuclear Agency (DNA) sponsored the project, believing that the bubble dosimeter could fulfill this need.

Although the bubble dosimeter is a rugged device, ideally suited for field work, three problems must be tackled and overcome before use of the dosimeter can be considered feasible. This project focussed upon evaluating and solving the problems of temperature dependence, bubble growth rate and accurate statistical analysis of the data. Extensive theoretical and experimental work was undertaken to design new detectors which would have a response which remained consistent with temperature. Furthermore, extensive experimentation was conducted at USNA's Neutron Generator Facility, with the purpose of evaluating the neutron detection characteristics of the bubble dosimeter.

ACKNOWLEDGEMENTS

The efforts of several people need to be mentioned here. First and foremost, I acknowledge the assistance of Professor Martin Nelson and Assistant Professor Mark Harper, who directed and guided me through every step of the project. I am also grateful to Larry Clemens at the Naval Academy's Nimitz Library for his aid in locating crucial references. Dr. Robert Schwartz of the National Institute of Standards and Technology provided valuable information and assistance. Dr. Schwartz graciously allowed me to use the facilities at NIST during the experimental phase of my research. Some of the most important help for this project came from Mr. Mike Gibbons, whose technical expertise in the nucleonics laboratory made the experimentation for this project run smoothly.

A special thanks is extended to Mr. Ed Hamilton of the Center for Verification Research and Lt. Col. Bernard Simelton of the Defense Nuclear Agency for their support.

I must also thank my parents for their continual support that has been vital to meeting the academic challenges I have encountered.

TABLE OF CONTENTS

PAGE

LIST OF TABLES

LIST OF FIGURES

NOMENCLATURE

English Symbols

A	atomic mass
a	dimensionless parameter
b	dimensionless parameter
E	Energy
dE/dx	stopping power
F	efficiency factor
GFR	group fractional response
h_{fg}	latent heat of vaporization
i	atomic species
j	type of nuclear reaction
L	effective ionic energy transfer length
M	molecular weight
N	Avogadro's number
n	neutron
P	pressure
p	proton
r	bubble radius
S	stopping power
T	temperature
V	volume
W	work

Subscripts

ℓ	liquid
v	vapor
o	initial
c	critical
min	minimum
j	type of neutron reaction
n	neutron
A	available
s	surface
e	expansion
k	inertia
J	acoustic

visc	viscous
h	thermal

Superscripts

i	component of compound

Greek Symbols

α	alpha particle
γ	gamma ray
Θ	scattering angle
ρ	density
σ	surface tension
σ	neutron cross section
ϕ	neutron flux
χ^2	Chi-squared test

CHAPTER I

BACKGROUND AND MOTIVATION

The Defense Nuclear Agency and the importance of nuclear treaty verification are discussed. Passive radiation detection, including neutron and gamma signatures, is described. The Trident Scholar Project is outlined.

1.1 MOTIVATION

One of the Defense Nuclear Agency's (DNA) missions is to develop and evaluate new technologies that could be applied to the NUCLEAR TREATY verification process.[1] The proliferation of nuclear weapons technology, especially to the Third World, and the ongoing reduction in the nuclear stockpile of the former Soviet Union as part of the Strategic Arms Reduction Treaty (START) have made nuclear treaty verification an extremely important issue. Now, more than ever, there is a need to develop reliable and non-intrusive technology that could be used in the field by inspection teams to evaluate whether nuclear weapons meet the specific guidelines delineated by the nuclear forces reduction treaties, specifically START. Inspectors must be able to determine both the presence of nuclear weapons and whether those weapons have less than the allowable number of warheads. Current verification technologies include radiography, gravimetric, and acoustic processes.[1] Although these procedures are effective, they can be extremely expensive and often reveal sensitive weapon design information. This is a problem because countries do not want to divulge unique weapon design specifications unless

obligated to do so by the treaty. Furthermore, the concept of reciprocity does apply to the verification techniques allowed under the current nuclear forces reduction treaties. If the United States expects foreign countries to accept certain inspection procedures, then it must also be prepared to do the same for foreign inspectors.

1.2 PASSIVE RADIATION DETECTORS

DNA currently believes that passive radiation detectors might non-intrusively provide the necessary information for nuclear treaty verifications.[2] In July 1989, this concept was evaluated outside the U.S. Government in a series of experiments conducted under the auspices of the Natural Resources Defense Council (NRDC) and the Academy of Sciences of the U.S.S.R..[3] The Soviet Navy provided the cruiser *Slava* armed with a single nuclear-armed SS-N-12 sea-launched cruise missile (SLCM). Using numerous gamma-ray detectors, the investigators detected the presence of a nuclear warhead without the need to have physical access to the weapon.

The Naval Research Laboratory (NRL) has proposed the use of passive neutron -- neutrons produced as a result of the bombardment of the earth by cosmic rays -- signatures for Nuclear Treaty verification applications.[4] The signature of the neutrons emitted by a body is potentially unique and depends on the internal structure and materials of the object. As a result, passive neutron measuring devices might be applied to verifications processes. Currently NRL is studying the use of a high efficiency Helium-3 neutron detector to measure these signatures accurately.[5]

DNA now believes weapon neutron signatures offer more promise for verification

than the aforementioned passive radiation detection techniques.[2] Nuclear warheads, because of their composition of enriched uranium and plutonium, can produce a characteristic neutron signature. An accurate measurement of this signature should yield specific information concerning the presence of a nuclear weapon and whether the weapons have more than the allowed number of nuclear warheads.

1.3 POSSIBLE NEUTRON DETECTORS

Neutron detection is inherently difficult and complex owing to the physical characteristics of neutron radiation. Neutrons are neutral particles and interact through a variety of mechanisms to form secondary charged particles. Neutron detection relies upon the indirect measurement of these secondary particles in order to deduce the amount and energy of the original neutron radiation.[6] However, the probability of a given nuclear interaction is dependent upon the kinetic energy of the incident neutron. Neutron capture dominates at lower energies and causes alpha, proton, or gamma emissions, while elastic scattering, which generates heavy recoil ions, is predominant among higher energy neutrons. Because typical neutron fields of interest cover a broad spectrum of energy, from 0.025 eV (thermal) to about 6 MeV, accurate neutron detection can be quite complicated due to the mixture of mechanisms involved.

There are several types of commercially available neutron detectors, each having its own unique advantages and drawbacks. Two of the devices that have been identified as possible candidates for development as field instruments are the Helium-3 (He-3) proportional counter and the neutron bubble dosimeter. The He-3 detector indirectly

measures the presence of neutrons using the ionizing gas Helium-3. When a neutron reacts with He-3 gas, the following reaction occurs:

$$_2He^3 + {}_0n^1 \rightarrow (_1H^3)^- + (_1p^1)^+ + \gamma \qquad (1\text{-}1)$$

The products of the reaction are a triton (i.e., *tritium atom with an extra electron*), a proton, and a 765 keV γ. When a potential is applied across a He-3 filled chamber, each neutron interaction produces a pulse. He-3 gas has an extremely high thermal neutron capture cross-section, but a small fast neutron capture cross section. As a result, the device must be equipped with a moderator when used to detect a multi-energy neutron spectrum so that the response of the detector will not be severely limited.

The basic operation of neutron bubble detectors is fundamentally the same as that of bubble chambers, the only difference being that instead of filling a chamber completely with superheated liquid, bubble detectors contain many superheated liquid droplets which act as individual microscopic bubble chambers. Both devices operate on the principle first explained by Glaser:[7] if enough energy is transferred from a moving ion to a superheated liquid, then complete vaporization of the liquid is possible. The recently developed bubble detectors utilize thousands of independent superheated liquid droplets suspended in a semi-viscous matrix. When neutrons interact with the droplet material, the secondary ions deposit sufficient energy to nucleate them into macroscopically observable vapor bubbles. The number of bubbles can be directly related to the amount of neutron exposure, thus providing a portable, self-reading, isotropic detector which is simple and fairly inexpensive. By varying the superheated liquid material or the amount of droplets suspended in the gel matrix, different energy thresholds and sensitivities can

be obtained. The Navy has conducted extensive research evaluating the bubble detector for personal dosimetry applications.[8]

There are currently two commercially available bubble dosimeters, each having a different scheme for counting the vaporizations. The Apfel detector,[9] a product of Apfel Enterprises, acoustically monitors the device during neutron irradiation and electronically records each event by means of a piezoelectric transducer.[10] Ing's device,[11] manufactured by Bubble Technologies Incorporated (BTI), is much simpler. The bubbles form in a more rigid matrix and are held in place after vaporization so that they can be visually counted either by eye or with a computer driven optical reader. Unlike the Apfel device, the BTI detector can be recompressed after reading to condense the bubbles, making it reusable and thus cheaper. Both versions of bubble dosimeters have been shown to be insensitive to gammas below 6 MeV.[12]

Although the He-3 proportional detector and the bubble neutron detector are both capable of counting neutrons, the question has arisen as to which device is better able to carry out the mission of nuclear treaty verification. In order to fulfill the needs of DNA, the neutron detector must be rugged, easily transportable, and non-intrusive. Detector weight becomes an extremely important issue when comparing the weights of current proportional counters to the weight of the bubble detector. The proportional detectors being evaluated have total weights ranging from four to 35 pounds,[2] while the bubble detector weighs only 0.125 pounds.

Only the bubble dosimeter, specifically the BTI device, meets all of these criteria. Because of the low level of technology associated with the device, the detector requires

no electronics. As a consequence, the device is much smaller and more reliable in the field than the He-3 detector or the Apfel device. Although the electronics associated with the Apfel device are minimal, the device has problems with background noise while acoustically monitoring bubble formations. Furthermore, the neutron response of the bubble detector is more related to the energy of the source neutrons than the He-3 detector. In Fig. 1-1, it can be seen that the typical response for a BTI bubble detector

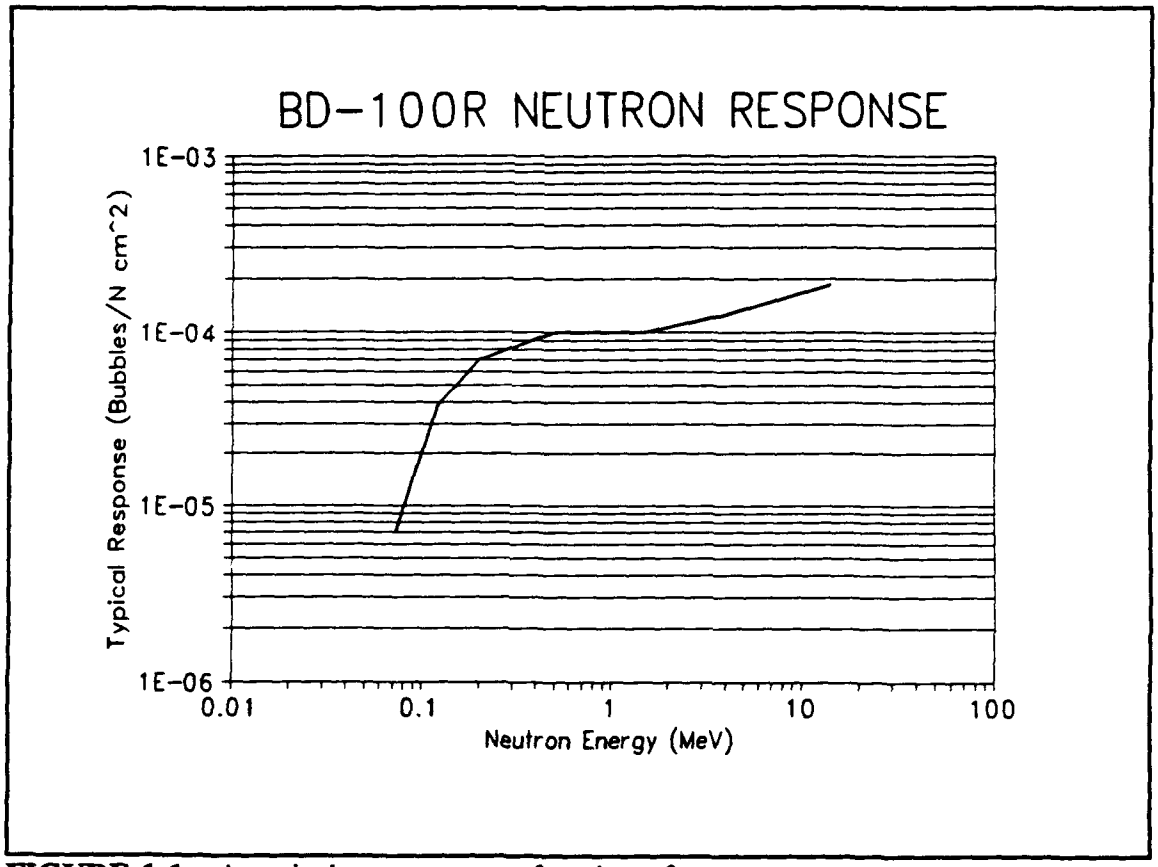

FIGURE 1-1. A typical response as a function of neutron energy for a neutron bubble dosimeter.

has a plateau from 0.3 MeV to 3 MeV, which is the majority of the neutron energy range of interest. As mentioned above, the He-3 detector is a thermal neutron detector. If it is used to measure a higher energy neutron field, then it must be equipped with a

moderator to slow the fast neutrons down into the thermal range.

Although the BTI device has the advantage of being more portable for the field environment than the He-3 detector, the He-3 detector does have some specific advantages. The two devices differ drastically in their means of counting neutrons. The He-3 detector, because of its design, is capable of achieving much higher counting efficiencies (provides a high neutron count rate) than the BTI device. As a result, the counting time associated with statistically accurate results is much smaller for the He-3 detector than for the BTI. Because of its higher counting efficiency, the He-3 detector would be better suited than the BTI device for the detection of concealed nuclear weapons where the neutron field is much smaller. However, the BTI device, because of its small weight and low level of technology, still remains a potential detector for verification purposes.

1.4 TRIDENT SCHOLAR PROJECT OUTLINE

Although the neutron bubble detector has been classified as a possible candidate for treaty verification applications, several drawbacks have been identified with the use of bubble dosimeters. First, most of the commercially available devices have a strong temperature dependence, which limits their use to constant temperature environments. As seen in Figure 1-2, the relative response of these devices increases non-linearly with increasing temperature. Second, not all the bubbles produced are immediately visible, but instead require a waiting time of several minutes or hours depending on the initial droplet size. Third, the devices have a limited dynamic range of about a thousand

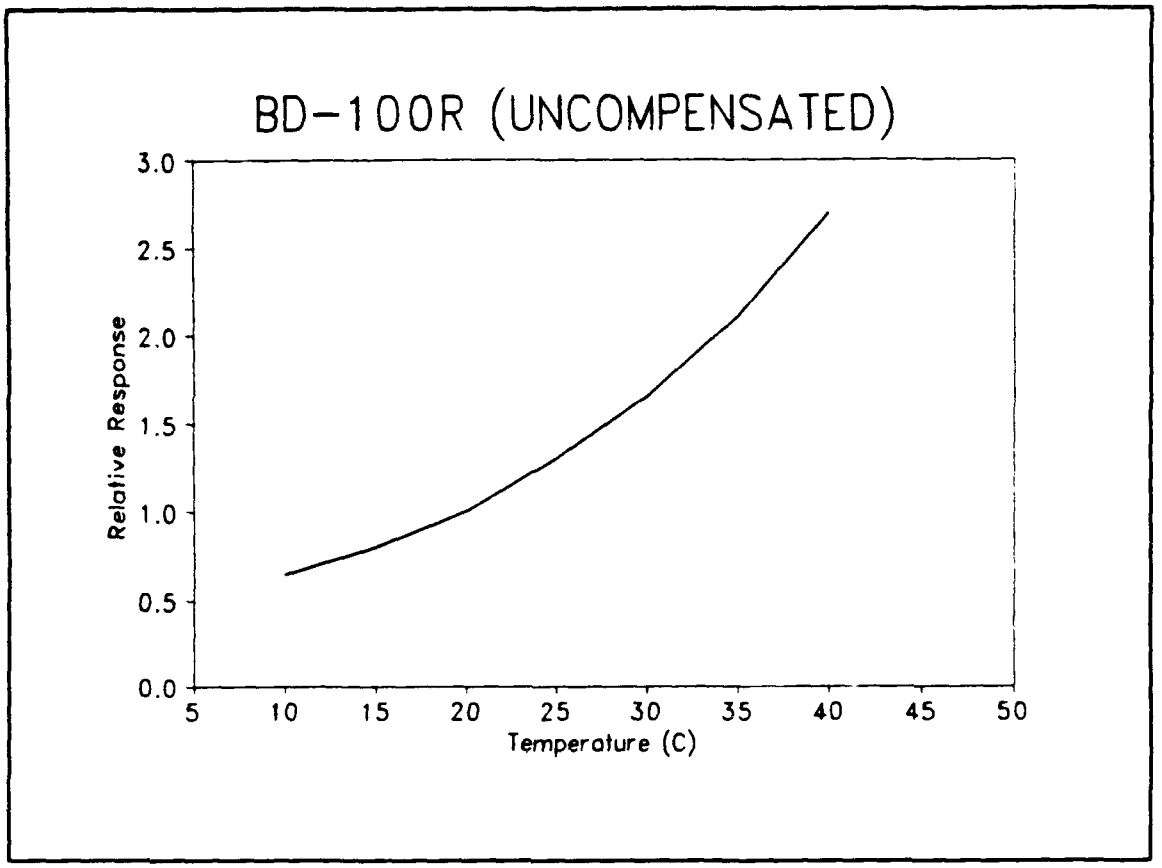

FIGURE 1-2. The relative response as a function of temperature for an uncompensated BD-100R neutron bubble dosimeter.

bubbles per exposure. Because of the statistical nature of the bubble formation process and the relatively small number of bubbles often produced, statistical uncertainty when counting also needs to be considered.

This Trident Scholar report is a feasibility study for the Defense Nuclear Agency as part of the Arms Control Research, Development, Test, and Evaluation Program (RDTE) and will evaluate the potential of the neutron bubble detector for START verification applications. The report will focus upon the effectiveness of the device as a neutron detector and will attempt either to solve or estimate the extent of the problems previously outlined.

A background of the nuclear reactions that occur in the detectors is provided in Chapter II. Using a theoretical model developed by Dr. Mark J. Harper,[6] the neutron→heavy ion→bubble process is presented.

Chapter III investigates the use of different droplet materials as a solution to the device's temperature sensitivity problem. The Harper model will be used extensively to establish and evaluate possible candidate materials theoretically.

Several experiments were conducted at the National Institute of Standards and Technology (NIST) to validate the theoretical model. The setups, results, and analyses of the data are reviewed in Chapter IV.

Additional experimentation was conducted at USNA to evaluate further the problems associated with the device and its potential as a reliable neutron detector. Chapter V presents the setups, results, and analyses of the data.

Chapter VI draws conclusions concerning the feasibility of using a neutron bubble detector as a field detector for nuclear treaty verification applications. Future ideas for further research are also discussed.

CHAPTER II

THEORETICAL MODEL

The significant neutron reactions in typical superheated liquid droplet materials are examined. The radiation-induced nucleation of bubbles in superheated liquid droplets is discussed. A model, developed by M.J. Harper,[6] that accounts for all probable neutronic interactions resulting in the formation of bubbles in superheated liquid droplets is outlined.

2.1 NEUTRONIC INTERACTIONS

Several conditions must be met for neutrons to cause a bubble to nucleate from a superheated liquid droplet. First, some type of reaction must occur between the neutron and the liquid material. The probability of this interaction is highly dependent upon the kinetic energy of the incident neutron, the overall inclination of the target atom for specific types of interactions (nuclear cross section), and the atomic density of the target material. Second, some type of ionizing particle or other radiation capable of dissipating energy across a very small distance must be created as a result of the nuclear reaction. Neutrons, being electrically neutral, are not capable of directly ionizing matter. The secondary radiations, which result from the primary neutron interactions, deposit *their* energy through electronic and nuclear collisions in the medium. Third, sufficient energy must be deposited within a small enough distance for a permanent phase transformation from liquid to vapor to occur.

Neutron interactions producing secondary ionizing radiation are classified as either scattering or absorption. Scattering reactions produce heavy recoil ions (the target atom stripped of its electrons) and a deflected, lower energy neutron. Such reactions are either elastic, where momentum and kinetic energy are conserved, or inelastic, where the target nucleus is left in an excited state, to decay later by beta or gamma emission. Absorption reactions, however, do not always re-emit a neutron. The energy of the incident neutron may appear either as a photon instantaneously released or as an energetic particle ejected from the nucleus. Fission may also result if the material is fissile. Spallation, which is possible at energies above about 20 MeV, ejects several nuclear fragments and particles.[13]

When a polyenergetic neutron radiation field characteristic of a nuclear warhead (0.025 eV to 6 MeV) is incident upon a neutron bubble detector, the only nuclear reactions possible are elastic scattering, inelastic scattering, and charged particle productions such as (n,p), (n,He_3), and (n,α).

Refrigerants are typically the best choice for the superheated liquids used in bubble detectors.[14,15] A combination of low boiling points at atmospheric pressure, high heats of vaporization, and favorable physical properties make refrigerants, specifically chlorofluorocarbons, fluorocarbons, and hydrocarbons, ideal materials for radiation induced nucleation. Since carbon, chlorine, fluorine, and hydrogen are the only elements found in these compounds, the probability and significance of all reactions can readily be determined for each isotope. If a reaction is physically possible and its cross section is non-trivial for the energy range considered, then the effects of the reaction must be considered.

2.2 BUBBLE NUCLEATION

Several theories have been offered as to the exact mechanism by which energy converts from the kinetic in charged particles to thermal during radiation-induced nucleation. However, the currently accepted theory is that of the "thermal spike."[16] According to Seitz, the originator of the concept, the intense energy deposition along the charged particle's track provides enough localized heating in the superheated liquid to cause nucleation.

There are two steps in bubble formation by the thermal spike processes. First, a small "seed" bubble is formed when a small amount of superheated liquid is directly vaporized by the energy transferred from the recoil ion. Second, the bubble grows to visible proportions. Once formed, this seed bubble begins to expand as it receives more thermal energy due to the propagation of the thermal spike's shock wave through the surrounding superheated liquid. However, the bubble must expand beyond a critical size if it is to grow and eventually consume the entire liquid droplet. A vapor bubble of "critical" radius r_c and pressure P_c will be in static equilibrium if

$$r_c = \frac{2\sigma}{P_c - P_l} = \frac{2\sigma}{\Delta P} \qquad (2\text{-}1)$$

where σ is the surface tension of the liquid, and P_l is the pressure of the saturated liquid. Since bubble detectors are usually operated at temperatures sufficiently removed from the critical temperature, the pressure difference between the bubble (inside) and the liquid (outside) is[17]

$$\Delta P = P_c - P_\ell \approx (P_{vap} - P_\ell)\left(1 - \frac{\rho_v}{\rho_\ell}\right) \qquad (2\text{-}2)$$

where ρ_v and ρ_ℓ refer to the densities of the saturated vapor and saturated liquid respectively, at the liquid's temperature.

Although the bubble-and-liquid system is mechanically determinate and in thermodynamic equilibrium, it is not thermodynamically stable. This condition of instability implies that were the bubble any smaller, it would collapse. However, if it gains one additional molecule, its radius will exceed r_c and will grow spontaneously until the initial liquid droplet has fully evaporated.

For the bubble to achieve and exceed the critical radius, a certain critical energy E_c must be deposited by the charged particle as it passes through the superheated liquid droplet. This minimum amount of energy, F_c, has been studied at great length and can be evaluated by examining the theoretical amounts of energy demanded by each of the mechanisms involved in bubble formation. An expression for E_c is

$$E_c = \frac{4}{3}\pi r_c^3 \rho_v h_{fg} + 4\pi r_c^2\left(\sigma - T\frac{\partial\sigma}{\partial T}\right) + \frac{4}{3}\pi r_c^3 P_\ell + W_k + W_J + W_{visc} + W_h \qquad (2\text{-}3)$$

Fundamentally, E_c consists of both reversible and irreversible components. The first three terms represent the thermodynamically reversible processes which account for the formation of the bubble surface, the evaporation of the liquid mass inside the bubble to the same mass of vapor, and the expansion work done against the pressure of the liquid. The final four terms represent irreversible processes and account for the kinetic energy imparted by the expanding bubble against the wall of the liquid, W_k; the acoustic energy

lost by the generation of sound waves ("popping), W_j; the energy lost during the bubble's growth by the action of viscous forces, W_{visc}; and the thermal energy lost during the time a bubble is expanding to its critical radius, W_h. Calculations of each term of Eq. (2.3) for various freon compounds at different temperatures predict that the first three reversible processes typically account for more than 99% of the critical energy.

All of the energy required to produce the bubble originates from the energy lost by the charged particle passing through the liquid. No bubble will form if the net energy deposited E_A is less than E_c. Furthermore, E_A must be deposited within a short enough time and inside a small enough volume to be effective. The effective length L over which a charged particle transfers its energy can be related to the dimensions of the "critical bubble." If the stopping power for the recoil ion is assumed to be constant, then the energy available for bubble formation is

$$E_A = L\left(\frac{dE}{dx}\right) \tag{2-4}$$

If the relationship between L and r_c were known, then predicting a minimum stopping power necessary to cause a bubble would be possible, assuming $E_A = E_c$.

Bell[18] defined this relationship by introducing the parameter a, such that

$$L = ar_c \tag{2-5}$$

Although the exact value of L is undetermined, one might intuitively think that the energy must be deposited within an interval of one critical bubble's diameter, making $a = 2$. Table 2-1 shows that several researchers have greatly differed in their estimation of the parameter a.

TABLE 2-1. Predicted Values of dimensionless parameter a, where $L = a\, r_c$.

Author	Year	Ref.	a
Norman and Spiegler	1963	[19]	2π
El-Nagdy and Harris	1971	[20]	2
Deitrich and Connolly	1973	[21]	2π to 12.96
Bell	1974	[22]	6.07
Apfel	1988	[23]	2

Harper[24] however, takes an unconventional approach and defines L in terms of a different parameter. A bubble which has been formed in a liquid may grow to visible dimensions if its radius exceeds a critical value r_c. Since the mass of vapor present in the critical bubble has not changed since it was in the liquid phase, (which is when the charged particle traversed it), then it would make sense to redefine the relationship between effective ion track length and bubble dimension in terms of this initial "seed" bubble's dimensions. The smaller seed bubble has a radius r_o equal to a sphere of liquid having the same mass as that of the vapor present in a critical bubble. Thus, the seed bubble, which contains this mass of vapor before expansion has begun, has a radius of

$$r_o = \left(\frac{\rho_v}{\rho_l}\right)^{\frac{1}{3}} r_c \qquad (2\text{-}6)$$

If the bubble radius r exceeds r_c when the ion-supplied energy E_A is expended, then it will continue to grow as further energy is received from the superheated liquid. Therefore, Harper argues, it seems appropriate to link the seed bubble radius r_o with the effective

track length L of the moving ion by creating the dimensionless coefficient b, such that

$$L = br_o \tag{2-7}$$

where b has been empirically shown to be 4.3 from experimental data.[24]

2.3 THEORETICAL RESPONSE MODEL

The response of a bubble detector will vary directly with the amount of superheated liquid, magnitude of neutron flux, microscopic cross section for a particular reaction and the efficiency factor for each constituent in the liquid. The response rate R (bubbles/sec) can be calculated in terms of these factors by the equation

$$R(T,E_n) = \phi(E_n)\, V_t \sum_i N^i \sum_j \sigma_j^i(E_n)\, F_j^i(T,E_n) \tag{2-8}$$

where T is the superheated liquid droplet temperature

E_n is the incident neutron energy

$\phi(E_n)$ is the neutron flux, n/cm^2/sec

V_t is the total volume of superheated liquid, cm^3

N^i is the atomic density of the ith species in the liquid, atoms/cm^3

$\sigma_j^i(E_n)$ is the microscopic cross section for a j-type reaction in the ith species, at neutron energy E_n, barns

$F_j^i(E_n,T)$ is the efficiency factor for a j-type reaction in the ith species for a particular liquid temperature T and the incident neutron energy E_n, dimensionless

i is one of the atomic constituents of the compound

and j is the type of neutron reaction.

The efficiency factor $F(E_n)$ refers to the fraction of knock-on ions that are capable of depositing the critical amount of energy (thus forming a bubble), considering their initial formation energy spectra and stopping powers in the superheated liquid of the detector. Because critical energy depends upon the superheated liquid's temperature, the efficiency factor will also be a factor of temperature.

If the neutron field is polyenergetic -- such as that found in spontaneous fission sources like californium and nuclear warheads -- then the total response rate at a given temperature is found by integrating over all energies

$$R(T) = \int_E \phi(E_n)\, V_t \sum_i N^i \sum_j \sigma_j^i(E_n)\, F_j^i(T,E_n)\, dE \qquad (2\text{-}9)$$

CHAPTER III

SEARCH FOR ALTERNATIVE DROPLET MATERIALS

The theoretical response model previously discussed is used to identify possible candidate materials which could provide a consistent response (Bubbles) with changing temperatures. The materials are classified as exceptional or poor candidates by assigning a Figure of Merit (FOM). For the three best candidates, a response is calculated. A protocol for determining constant responses is established. The "flat" regions of response provided by the candidate materials are graphically displayed.

3.1 CANDIDATES EVALUATED

Current superheated liquid neutron detectors are inherently temperature dependent. Although both Apfel Enterprises and BTI claim to have overcome this problem through computer algorithms and pressure compensating devices, the fundamental principle that the critical energy E_c changes with temperature remains unchanged. The critical energy is directly linked to the thermodynamics of the bubble formation process and must be temperature dependent. The methods used by Apfel Enterprises and BTI could work; however, it would be best to attack the temperature dependence problem at its root and identify a possible superheated liquid droplet material that would naturally provide a "flat" detector response over a reasonable temperature range. Consequently, a study was conducted to find suitable liquids other than those currently employed that would have little or no variation in detector response over a range of temperatures.

The evaluation process was conducted in several steps. First, a large number of refrigerants were surveyed by studying the thermodynamic properties and calculating the critical energy E_c as a function of temperature. Refrigerants were chosen as the possible candidate materials because of their favorable thermophysical properties. A combination of low boiling temperatures at atmospheric pressure, high heats of vaporization, and low surface tensions make refrigerants ideal materials to be used as the superheated liquid candidates for nucleation. The critical energy calculations were performed by evaluating only the reversible work terms of Eq. (2-3). The modified equation for E_c,

$$E_c = \frac{4}{3}\pi r_c^3 \rho_v h_{fg} + 4\pi r_c^2 \left(\sigma - T\frac{\partial \sigma}{\partial T}\right) + \frac{4}{3}\pi r_c^3 P_l \qquad (3\text{-}1)$$

was calculated using thermodynamic properties obtained from Dupont Laboratories,[25] Stanford,[26] and the National Institute of Standards and Technology (NIST).[27] Figures 3-1, 3-2, and 3-3 show the critical energy E_c and critical radius r_c as a function of temperature for propylene, propane, and HFC-134a respectively. Table 3-1 lists the thermophysical properties and energy requirements for the three candidates at selected temperatures. It is important to note that HFC-134a has a much higher critical energy E_c and boiling temperature than both propylene and propane.

The critical energy needed to form a bubble is less dependent upon temperature near the material's critical temperature. Thus, having a critical temperature close to the normal operating temperatures of bubble detectors is a favorable characteristic for possible superheated liquid droplet candidates. However, by operating so close to the critical temperature, the issue of homogeneous nucleation, the spontaneous vaporization

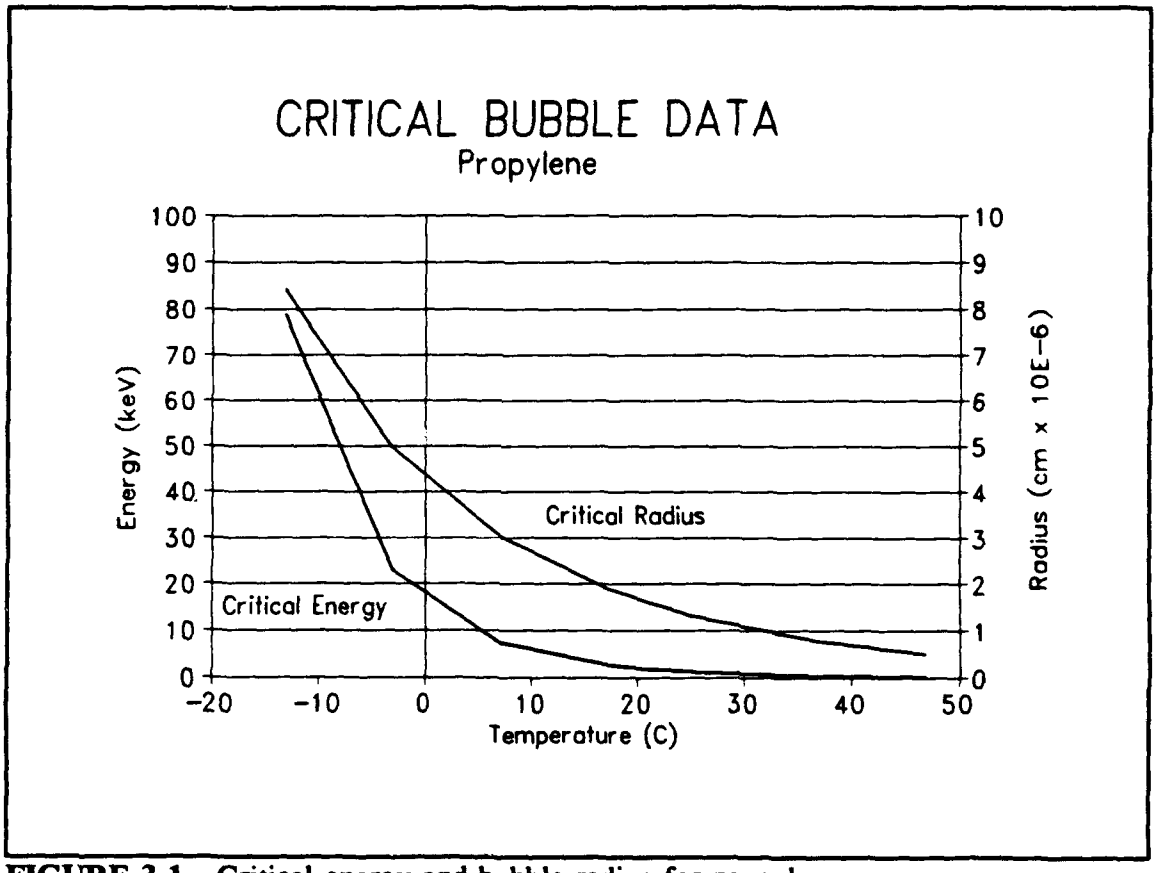

FIGURE 3-1. Critical energy and bubble radius for propylene as a function of temperature at 1 atmosphere.

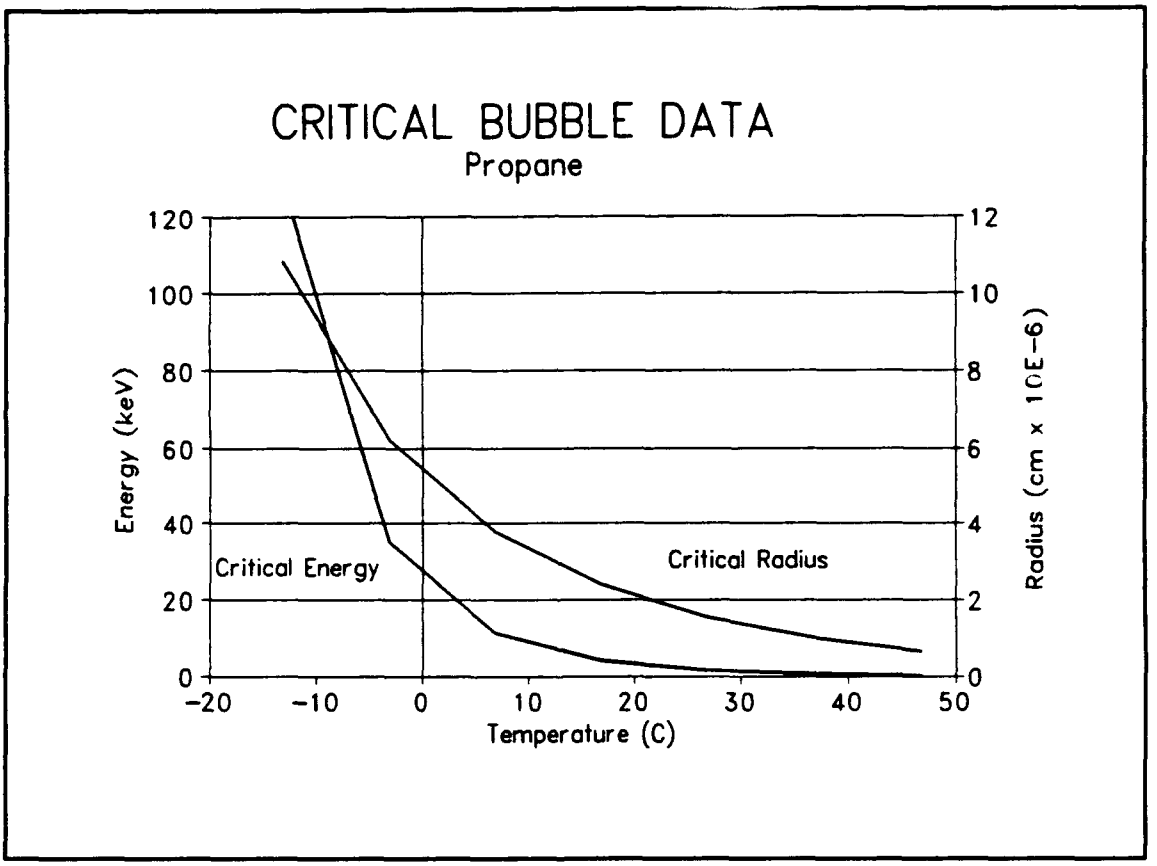

FIGURE 3-2. Critical energy and bubble radius for propane as a function of temperature at 1 atmosphere.

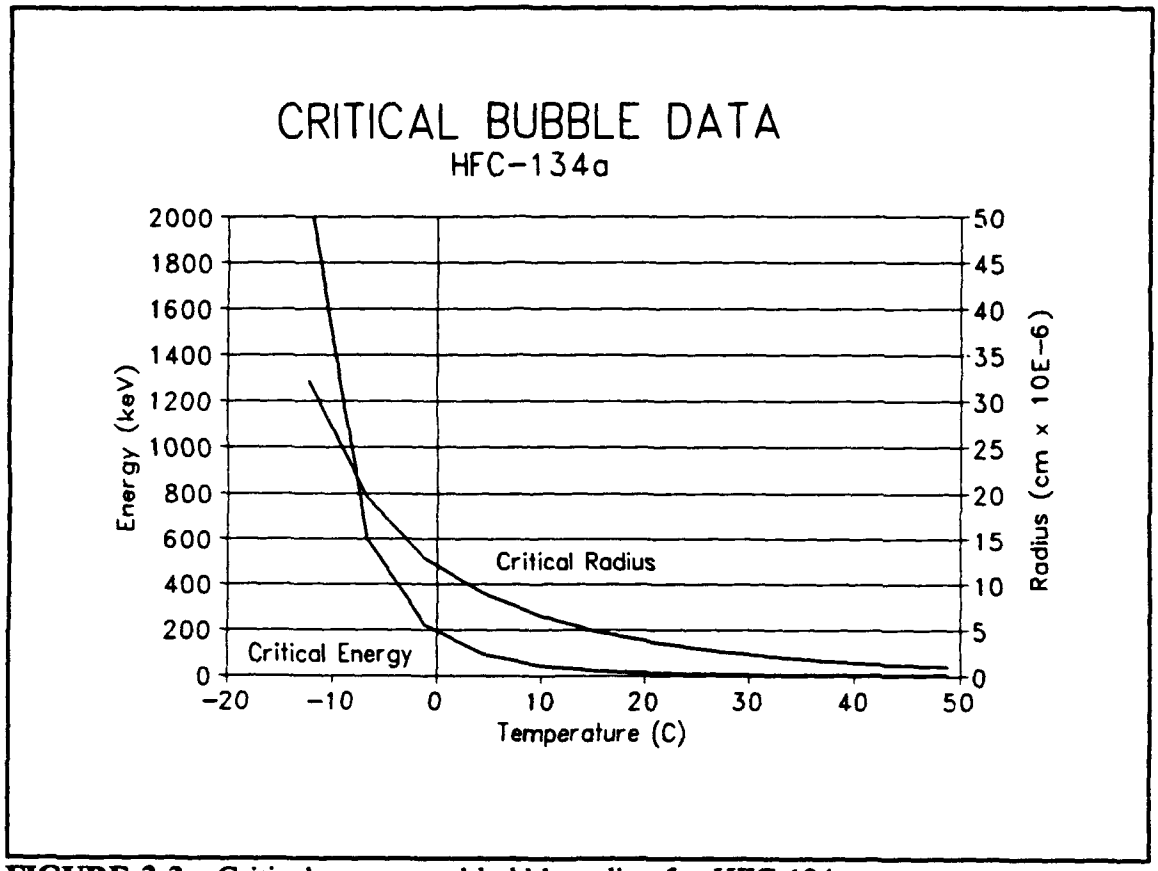

FIGURE 3-3. Critical energy and bubble radius for HFC-134a as a function of temperature at 1 atmosphere.

TABLE 3-1. Thermophysical properties and energy requirements for alternate bubble dosimeter compounds.

Compound Name		Propylene	Propane	HFC-134a
Chemical Formula		C_3H_6	C_3H_8	CH_2FCF_3
Boiling Point	°C	-47.7	-42.07	-26.50
Temperature	°C	26.9	26.9	26.7
Vapor Density (ρ_v)	kg/m^3	25.5	21.7	32.6
Liquid Density (ρ_l)	kg/m^3	503.3	489.2	1192.9
Vapor Pressure	atm	11.9	9.8	6.9
Surface Tension (σ)	dyn/cm	6.4	6.6	7.7
Critical Radius r_c	10^{-6}cm	1.22	1.55	2.67
Surface Formation Energy W_s	keV	0.54	0.75	2.54
Vaporization Energy W_v	keV	0.40	0.70	3.02
Expansion Energy W_e	keV	0.00	0.01	0.05
Total Critical Energy $E_c = W_s + W_v + W_e$	keV	0.95	1.46	5.61

of droplets without neutron interaction, became a definite consideration. Therefore, the theoretical temperature at which spontaneous nucleation occurs, the "foam limit," was calculated at one atmosphere pressure using Spiegler's method.[28] Based upon the van der Waals equation, Spiegler's unique derivation uses only the critical constants of the liquid to determine the foam limit. The guideline,[10] that for small volumes homogenous nucleation will very rarely (once per million years) occur at temperatures more than 3°C

below the foam limit, was used when evaluating the candidate materials.

After the critical energies and foam limit temperatures had been calculated, the materials were classified as possible candidates by assigning each one a non-dimensional Figure of Merit (FOM). The FOM was calculated by finding each candidate's change in critical energy for a given change in temperature ($\Delta E_c/\Delta T$) for the temperature range of 290°K to 310°K, the normal operating region of bubble detectors, and dividing it by the lowest $\Delta E_c/\Delta T$ (Freon 23) of all the candidates. By assigning the FOM, seventeen different candidate materials could be compared to one another in terms of their ΔE_c over the temperature region of interest. It was only after comparing both the FOM and foam limit temperatures however, that a decision could be made concerning which materials made the best candidates. The results of the FOM comparisons may be found in Table (3-2). From the table it can be seen that although a candidate might have a favorable FOM, the foam limit temperature is often well below the temperature region of interest. Furthermore, the great disparities in FOM for the different candidates should be noticed. After evaluating the data, five candidates stood out as potentially offering the best chance of achieving a *non-temperature dependent* response for the normal operating region. These candidates included: Freon 22, Freon 500, HFC-134a, Propylene, and Propane. Information concerning the critical properties of some of the other compounds considered is located in the Appendix.

TABLE 3-2. Figure of Merit (FOM) for the Candidate Alternate Materials.

Liquid	ΔE_c (keV)	$\Delta E_c/\Delta T$ (keV/K)	FOM	Foam Limit (K)
Freon-12	19.74 (290K-310K)	0.99	7581	326
Freon-13	0.001 (290K-295K)	0.00	2.104	256
Freon-22	5.383 (290K-310K)	0.27	2067	312
Freon-23	0.001 (290K-295K)	0.00	1.000	253
Freon-114	3693 (290K-310K)	185	$> 10^4$	355
Freon-115	1.156 (290K-300K)	0.12	887.7	299
Freon-C318	150.9 (290K-310K)	7.55	$> 10^4$	330
Freon-500	7.028 (290K-310K)	0.35	2699	321
Freon-502	1.453 (290K-310K)	0.07	558.1	301
HCFC-124	226.5 (289K-311K)	10.2	$> 10^4$	335
HFC-125	0.740 (289K-311K)	0.03	255.7	287
HFC-134a	19.19 (289K-311K)	0.86	6633	317
Butane	1480 (290K-310K)	74.0	$> 10^4$	359
Ethane	0.003 (290K-300K)	0.00	2.074	259
Isobutane	115.0 (290K-310K)	5.75	$> 10^4$	347
Propylene	2.286 (290K-310K)	0.11	877.7	309
Propane	3.401 (290K-310K)	0.17	1306	313

3.2 RESPONSE CALCULATIONS USING THEORETICAL MODEL

Of the five candidates listed above, propylene had the smallest FOM and was designated the candidate with the most potential for achieving a "flat" response over the

normal operating region. In order to establish the theoretical response for a device using propylene as the droplet material, the Harper model was applied to a bare Californium source having a median neutron energy of 1.678 MeV. The spectrum for the Californium source was broken into 44 groups, or bins, of energy based on the standard groups recommended by NIST.[29] Individual mean energies for the groups ranged from 0.025 MeV to 17 MeV. The individual groups' relative strengths were also obtained from reference [29]. Figure 3-4 illustrates the bare Californium spectrum. The

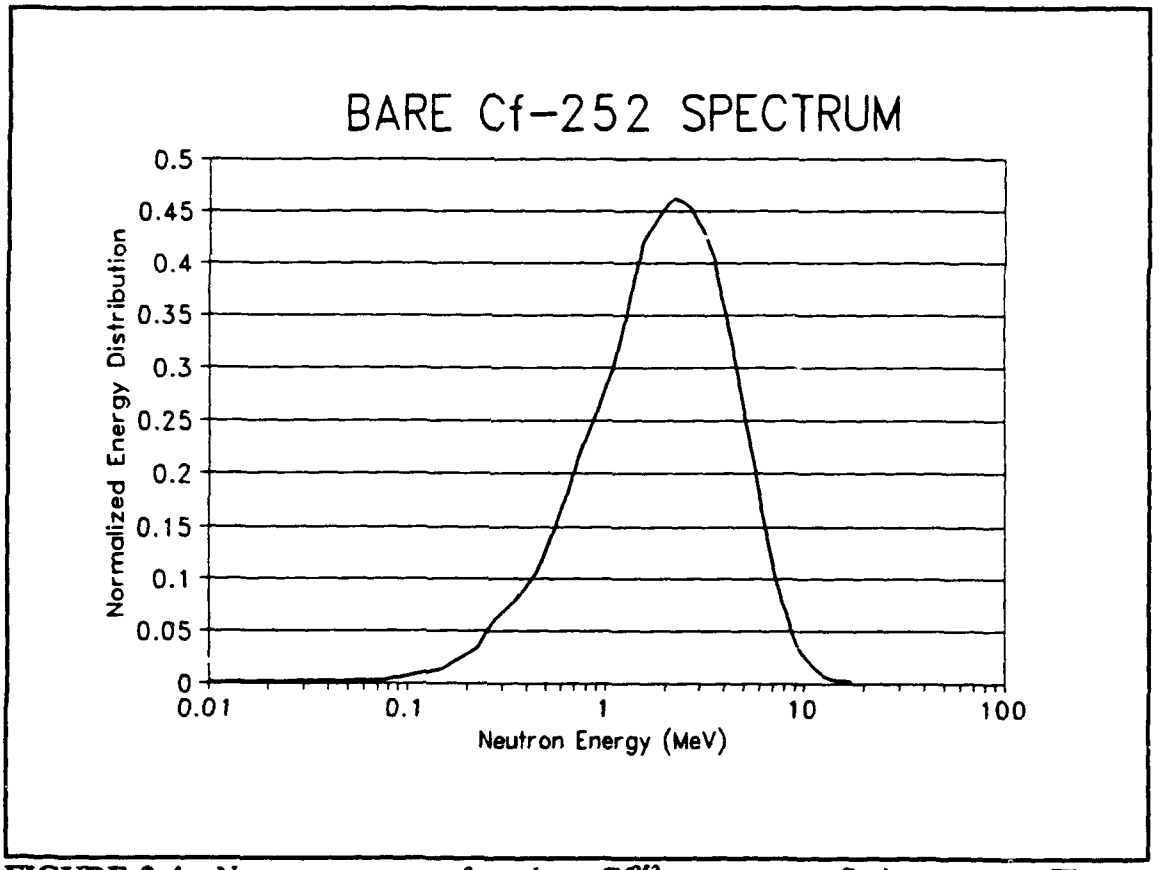

FIGURE 3-4. Neutron spectrum from bare Cf^{252} spontaneous fission source. The spectrum has an average energy of 1.678 MeV.

Californium spectrum was chosen for the calculations because it is a self-fissioning neutron source whose neutron energy spectrum is well characterized and useful for model

validation.

The relative contribution of each group's flux to the overall response, or group fractional response (GFR), was calculated by dividing the group's differential source strength by the total strength given in reference [29]. Dividing the spectra into individual bins allows the conversion of the energy integral of Eq. (3-9) into the summation

$$\int_E \phi(E_n)\, dE_n = \sum_{n=1}^{n=44} GFR\ (E_n) \qquad (3\text{-}2)$$

Microscopic elastic scattering cross section data was obtained from Lawrence Livermore National Laboratory (LLNL)[30] and the BNL-325 publication[31] for each element

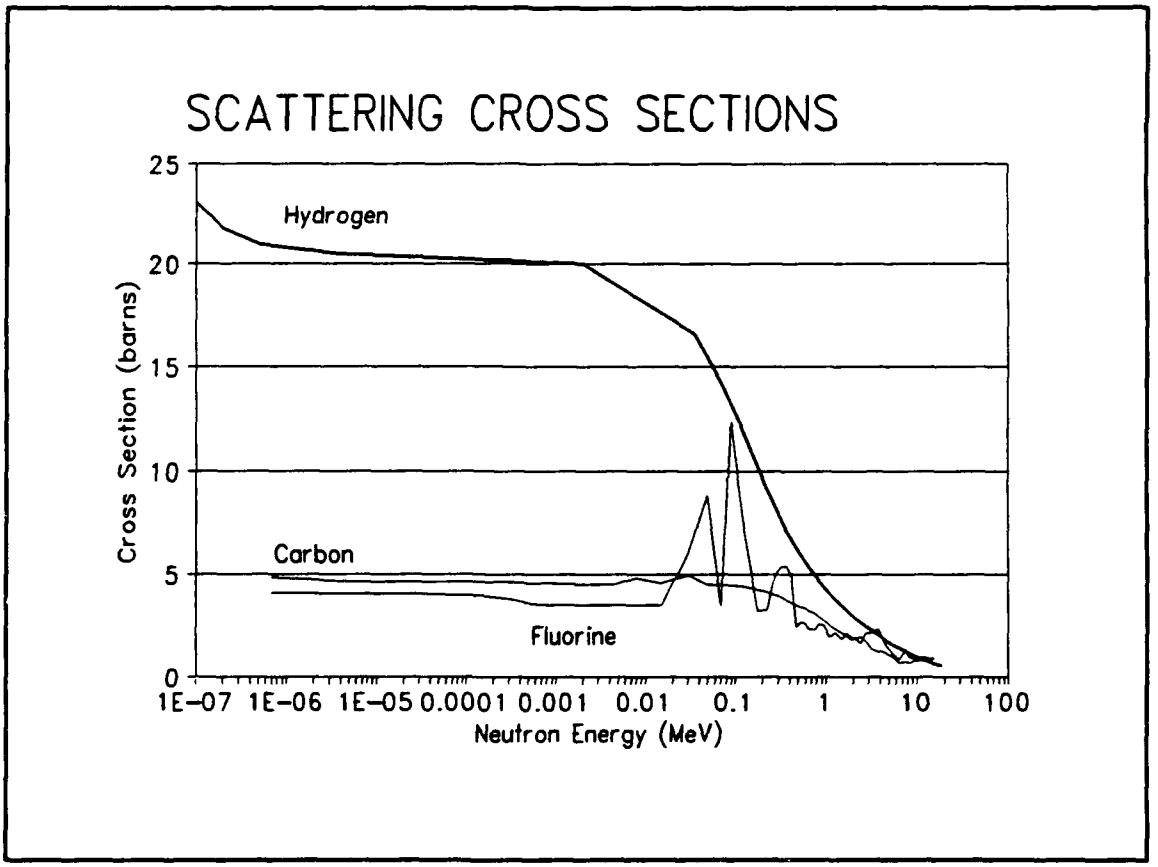

FIGURE 3-5. Neutron elastic scattering cross sections for H, C, and F.

of propylene. An average cross section was calculated for each bin, such that the area of the rectangle as high as the bin and as wide as the energy group was exactly equal to the total area bounded by the continuous cross section versus energy curve, evaluated over the energy of that particular group. This averaging procedure accounted for any possible resonances which occurred within the bin. Figure 3-5 shows the elastic cross sections versus neutron energy for common refrigerant elements such as carbon, hydrogen, and fluorine. Values for other microscopic cross sections, such as inelastic scattering and absorption reactions, were negligible and were not used in the response calculations.

The atom density (atoms/cm^3) N^i used in the response calculations was computed using the standard formula

$$N^i = \frac{N_A \rho \gamma^i}{M} \tag{3-3}$$

where N_A is Avogadro's number, ρ is the superheated liquid's density, γ^i is the isotopic abundance of the particular isotope i, and M is the liquid compound's molecular weight. This number, multiplied by the number of atoms of the ith species per molecule, gives the isotope's individual atom density.

The efficiency factor, $F(E_n,T)$, was evaluated for each possible recoil ion by considering both the recoil ion's initial energy spectra as well as its stopping powers in the superheated liquid of the detector. $F(E_n,T)$ accounts for the expected fraction of knock-on ions capable of depositing the critical amount of energy within the detector droplets.

Using Harper's assumption that the amount of energy made available, E_A, by a charged particle transiting a distance $L = br_o$ through a liquid droplet, is equal to the critical energy, E_c, an expression for minimum stopping power $(dE/dx)_{min}$ can be written as

$$\left(\frac{dE}{dx}\right)_{min} = \frac{E_c}{L} = \frac{E_c}{br_o} \qquad (3\text{-}4)$$

Note that the right-hand side of Eq. (3-4) depends only on the thermophysical properties of the superheated liquid. Because stopping powers can be calculated as a function of an ion's energy, it is possible to determine exactly how much energy the individual ions of the superheated liquid must have in order to exhibit the minimum required stopping power, $(dE/dx)_{min}$. Figures 3-6, 3-7, and 3-8 are graphical representations from Ziegler's Transport of Ions in Matter (TRIM-90) code[32] of the stopping powers for the possible recoiling ions produced in propylene, propane, and HFC-134a. For propylene, 3.52 MeV per mg/cm^2 is the minimum stopping power required by Eq. (3-4) for a carbon ion to form a bubble at a temperature of 6.9°C. Entering Fig. 3-6 with a value of 3.52 on the *dE/dx* axis, the corresponding value for the required carbon energy is found to be approximately 0.13 MeV. As a result, only carbon ions with more energy than 0.13 MeV are capable of depositing the necessary critical energy within the propylene liquid droplet.

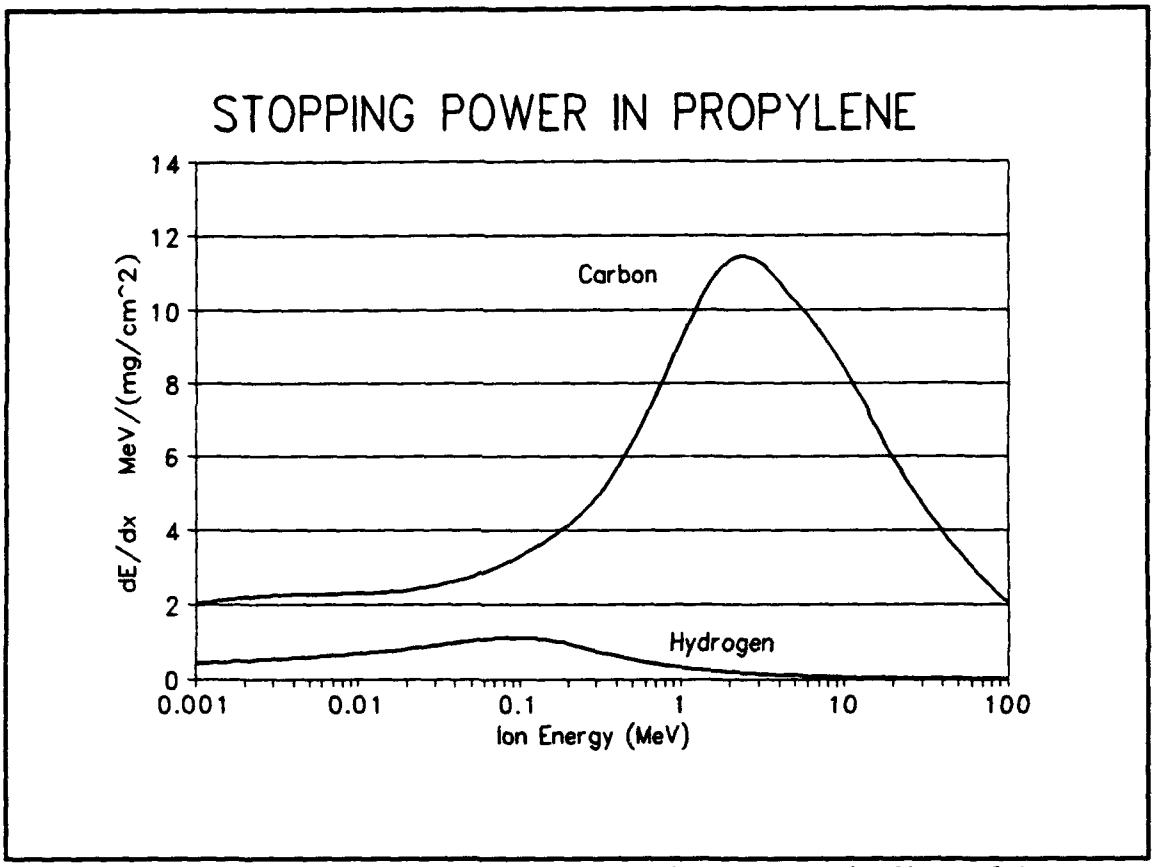

FIGURE 3-6. Total (compound) stopping power in propylene for H and C ions as a function of ionic energy, generated from Ziegler's Trim-90 code.

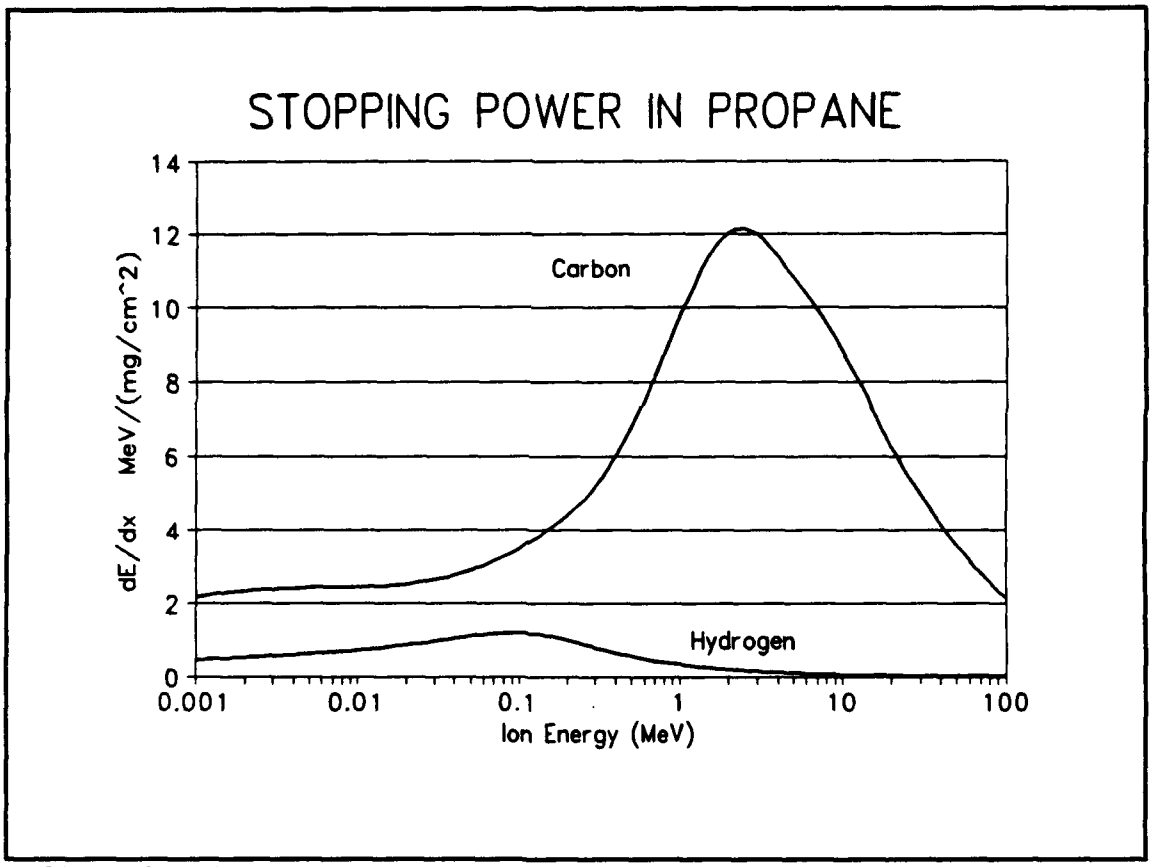

FIGURE 3-7. Total (compound) stopping power in propane for H and C ions as a function of ionic energy, generated from Ziegler's Trim-90 code.

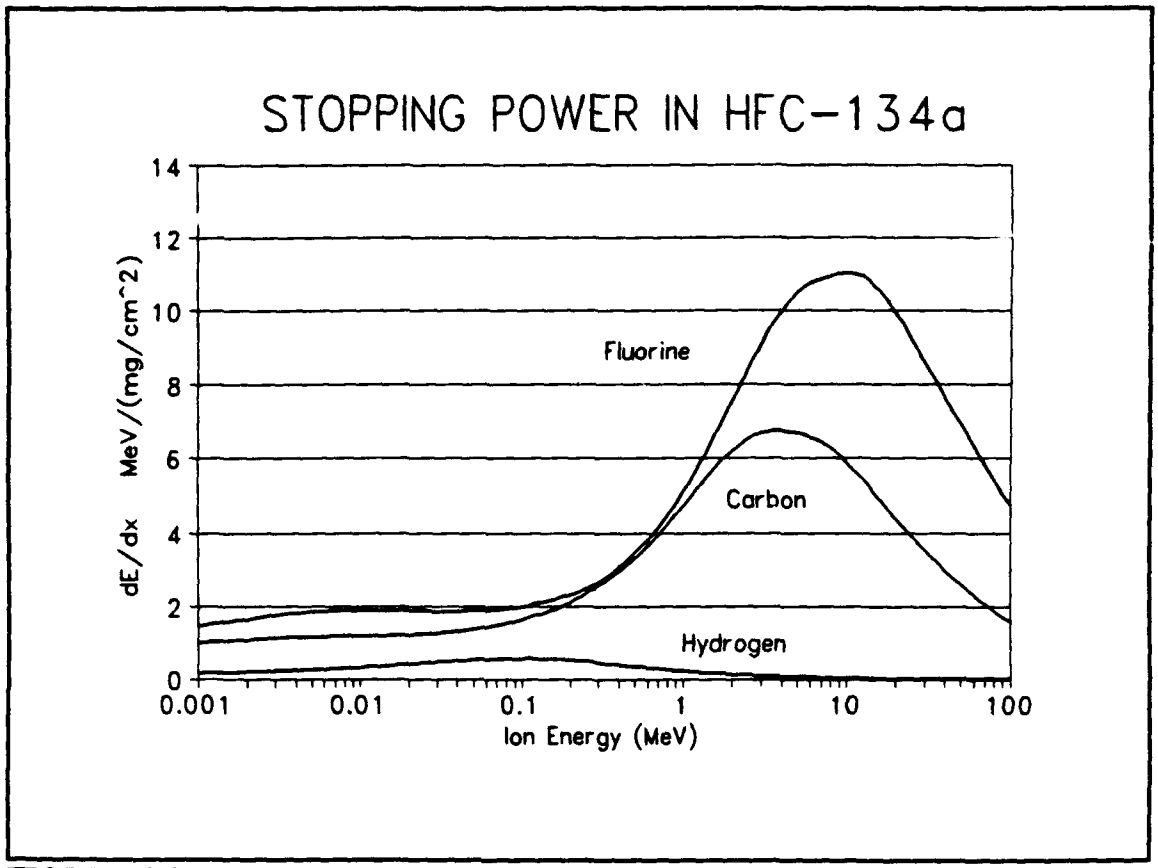

FIGURE 3-8. Total (compound) stopping power in HFC-134a for H, C, and F ions as a function of ionic energy, generated from Ziegler's Trim-90 code.

According to the Harper model, all possible neutron interactions must be evaluated to determine whether the required *(dE/dx)* can be provided by the recoil ions. For the case considered, elastic scattering was the dominating interaction and resulted in fairly predictable knock-on ion spectra. The energy of elastically scattered ions, E_R, depends on both the incident neutron energy, $E_{n,i}$, and the center-of-mass scattering angle, Θ_c, such that

$$E_R = \frac{2A}{(A+1)^2}(1-\cos\Theta_c)\, E_{n,i} \qquad (3\text{-}5)$$

As a result, for a particular $E_{n,i}$, the relative distribution of recoiling ions follows a

unique curve related to the possible center-of-mass scattering angles Θ_c.

Using LLNL's library of evaluated nuclear data,[30] the expected elastic scattering distributions were generated for carbon, hydrogen, and fluorine at all energies of interest. Figure 3-9 shows the relative distribution of carbon ions scattered by an incident 3.50 MeV neutron. Considering the carbon ions, it can be seen that there is a relatively high probability that Θ_c will be close to either 0° (slight glancing collision, almost a complete

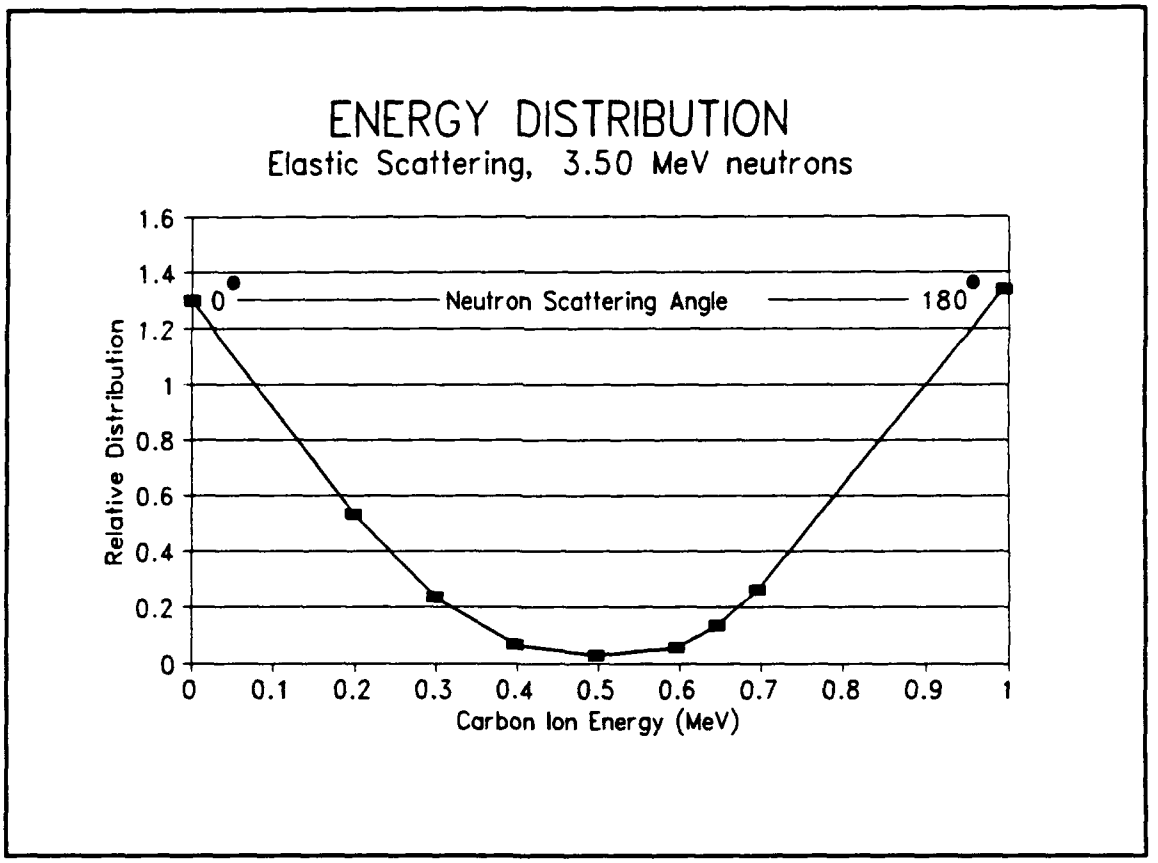

FIGURE 3-9. Relative distribution as a function of carbon ion energy after elastic scattering 3.50 MeV neutrons, generated from LLNL data,showing extreme forward and backward scattering.

miss) or 180° (head-on collision, complete back-scattering). From the ion distribution, it is possible to calculate the fractions of ions generated that have either energies greater

than a certain value or energies which lie in a certain energy band. For propylene, at 6.9°C, it was earlier stated that the carbon ions needed to have a minimum energy of 0.13 MeV in order to form a bubble. The fraction of all carbon ions capable of creating a propylene bubble is found by comparing the shaded area of Fig. 3-10 to the total area under the relative distribution curve produced by elastic scattering with a 3.50 MeV neutron. This fraction is the efficiency factor, $F(E_n,T)$, and was calculated to be 0.73. An efficiency factor of 0.73 implies that 73% of the recoil carbon ions created from

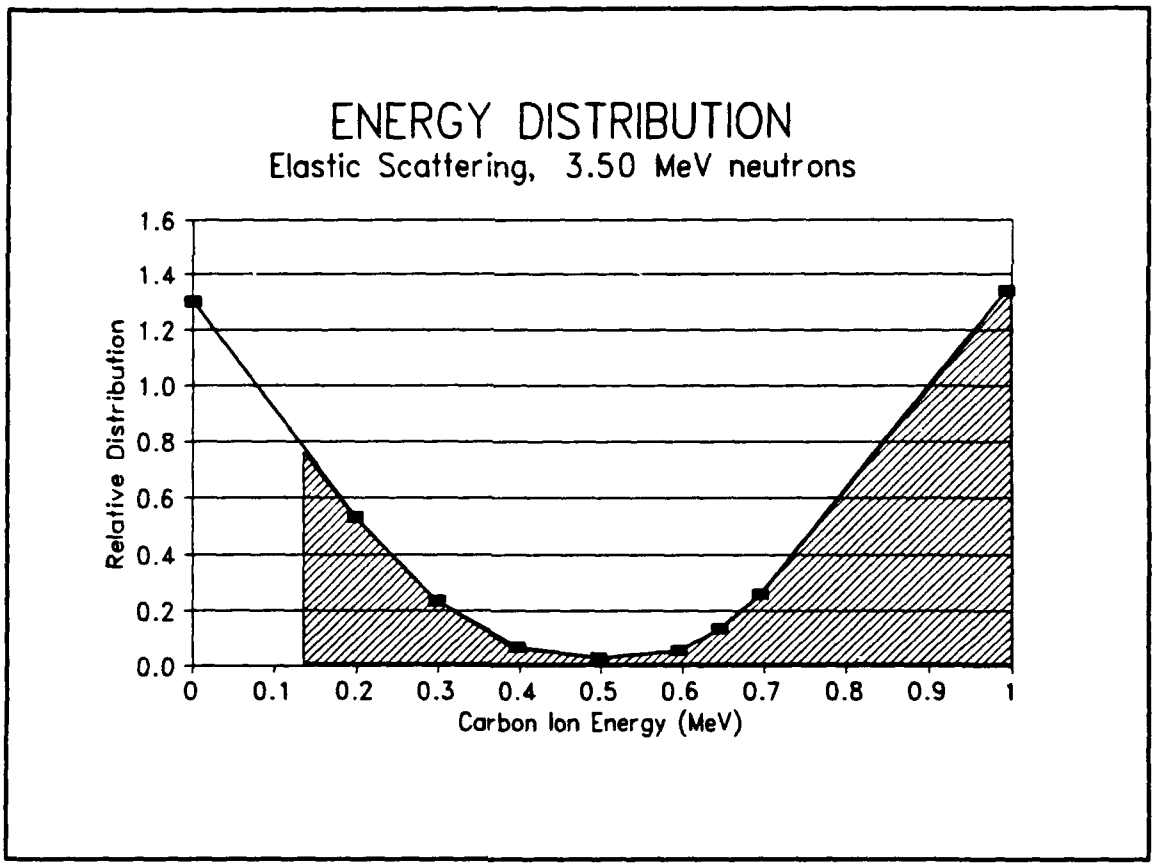

FIGURE 3-10. Relative distribution of carbon ions after scattering by 3.50 MeV neutrons. Shaded area indicates fraction of recoiling ions which supply E_c.

elastic scattering with a 3.50 MeV neutron have sufficient energy to form a bubble.

Figure 3-11 also demonstrates the computation of $F(E_n, T)$ for hydrogen ions elastically scattered by a 2.0 MeV neutron in propylene at 36.9°C. Unlike the carbon ion, the hydrogen ion has an upper bound for the ion energies which can produce nucleation. The upper energy boundary results from the unique shape of the hydrogen ion stopping power curve. From Fig. 3-6, it should be observed that hydrogen ion energies greater than 0.1 MeV begin to provide a decreasing *(dE/dx)* with increasing ion energy. As

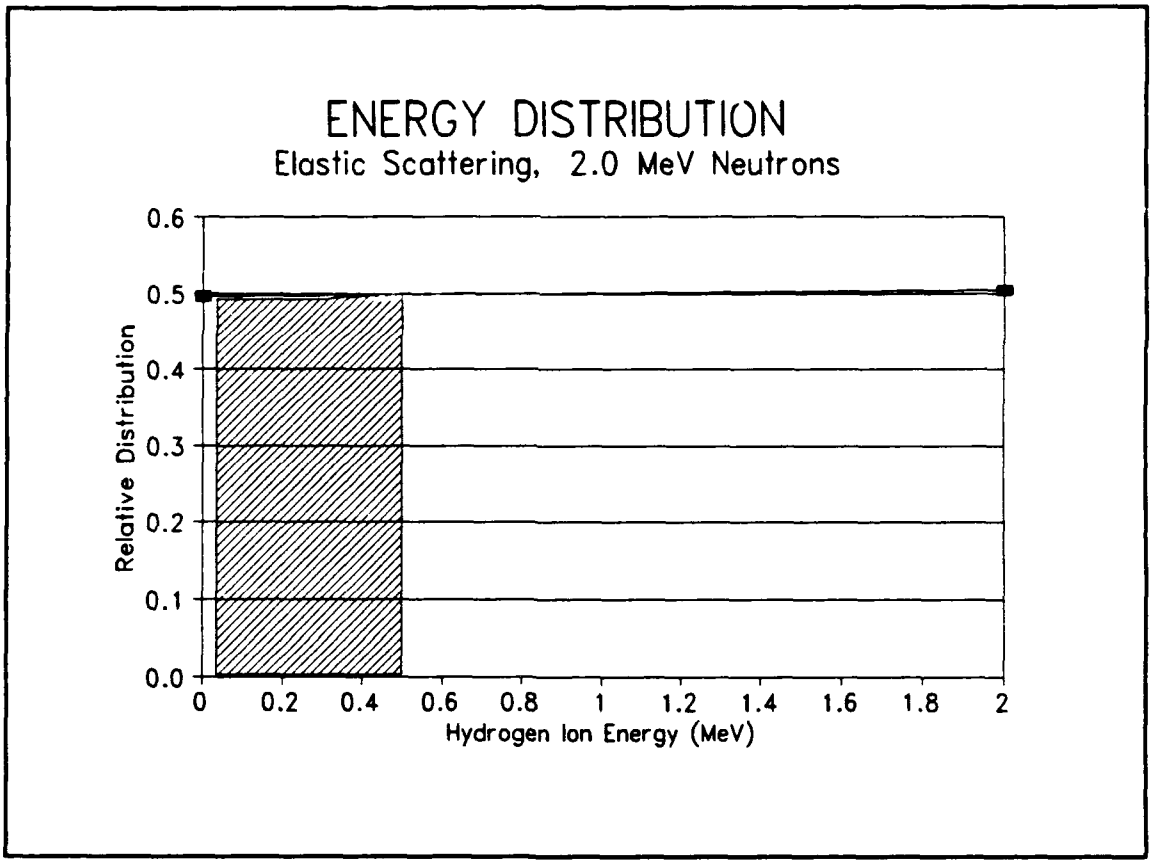

FIGURE 3-11. Relative distribution of hydrogen ions after scattering by 2.0 MeV neutrons. Shaded area indicates fraction of recoiling which supply E_c.

demonstrated in Fig. 3-6, some higher energy hydrogen ions are not capable of supplying a *(dE/dx)* which lower energy ions were able to.

In determining the propylene response for a bare Californium spectrum, efficiency

factors were calculated for elastic scattering with neutrons from each of the 44 different energy bins, having energies ranging from 0.0253 eV to 14 MeV. Furthermore, $F(E_n, T)$was evaluated at temperatures ranging from -13.2°C to 46.9°C. Figure 3-12 shows how the $F(E_n, T)$ for carbon ions varies for a range of temperatures and neutron energies within propylene. As seen in the plot, the higher the incident neutron's energy or the higher the liquid's temperature, the closer the efficiency factor will be to unity.

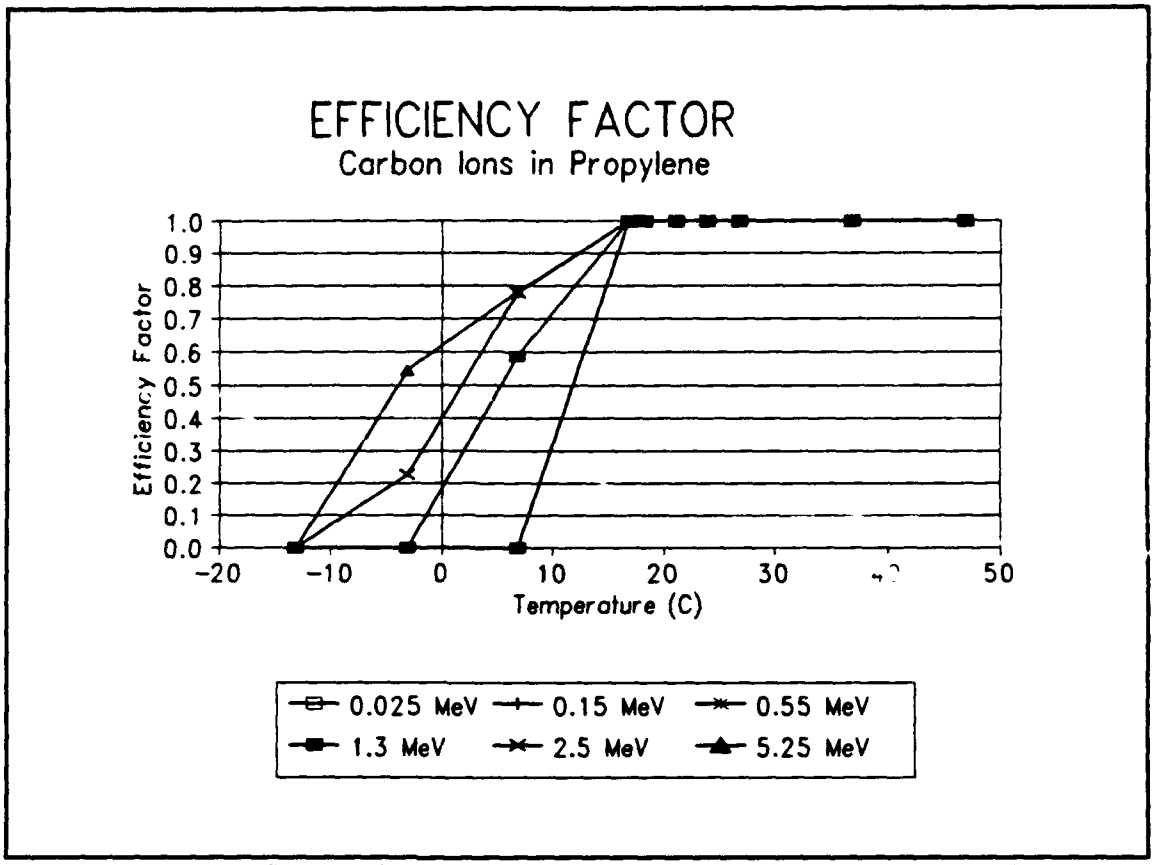

FIGURE 3-12. Efficiency factor $F(E_n, T)$ for carbon ions in propylene as a function of temperature. Efficiency factor represents fraction of ions providing E_c.

This is the normal trend for most ions. However, as shown in Fig. 3-13, the $F(E_n, T)$ for hydrogen ions behaves quite differently. Because hydrogen ions are not capable of providing a large (dE/dx), the stopping power curve is very unique when compared with

other ions. As the ion energy increases above 1 MeV, the *(dE/dx)* provided by the ion becomes too small to form a bubble. As a result, the efficiency factor decreases with increasing neutron energy. However, because the required *(dE/dx)* decreases with increasing temperature, the efficiency factors always increase with increasing temperature. When $F(E_n, T)=1$, then every recoil ion is capable of producing a bubble. Consequently, the detector response will be "flat" when the total efficiency factor for all

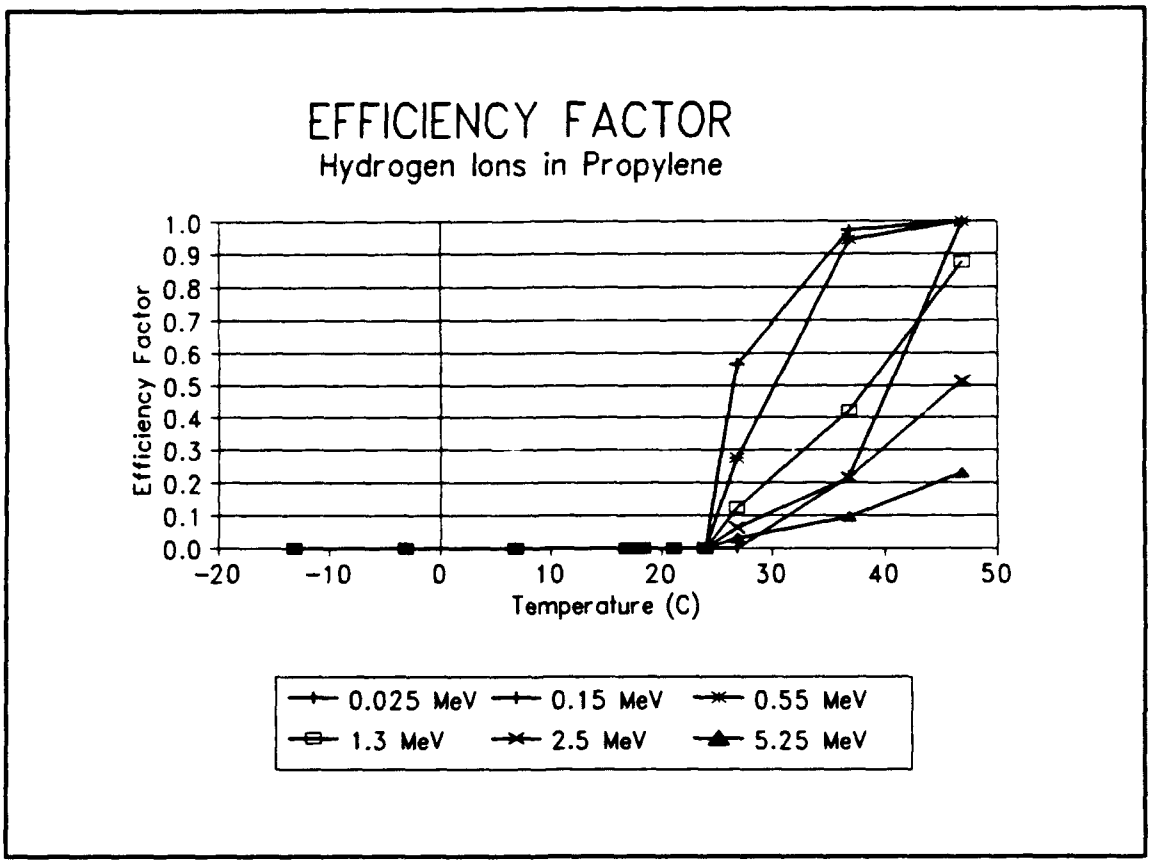

FIGURE 3-13. Efficiency factor $F(E_n, T)$ Hydrogen ions in propylene as a function of temperature. Efficiency factor represents fraction of ions providing E_c.

recoil ions achieves unity.

A close evaluation of the stopping power plots for carbon and hydrogen ions in propylene reveals that there are threshold stopping powers below which all recoil ions of

a particular type can satisfy the critical energy requirements. As a result, if the required *(dE/dx)* is less than the threshold for a particular ion, recoil ions of all energies will have more stopping power than the minimum required, and thus be capable of supplying the necessary critical energy, E_c. For the case of propylene, as seen in Fig. 3-6, if $(dE/dx)_{min}$ is less than 2 MeV per mg/cm^2, then recoiling carbon ions of all energies are capable of providing the critical energy. As a result, $F(E_n,T)$ will equal one for carbon ions of all energies. The propylene response will continue to be constant until $(dE/dx)_{min}$ decreases below the upper threshold (largest *dE/dx* provided by ion) for hydrogen ions. Previously, hydrogen ions of all energies had been incapable of supplying the required *(dE/dx)*. Once the upper threshold is passed, hydrogen ions will begin to contribute to the response, resulting in a total response that is no longer flat. The propylene response cannot become constant again until the required *(dE/dx)* becomes less than the lower hydrogen threshold (*dE/dx* below which all resulting ions are capable of depositing E_c). However, when this occurs, the temperature would have increased so much that the material would have already previously reached its foam limit of 35.7°C. Figure 3-14 shows the propylene response for the polyenergetic neutrons of bare Californium. The response has several important characteristics that should be noted. First, there are no hydrogen effects until 24°C because at lower temperatures, $(dE/dx)_{min}$ is too high and cannot be supplied by any energy hydrogen ion. It is not until temperatures greater than 24°C are reached that E_c is low enough for $(dE/dx)_{min}$ to be satisfied by hydrogen ions. Second, one can see the $F(E_n,T)$ curves echoed in the individual ion's responses as expected by Eq. (2-9). For carbon, all possible ions have a $F(E_n,T)=1$ at a temperature of 16.85°C.

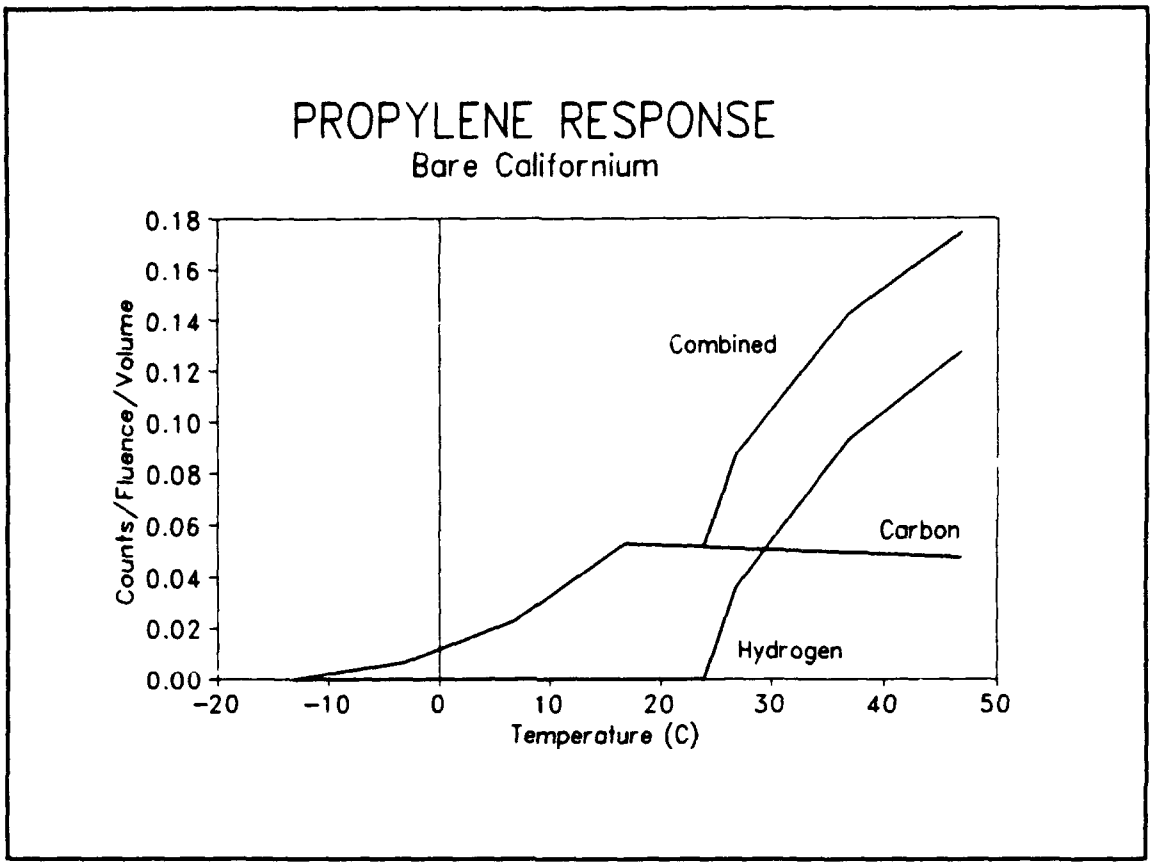

FIGURE 3-14. Theoretical model's predicted response for propylene (C_3H_6) to bare Californium neutron spectrum at 1 atmosphere. "Flat" response (15°C-24°C).

The theoretical responses for 2.1 MeV neutrons were calculated for propane and HFC-134a. As shown in Figs. 3-15 and 3-16 respectively, plateau regions of relatively constant response also exist in unique temperature bands for these other alternate materials. Although the response was only calculated for a 2.1 MeV neutron source and not for every energy bin, it still gives a good indication of the trends of the complete response. The constant temperature plateau should span the same temperature band, only the response before and after the plateau should change. The boundaries of the response plateau are determined more by $(dE/dx)_{min}$ than the incident neutron energy. A 2.1 MeV

neutron has sufficient energy so that at least a portion of the knock-on hydrogen ions created will have enough energy to form a bubble if $(dE/dx)_{min}$ is less than the upper threshold for hydrogen. Because the response only considers 2.1 MeV neutrons, the response before and after the plateau does not account for the combined responses of the other 43 energy bins as dictated by Eq. (2-9).

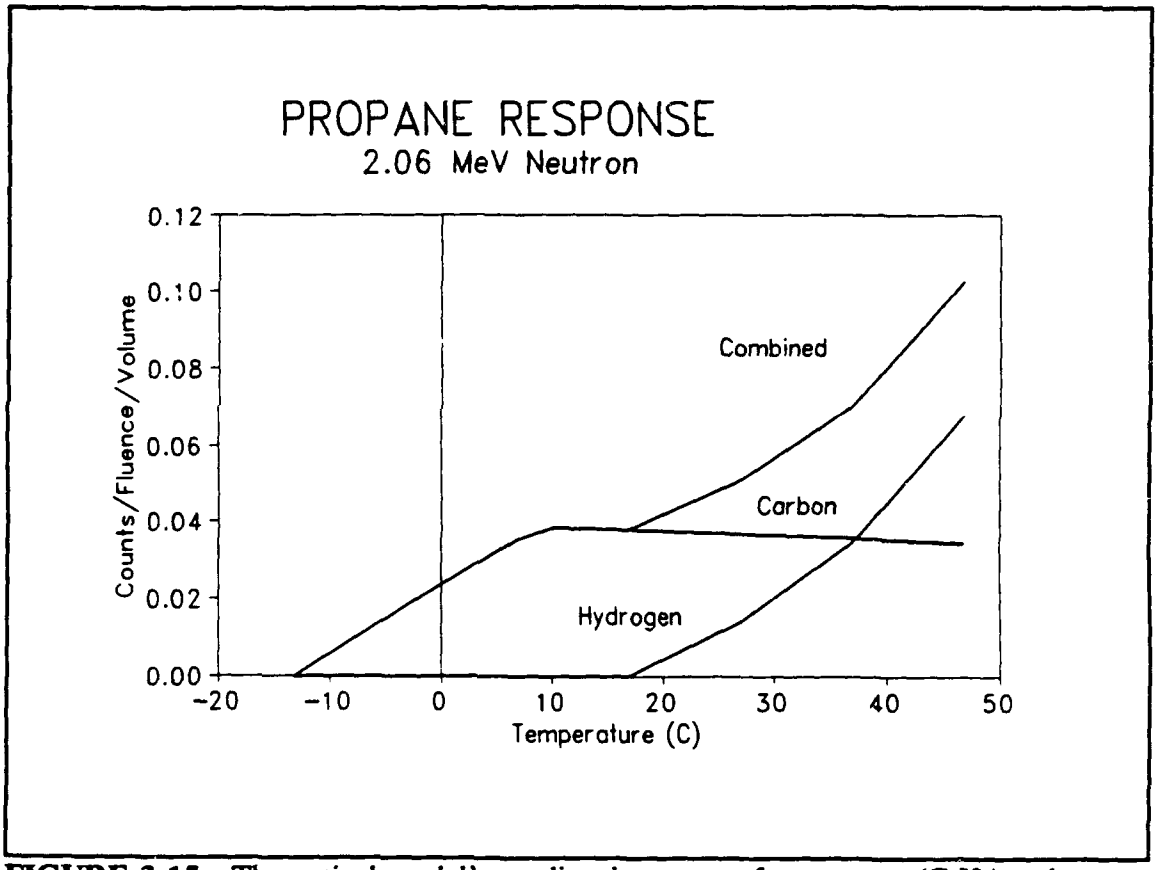

FIGURE 3-15. Theoretical model's predicted response for propane (C_3H_8) to bare Californium neutron spectrum at 1 atmosphere. "Flat" response (10°C-18°C).

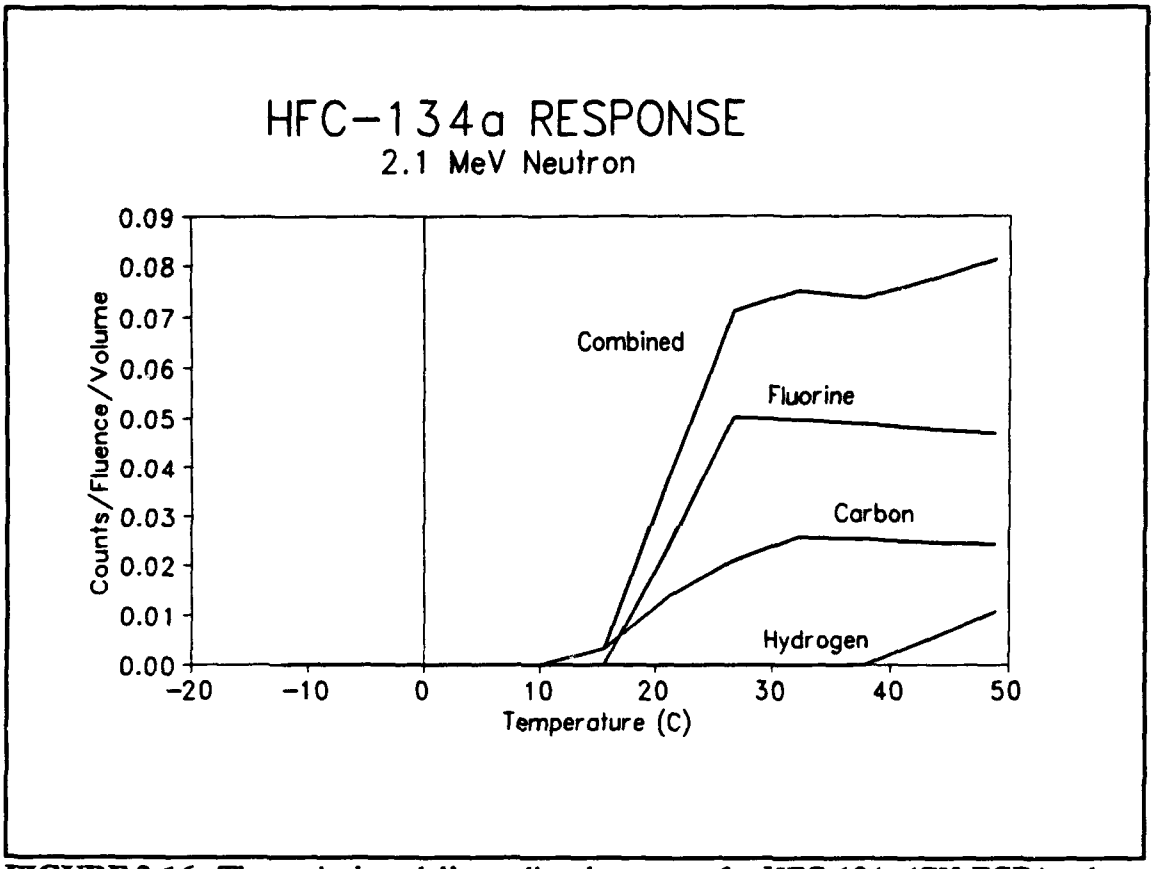

FIGURE 3-16. Theoretical model's predicted response for HFC-134a (CH_2FCF_3) to bare Californium neutron spectrum at 1 atmosphere. "Flat" response (31°C-38°C).

3.3 CONCLUSIONS

The extent of the regions of constant response is directly related to both the required stopping power, $(dE/dx)_{min}$, of each material and the stopping power thresholds of the individual components of the materials. This is very clear when considering propane and propylene. For these simple hydrocarbons, the plateau begins once the required $(dE/dx)_{min}$ falls below the minimum lower threshold for the recoil carbon ions. At this point, the upper threshold for a hydrogen response is significant when compared with the

required stopping power. However, as the temperature increases, the required *(dE/dx)* gradually decreases in value and eventually becomes less than the upper threshold of the hydrogen recoil ions. When this occurs, the response is no longer flat because the combined response is a summation of both the flat carbon response and the increasing hydrogen response. HFC-134a has a slightly more complicated response. In order for the response to be flat, the required *(dE/dx)* must be less than the lower threshold for both carbon and fluorine. Once again, the overall response will no longer be constant once the required *(dE/dx)* falls below the upper threshold for hydrogen ions.

As a result of this alternatives study, a specific protocol has been established in order to determine if a candidate material will have a constant response over a specific temperature band. First, a candidate material's $(dE/dx)_{min}$ must be evaluated over the operating region of interest. If $(dE/dx)_{min}$ is of small value and changes little over the specific temperature band, then the material is classified as a possible candidate. Second, the foam limit temperature must be checked to see if it lies within the temperature range of interest. If $(dE/dx)_{min}$ is relatively small and constant, then the material is probably close to its critical temperature, and the foam limit temperature is of concern. Third, the stopping power curves for the component ions within the candidate material must be evaluated for any lower thresholds below which all ions of a certain kind can deposit E_c. The response for an individual constituent will be constant if $(dE/dx)_{min}$ is less than the lower threshold for that constituent. If the responses for each constituent are either constant or zero, then the combined response will also be constant.

Although the temperature band for a constant response is usually limited to about

10°C, devices theoretically can be manufactured to meet selected temperature ranges by using different alternate materials. If one knows approximately what the anticipated operating temperature band will be, one could choose the appropriate device so that a detector with a flat response is used. Figure 3-17 demonstrates this concept. In this plot,

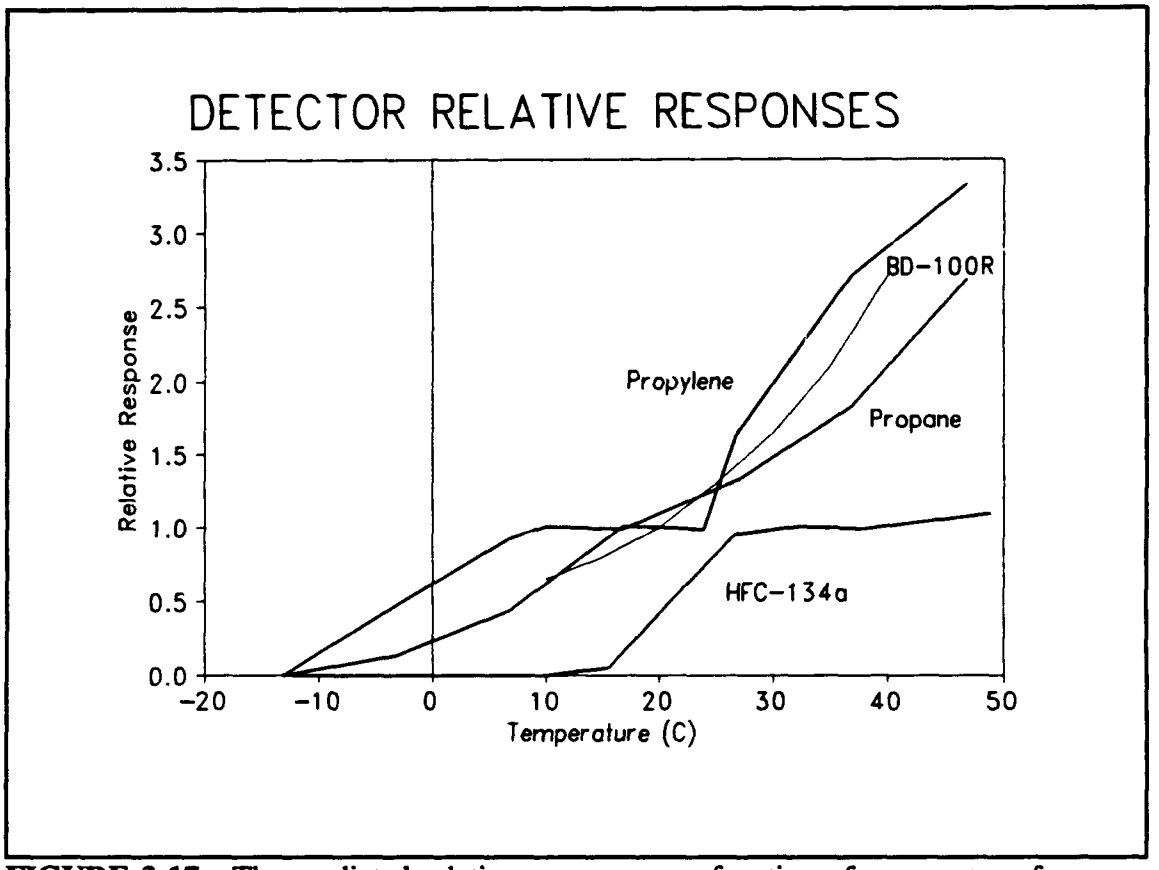

FIGURE 3-17. The predicted relative response as a function of temperature for a propylene, propane, and HFC-134a bubble detector.

the relative responses of four different devices are superimposed upon each other. BTI's commercially available uncompensated BD-100R clearly demonstrates a non-linear response versus temperature. However, the three alternative material devices considered in this report each have a unique region of constant response. Clearly, there is a particular material for a specific temperature band. The flat region which has a change

in response of plus or minus five percent for propane, propylene, and HFC-134a is approximately 7.5°C to 18.1°C, 15.9°C to 24.0°C, and 27.0°C to 44.2°C, as illustrated in Fig. 3-18. When evaluating Fig. 3-18, one must remember that the bars for propane

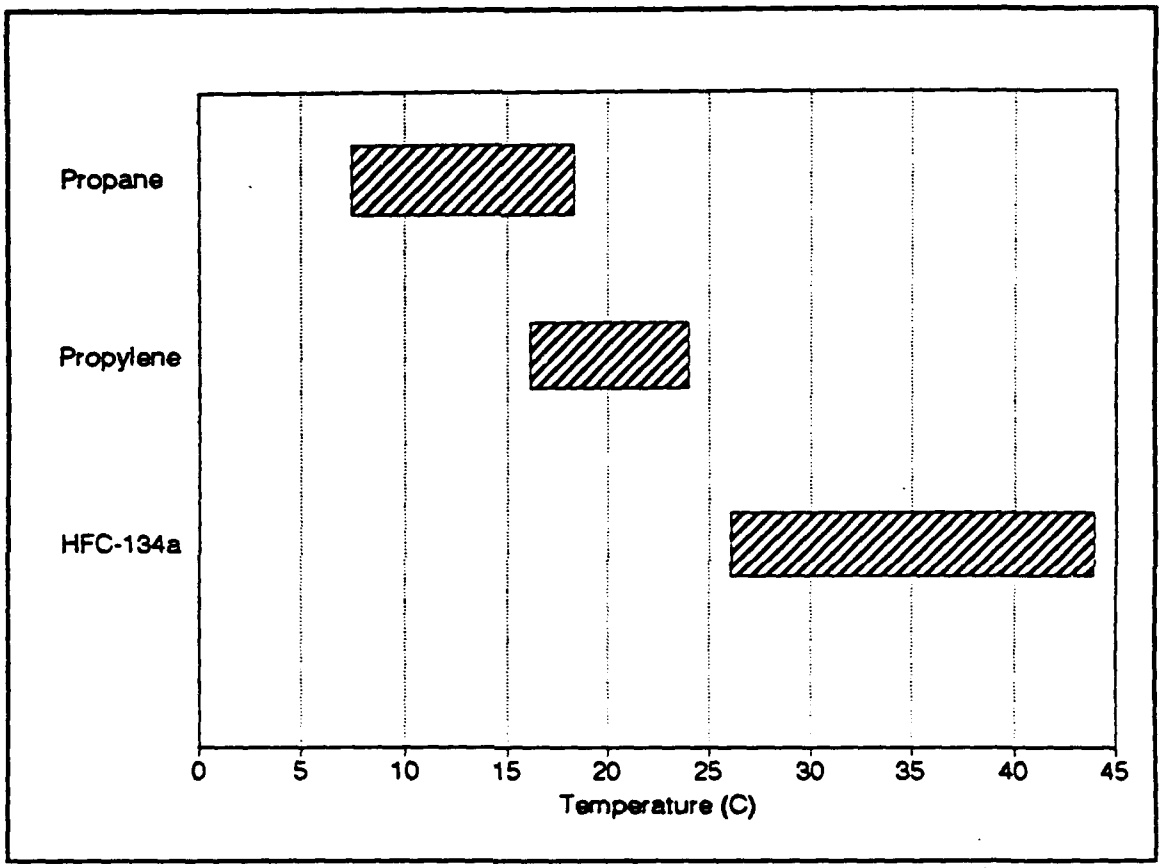

FIGURE 3-18. The predicted flat region for propylene, propane, and HFC-134a which has a change in response of ± 5 percent.

and HFC-134a only consider a 2.1 MeV neutron response. Because the regions were determined by a change in response of plus or minus five percent, they are defined beyond the response plateau. Consequently, the actual "flat" regions for propane and HFC-134a will be smaller when considering the response for a poly-energetic source.

CHAPTER IV

VERIFICATION OF THE THEORETICAL MODEL

The theoretical model is verified through experimentation conducted at the National Institute of Standards and Technology (NIST). The experimental set-up is presented. Test results are presented and discussed.

4.1 PROPOSED EXPERIMENT

The theoretical response predications presented in Chapter III depend heavily upon the validity of the Harper model. Although Harper has proven the soundness of his theory through prior experimentation,[6] it was decided that further experimentation was necessary to confirm the theoretical model. In the proposed experiment, Freon-12 detectors produced by Apfel Enterprises are irradiated at various temperatures using a pure thermal neutron beam (0.0253 Ev) from the Test Reactor at NIST. The detector responses at the different temperatures are then compared to the predictions of the theoretical model in order to test the model's validity.

4.2 THEORY

Because the efficiency factors for elastic scattering reactions by thermal neutrons in Freon-12 are zero, there is no expected response for any temperature from this type of reaction. However, there is a non-negligible (0.4 barn) thermal neutron cross section for the $Cl^{35}(n,p)S^{35}$ reaction. This particular reaction liberates 615 keV of energy, divided

between the heavier sulfur ion (17 keV) and the lighter proton (598 keV). Although it contains more energy, the proton's stopping power in Freon-12 is only 9% of sulfur's (0.33 keV per 10^{-6} cm as compared to 3.68 keV per 10^{-6} cm) and thus, is unable to deposit more than about 1 keV within the effective ionic energy transfer length L. Because the thermal neutron absorption reaction with chlorine-35 is the only possible source of energy, the total amount of energy made available to the superheated liquid can be calculated as the sum of the energies deposited by both ions, approximately 18 keV. Using Eq. (3-1),

$$E_c = \frac{4}{3}\pi r_c^3 \rho_v h_{fg} + 4\pi r_c^2 \left(\sigma - T\frac{\partial \sigma}{\partial T}\right) + \frac{4}{3}\pi r_c^3 P_l \qquad (3\text{-}1)$$

the critical energy required to form a bubble at different temperatures can be calculated. Table 4-1 provides the critical bubble data for Freon-12 at some temperatures of interest.

TABLE 4-1. Critical Bubble Data for Freon-12 at Selected Temperatures.

Freon-12 (CCl_2F_2)				
Temperature °C		18.9	19.1	20.0
Vapor Density (ρ_v)	kg/m^3	31.5	31.6	32.4
Liquid Density (ρ_l)	kg/m^3	1334	1333	1330
Surface Tension (σ)	. dyn/cm	9.9	9.8	9.7
Critical Radius r_c	10^{-6} cm	4.51	4.47	4.28
Total Critical Energy E_c	keV	18.2	17.8	16.1

Figure 4-1 illustrates the critical bubble data found in Table 4-1 and indicates that if 18 keV of energy were deposited, it would be sufficient to cause vaporization of Freon-

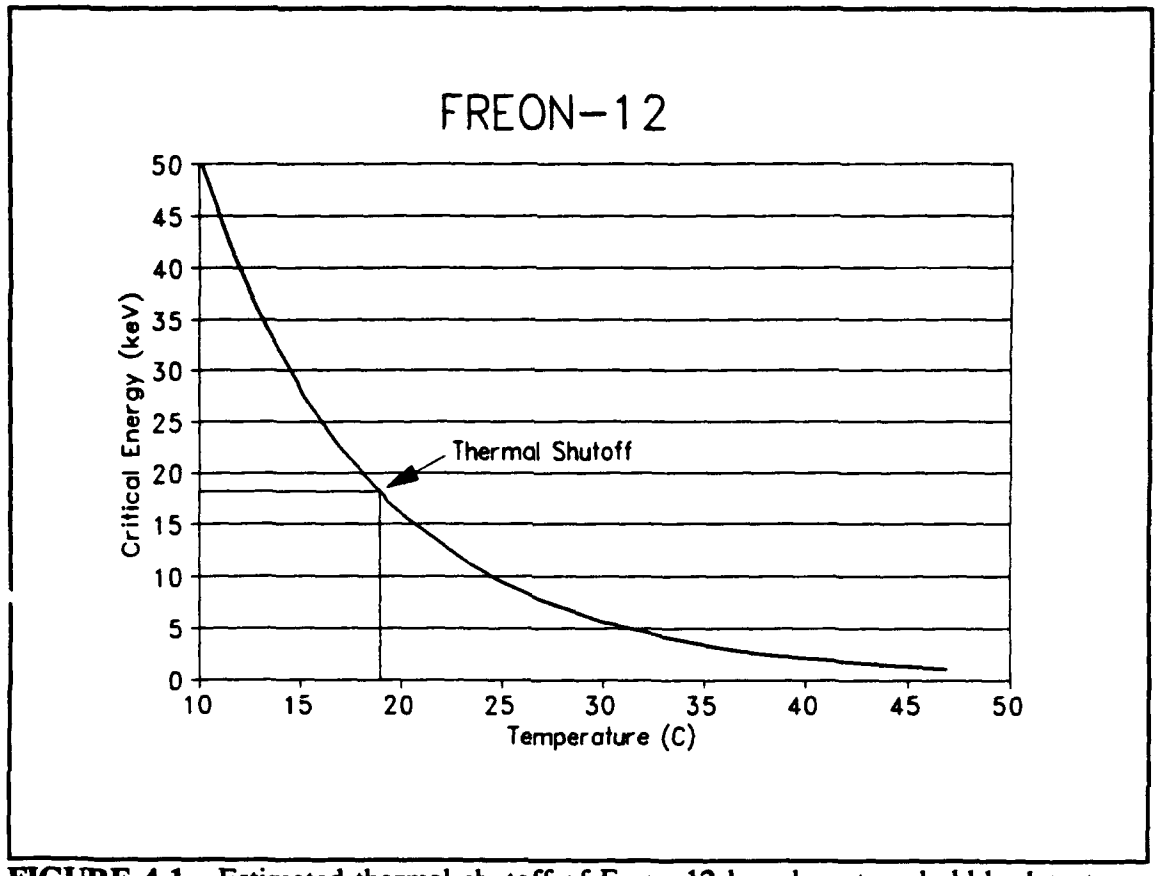

FIGURE 4-1. Estimated thermal shutoff of Freon-12 based neutron bubble detector based upon theoretically predicted critical energy, E_c.

12 droplets at a temperature greater than or equal to 19°C. Thus, by irradiating Freon-12 detectors at temperatures below and above 19°C, it is possible to validate the theoretical 19°C shutoff / turn-on temperature.

4.3 EXPERIMENTAL SET-UP

The detectors used in the NIST experiments utilize superheated liquid Freon-12 droplets uniformly distributed throughout a semi-viscous gel matrix. The detector system, manufactured by Apfel Enterprises, uses a personal computer driven device that holds a glass vial containing approximately 30,000 of the freon liquid droplets. Each

droplet measures about 100μm in diameter and forms a bubble of about 650μm diameter when activated by sufficient energy. When the individual droplets vaporize, they produce a pressure pulse lasting 15-30 msec with a frequency spectrum primarily in the 1kHz-10kHz range. A piezoelectric acoustic transducer is coupled to the glass vial in order to detect each pulse. The output is electronically filtered to discriminate authentic neutron events from any background noise and then is downloaded on to a personal computer via the Apfel detector.

Detector responses were measured at the research reactor located in NIST. The

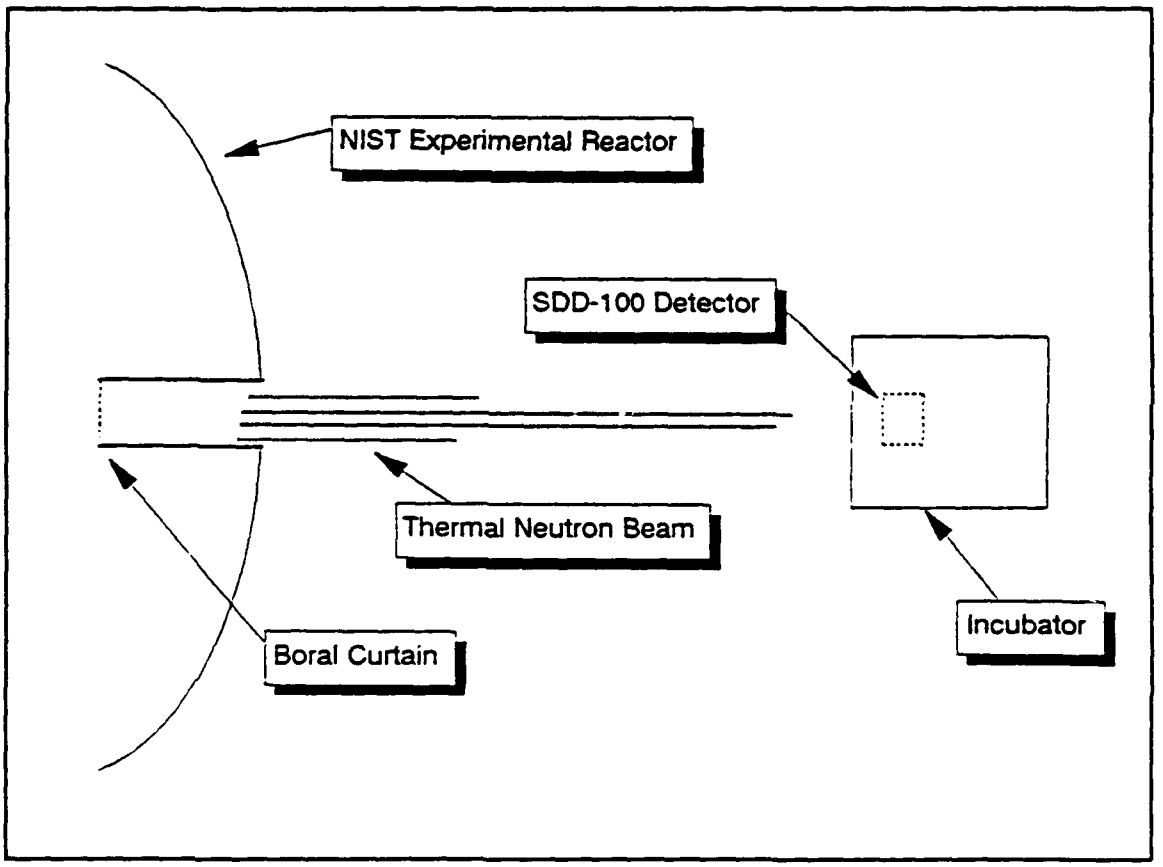

FIGURE 4-2. Schematic of the experimental set-up at NIST. The incubator was located approximately five feet from the entrance of the thermal neutron beam.

thermal neutron irradiations were performed using the 10-inch filtered pure thermal beam of the research reactor. The filtered thermal beam had a cadmium ratio of 10^4 and measured 1.2 x 10^4 neutrons per $cm^2 \cdot sec$ ($\pm 3\%$) for all irradiations. The irradiations were performed with the devices held at various temperatures maintained by a Fisher Scientific low temperature incubator. Figure 4-2 depicts the experimental setup.

4.4 EXPERIMENTAL RESULTS

Seven of Apfel's Freon-12 based SD-100 devices were irradiated using the NIST thermal beam. The irradiations lasted from ten to twenty minutes, and were conducted at five different temperatures ranging from (14°C to 26°C). The measured response rates (Bubbles/sec) are shown in Figure 4-3. It is important to note the distinct lack of response below 19°C and the noticeable increase in detector sensitivity above this shutoff point. Although the detectors' responses were significantly different from one another due to differing sensitivities, each detector demonstrated a definite shutoff at approximately 19°C.

4.5 EXPERIMENTAL CONCLUSIONS

The thermal irradiation experiments conducted with the Freon-12 based detectors proved that the model's prediction of the minimum critical energy required to nucleate a bubble is valid. From Eq. (3-1) the predicted shutoff temperature for thermal response by Freon-12 superheated liquid detectors was 19°C, exactly the same as that observed during the tests. Although Harper has done so in previous experimentation, this set of

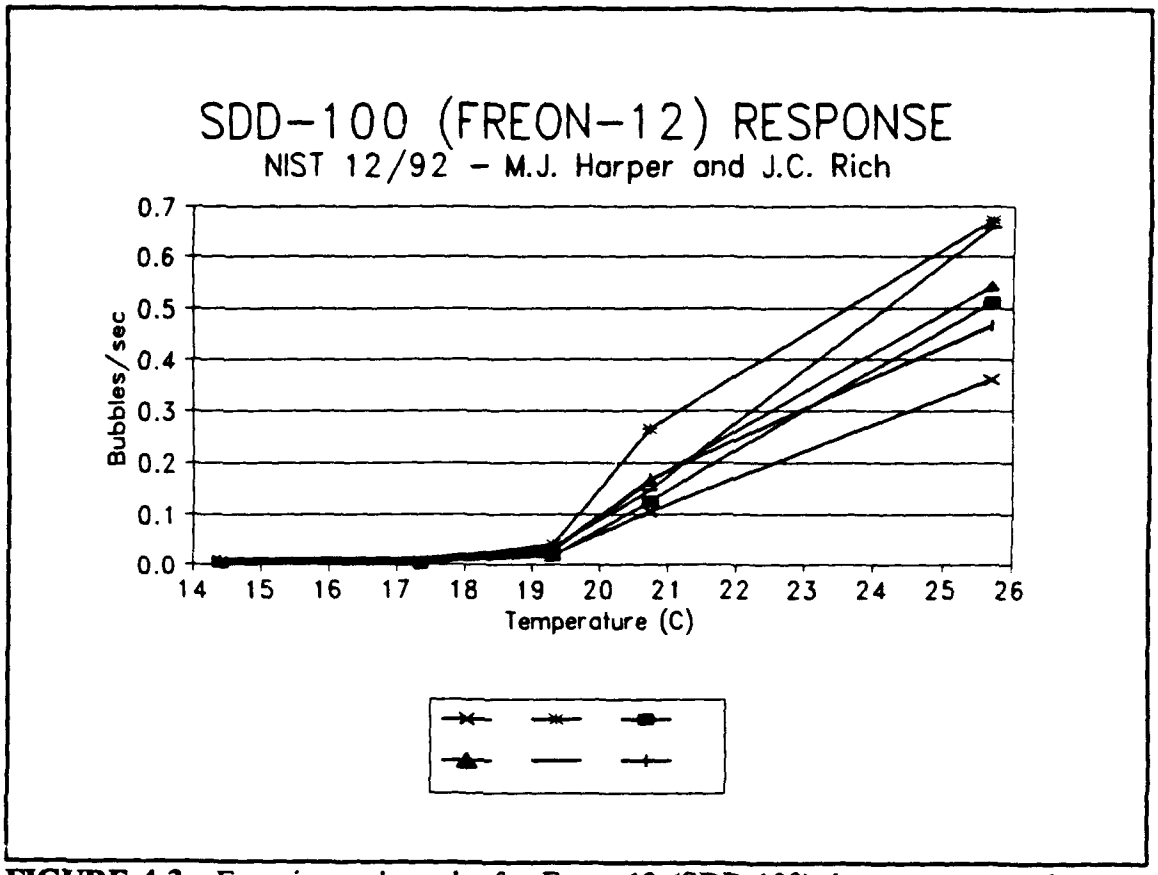

FIGURE 4-3. Experimental results for Freon-12 (SDD-100) detectors exposed to thermal neutron beam. Detectors effectively shutoff at 19°C.

tests could do nothing to validate the second criterion for nucleation, that dE/dx be such that $(dE/dx) \times L \geq E_c$. It does not matter whether one assumes $L = 2 \times r_c$ or $L = 4.3 \times r_o$, since the shutoff temperature for this criterion to be satisfied is lower than 19°C. At this point the detectors have ceased to function because the energy supplied by the charged particles, E_A, is less than the minimum critical energy required, E_c.

CHAPTER V

EXPERIMENTAL EVALUATIONS OF THE BUBBLE DETECTOR

A series of experiments were conducted at the U.S. Naval Academy's neutron generator facility to evaluate the characteristics of the neutron bubble detector. The experimental set-ups are provided and the results are discussed. Conclusions are drawn as to the suitability of the bubble detectors as on-site treaty verification tools.

5.1 REPEATABILITY STUDY

There are currently two different manufacturers of bubble detector devices, Apfel Enterprises and BTI Industries (BTI). Although both types of devices perform on the same theoretical principles, their characteristics and modes of operation are quite different. One of the greatest differences between the devices is the inability of the Apfel device to be reused. The viscous gel matrix which holds the initial liquid droplets is not rigid and consequently, is unable to keep the vapor bubbles from joining together once they have formed. As a result, it is impossible to return the vapor back into the original liquid droplets. The BTI device however, utilizes a rigid matrix which keeps the newly formed vapor bubbles in place. After the bubbles have formed and the detector has been read, it is relatively easy to re-condense the bubbles back into their original liquid form.

One of the greatest advantages of the BTI device over the Apfel detector is its capacity for reuse. A device which can be reused is more practical because of its lower cost and reduced calibration requirements. However, for the reusable detector to be of

any value, the device's sensitivity must remain constant after repeated use. In the following experiment, several of BTI's temperature compensated BD-100R devices were repeatedly irradiated in order to determine the effect of reuse on device sensitivity.

EXPERIMENTAL SET-UP

The BTI BD-100R bubble detector responses were measured in the Nucleonics Lab located in Rickover Hall. Neutron irradiations were performed using a bare Californium source (Cf^{252}) which provided an emission rate of 6.136×10^6 neutrons per second. Fourteen high sensitivity (30-60 bubbles/mrem) BD-100R detectors were attached and evenly spaced on a circular aluminum ring having a diameter of 41.3 cm. As seen in Fig. 5-1, the Californium was placed in the exact center of the ring so that each device would receive the same neutron exposure from the isotropic source during each successive test. The neutron irradiations lasted exactly five minutes for each run. An irradiation time of five minutes was chosen because calculations indicated that approximately 350 bubbles would be formed. This number of bubbles is statistically significant for data analysis. It was assumed that scattering effects would be identical for all devices in each successive exposure. All irradiations were conducted at standard atmospheric pressure and constant room temperature (22°C). The bubbles were counted using a BTI BDR-Series II Bubble Reader which is shown in Fig. 5-2. A full description of the optical reader is provided in Section 5.5.

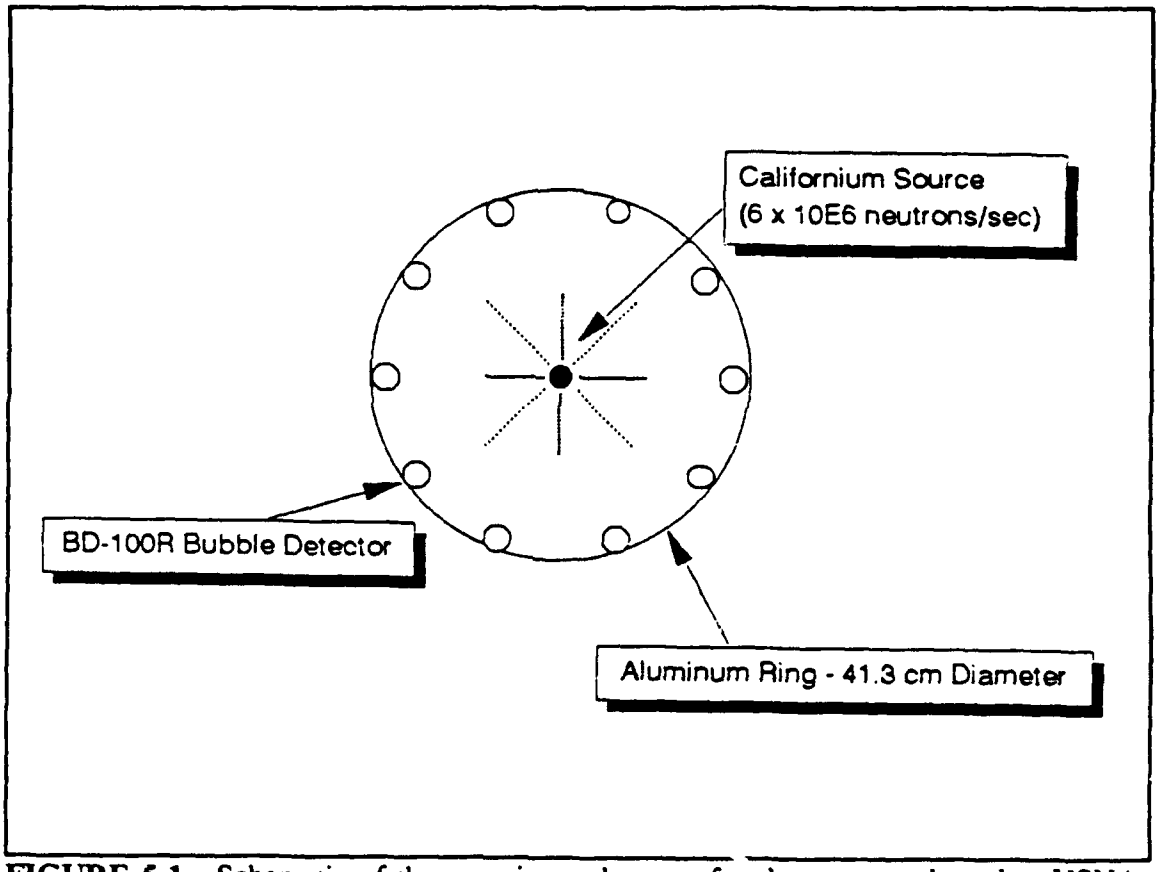

FIGURE 5-1. Schematic of the experimental set-up for the tests conducted at USNA neutron generation facility.

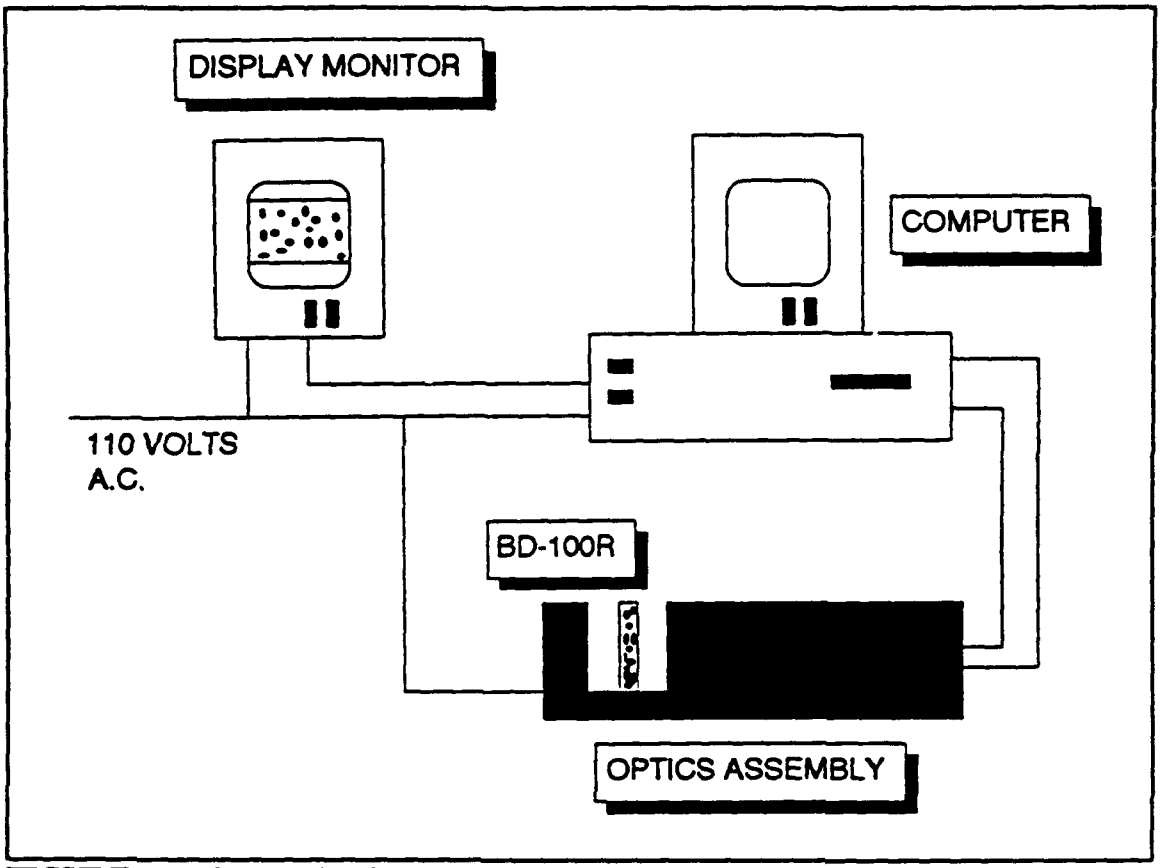

FIGURE 5-2. Schematic of the BTI BDR-Series II Optical Reader. The reader uses two cameras and a computer to count the bubbles.

DISCUSSION OF RESULTS

In this study, each device was irradiated ten separate times. Figures 5-3, 5-4, 5-5 provide a graphical display of the data acquired for each of the devices, which are labeled A through N. In these plots, the normalized relative response of each device is given for individual runs. The normalized response was obtained by dividing the observed number of bubbles for a given run by the average number of bubbles observed over all exposures. The shape of the individual three-dimensional relative response plots provide an indication of how the bubble counts for a particular run compared to the average. The flatness of the ribbons is evidence of the response consistency with each consecutive run.

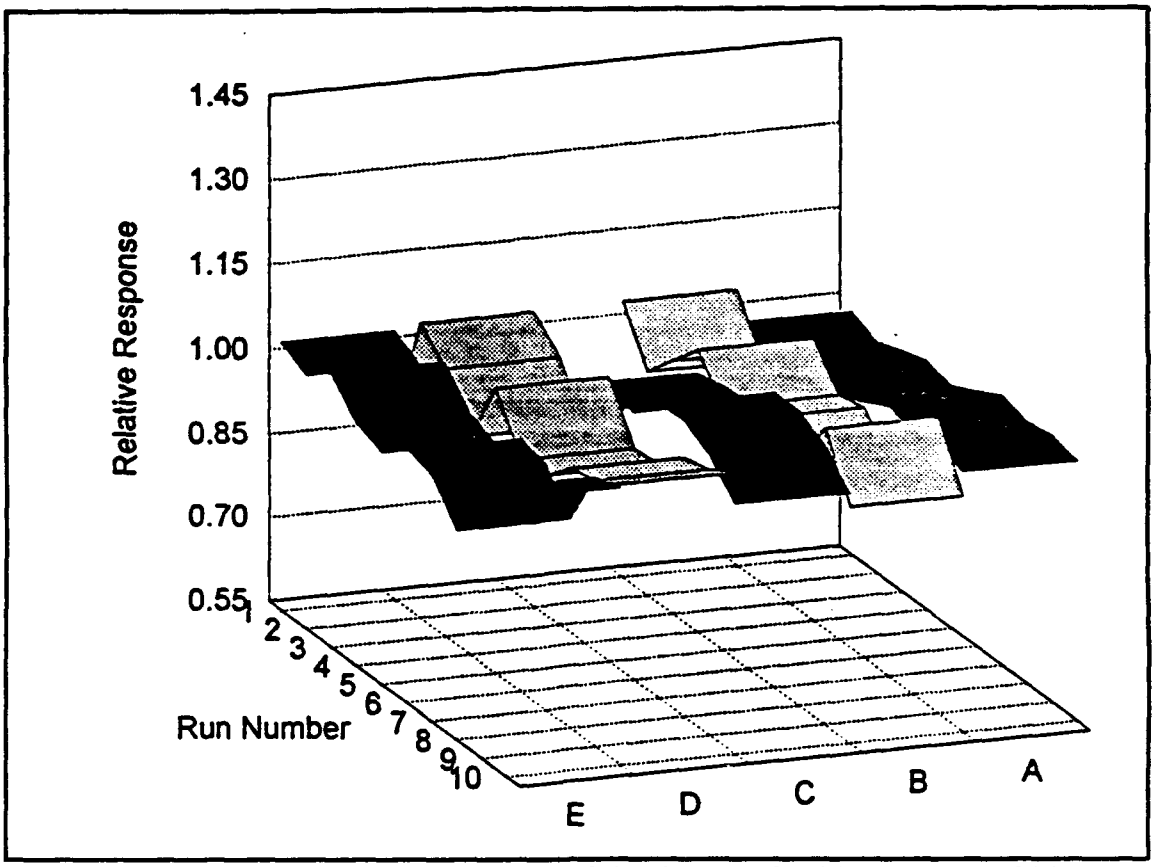

FIGURE 5-3. Three-dimensional display of the data obtained in the repeatability test. Flatness indicates consistency of response.

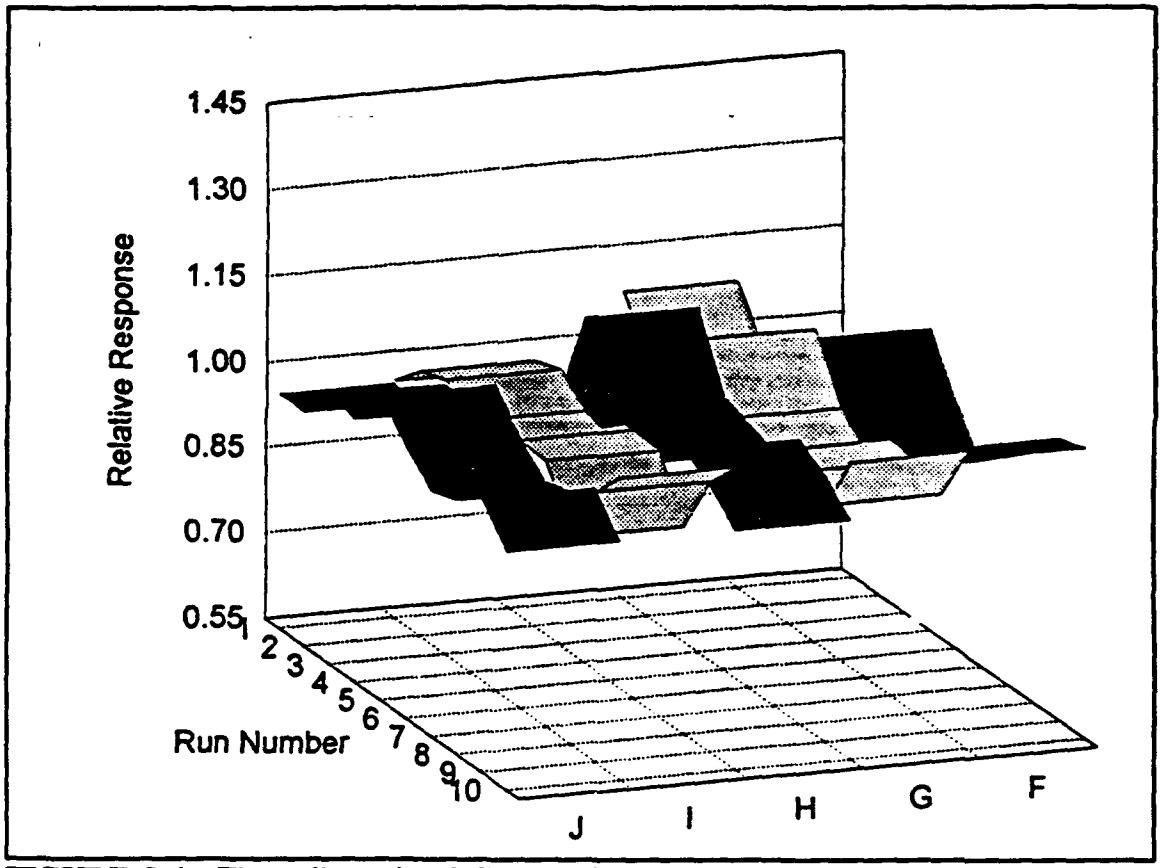

FIGURE 5-4. Three-dimensional display of the data obtained in the repeatability test. Flatness indicates consistency of response.

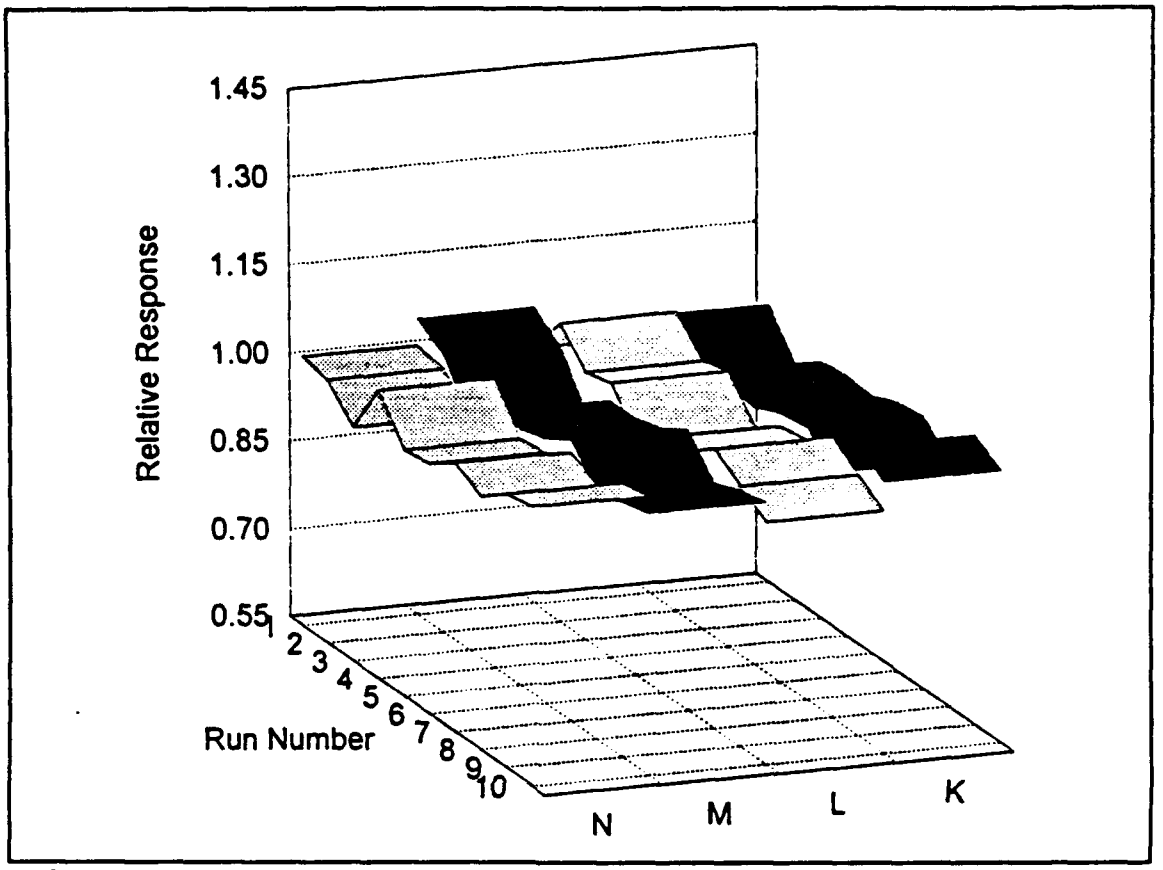

FIGURE 5-5. Three dimensional display of the data obtained in the repeatability test. Flatness indicates consistency of response.

Since radiation interactions are random in nature, any observation is subject to some degree of statistical fluctuation. These inherent fluctuations provide a means to check the normal functioning of any piece of nuclear counting equipment. If the amount of fluctuation associated with the collected data is not consistent with the predictions of statistical tests, it can be concluded that an anomaly exists in the detection system. Since nuclear events are typically described by a Poisson distribution, the "Chi-squared Test" (χ^2)[33] can be used to determine if the experimental data follows this distribution.

For this experiment, the two percent χ^2 test was applied to the data collected. The test indicated that the fluctuations in the data for all devices, except one, fell within the

normal bounds allowed. Device A failed the test because it was too consistent (i.e. its response did not exhibit enough statistical variation). However, this result was not unexpected, since statistically one device in 25 should fail the two percent χ^2 test.

Counting statistics were further used to give an indication of the consistency and uncertainty associated with the data obtained from the fourteen devices. Figure 5-6

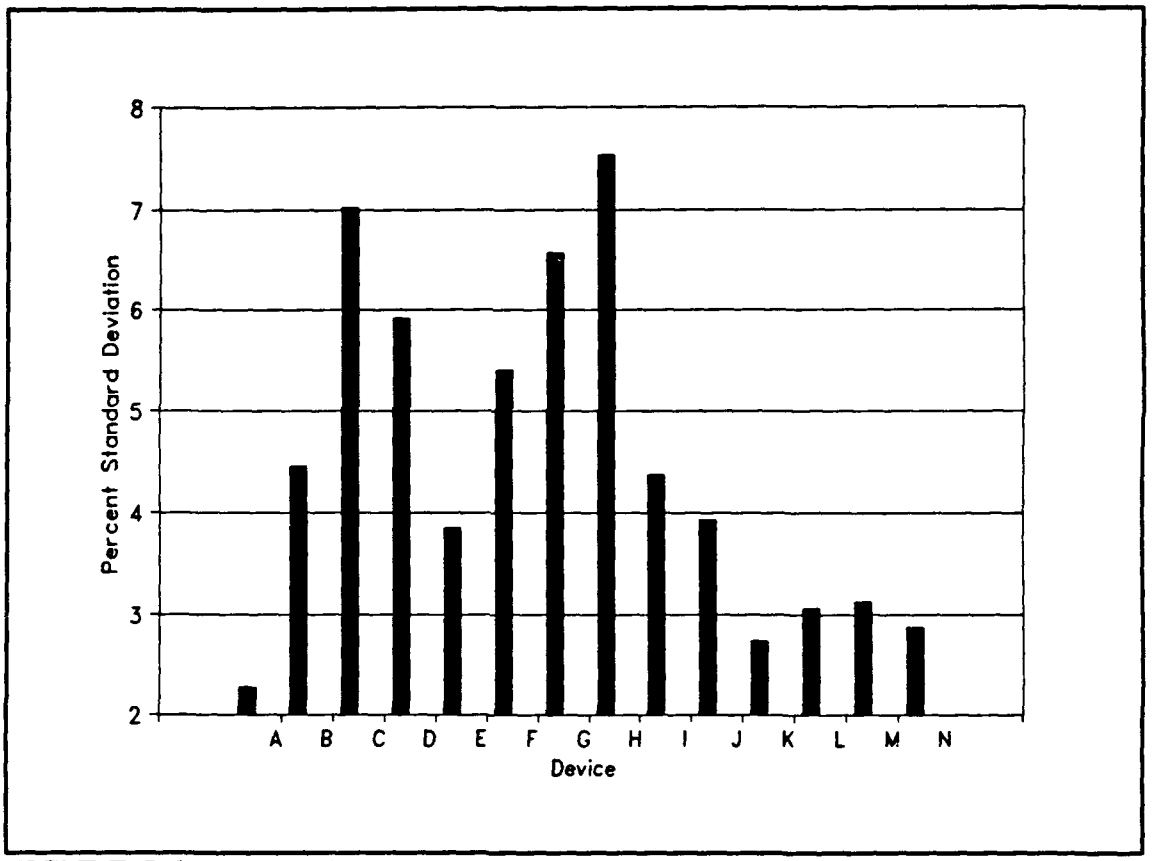

FIGURE 5-6. Bar graph represents the percent standard deviation for each of the fourteen devices. $N = 365$.

provides a measurement of the percent standard deviation in the data for each device. In this figure, it can be seen that the percent standard deviation ranges from approximately two percent to seven percent. Since the average number of bubbles formed for each run was 365, it was expected based on Poisson statistics that

approximately one third of the devices would have a percent standard deviation greater than 5.2 percent. As can be seen in Fig. 5-6, five of the fourteen devices, approximately one-third, had percent standard deviations greater than 5.2 percent. It can be concluded from this study, that the manufacturer's claim of a sensitivity which remains consistent with each reuse is valid.

5.2 BUBBLE GROWTH STUDY

After a superheated liquid droplet vaporizes, the resulting bubble formed in the BD-100R is not in dynamic equilibrium with the rigid gel matrix. The bubbles continue to grow for a significant period of time after their initial formation. Studies conducted with the early models of the BD-100R[34] indicated that the readings obtained changed drastically over time. It was not until upwards of ten hours after irradiation that the devices were able to be read with the confidence that the data acquired had stabilized and was accurate. When considering the BD-100R for operational use by nuclear weapons on-site inspection teams, this feature is a major drawback. Ideally, it would be best if the devices could be read as soon as possible after irradiation so that instant feedback could be obtained. Furthermore, the question as to how much time must elapse before the devices are read with confidence must be answered.

The currently marketed temperature compensated BD-100R devices are quite different from their predecessors. The processing of the liquid droplets and the gel has been changed in the newer devices. Furthermore, BTI, the manufacturer, insists that the bubbles are visible immediately upon nucleation. Consequently, it was determined that

the phenomena of bubble growth should be studied in greater depth than heretofore. This study examined bubble growth in two steps. The first step involved quantifying the actual change in size of a bubble over time by measuring the changing bubble diameter. In the second step, the devices were continuously read over time and the change in response with time was evaluated.

EXPERIMENTAL SET-UP

For step one, two different high sensitivity (45-50 bubbles/mrem) BD-100R devices were each irradiated for exactly ten seconds using the Cf^{252} source mentioned earlier. Each detector was exposed to the same radiation field. Furthermore, each radiation was conducted at standard atmospheric pressure and constant room temperature (22°C). The bubble growth was observed by measuring the actual diameter of a single bubble over time using the Buehler Omnimet Image Analysis System.

In the second step of the experiment, separate groups of BD-100R devices were irradiated using different neutron sources. First, ten high sensitivity (48-60 bubbles/mrem) BD-100R devices were independently irradiated twice for thirty seconds using the Cf^{252} source. Thirty seconds was chosen because approximately sixty bubbles would be provided in each device. This number of bubbles can be counted very accurately with the BTI BDR-Series II Reader. To evaluate the bubble growth effect upon bubble counting, the devices were read every 30 seconds between one and six minutes after irradiation and every minute between six and twelve minutes after irradiation. Second, ten high sensitivity (48-60 bubbles/mrem) BD-100R devices were

independently irradiated once for thirty seconds using a Plutonium-Beryllium (Pu-Be) source. For this source, the Pu^{239} in the Pu-Be source emits alphas which react with the beryllium to produce neutrons with an approximate average energy of 4.0 MeV. The source provided an emission rate of 2×10^6 neutrons per second. For this test, the devices were read every 30 seconds between one and six minutes after irradiation and every minute between six and twelve minutes after irradiation. Finally, four additional high sensitivity (48-49 bubbles/mrem) BD-100R devices were irradiated for 30 seconds using the Cf^{252} source. These devices were read periodically over an 1880 minute period so as to determine the effects upon long term counting. Each group of irradiations for the bubble growth analysis were conducted under the same conditions. Furthermore, each group of irradiations, except for minor variations (different source, different number of detectors), used the same experimental set-up as that outlined in Fig. 5-1.

DISCUSSION OF RESULTS

The results of the first step are presented in Fig. 5-7, where the changing bubble diameters are plotted with respect to time. From Fig. 5-7, it is evident that the initial rate of growth is quite large, and with time, the rate of growth will continually decrease until the bubble achieves a state of equilibrium. Although the growth curves for the two different bubbles are not exactly the same, a clear understanding of the growth characteristics can be obtained. The growth of the two bubbles follow the same trends, differing only slightly in their growth rates. Differing growth rates can be rationalized

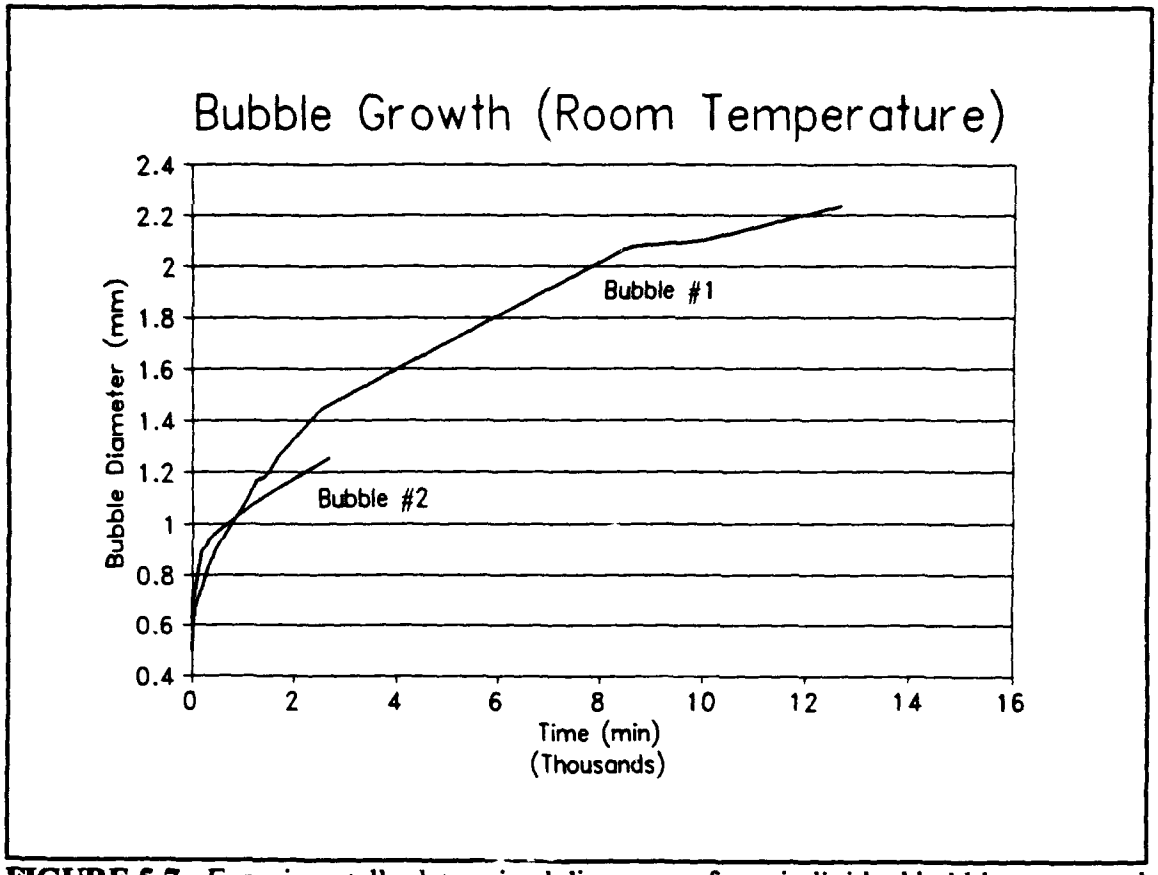

FIGURE 5-7. Experimentally determined diameters of two individual bubbles measured over time. Initial bubble growth is rapid.

by various factors such as slight deviations in temperature and dissimilar liquid droplet densities within the gel matrix. The growth curves of the two bubbles appear to follow an exponential relationship of the form $(1\text{-}e^{\lambda t})$ expression. The growth is very large initially and then tapers off over time. As demonstrated by bubble #1, the diameter does asymptotically reach some value.

The initial growth study indicates that it takes a considerable amount of time, approximately 14,000 minutes (10 days), for a bubble to reach a state of equilibrium. It is clear that the initial rate of growth is considerable, but the question of how much of an effect the growth rate has upon the reader's ability to detect and count accurately a

still growing bubble must be determined. However, since the human eye can discern a bubble approximately 0.3 mm in diameter, the bubble dosimeter can be read visually within one minute after irradiation.

The second step of the bubble growth analysis involved irradiating different groups of bubble detectors with different sources and reading them at various times after irradiation. The goal of the study was to determine if the number of bubbles counted by the optical reader varied significantly with time after irradiation, and also whether a different energy neutron source yielded an effect upon those readings.

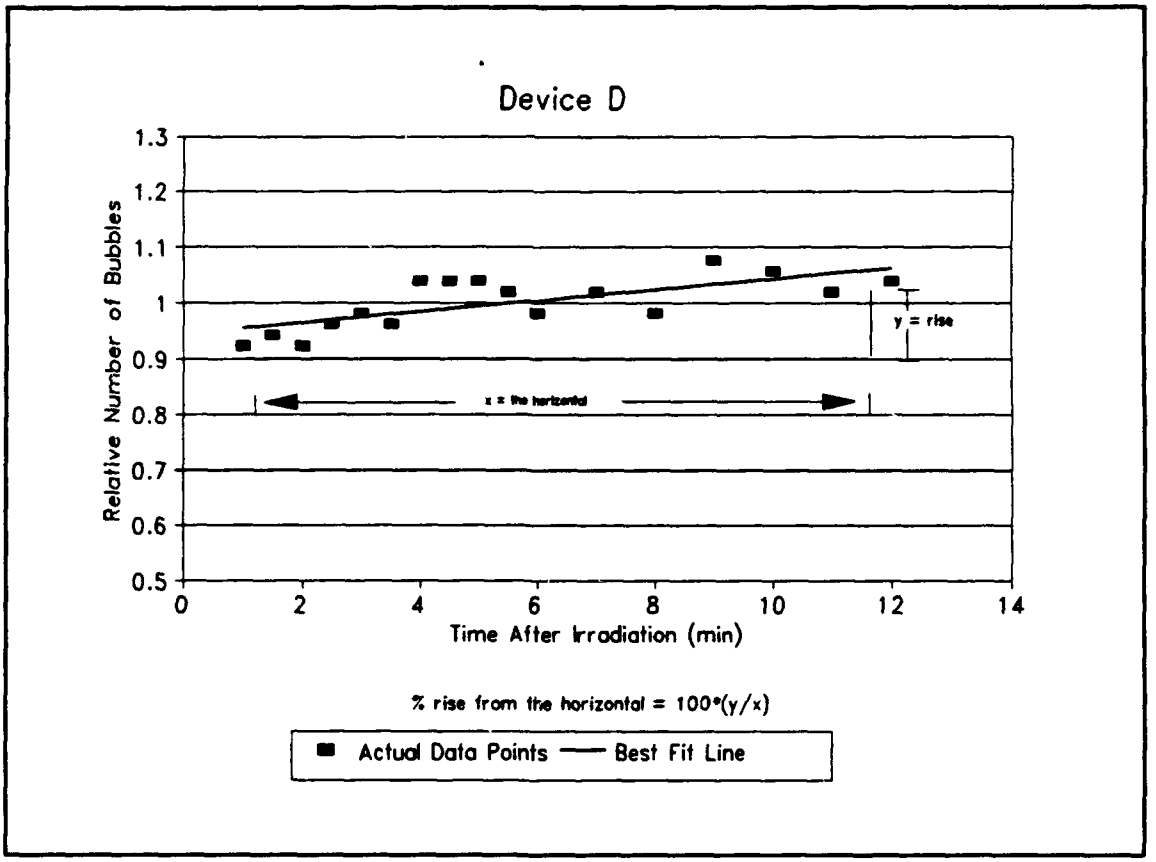

FIGURE 5-8. The percent rise from the horizontal is defined for device D. The percent rise represents the percent increase in response per minute.

The first group of ten devices were each irradiated twice using the Cf^{252} source. The experimental results of the first two runs were analyzed by using the concept of the "percent rise from the horizontal." Figure 5-8 provides a graphical representation of this concept. In this figure, the normalized relative response is plotted with respect to time after irradiation. The response was normalized by dividing the number of bubbles counted at a specific time by the average number of bubbles for all counts. A linear regression was performed on the data so that the best fit line which approximated the data could be determined. The percent rise above the horizontal was next defined by multiplying the slope of the best fit line by 100 percent. This calculation provides a number which represents the change in the bubble counts with time in terms of a percent relative increase or decrease above the horizontal. Thus, a percent rise above the horizontal of zero would indicate a response which does not change with time, while a percent rise above the horizontal of one would indicate a response which increased by one percent every minute.

Figures 5-9 and 5-10 provide the percent rise above the horizontal for the two runs of the devices irradiated by the Cf^{252} source. In the two plots, the percent rise varies between -0.54 percent and 1.7 percent, with the all of the devices except for one having a percent rise below 1.0 percent. These values indicate that the bubble counts for all the devices varied little with time. Although the bubble counts for the devices did for the most part increase with time, it can be concluded from this test that the bubbles, when formed, are generally large enough to be counted by the reader. However, a very small number of bubbles will sometimes be initially too small and will be below the minimum

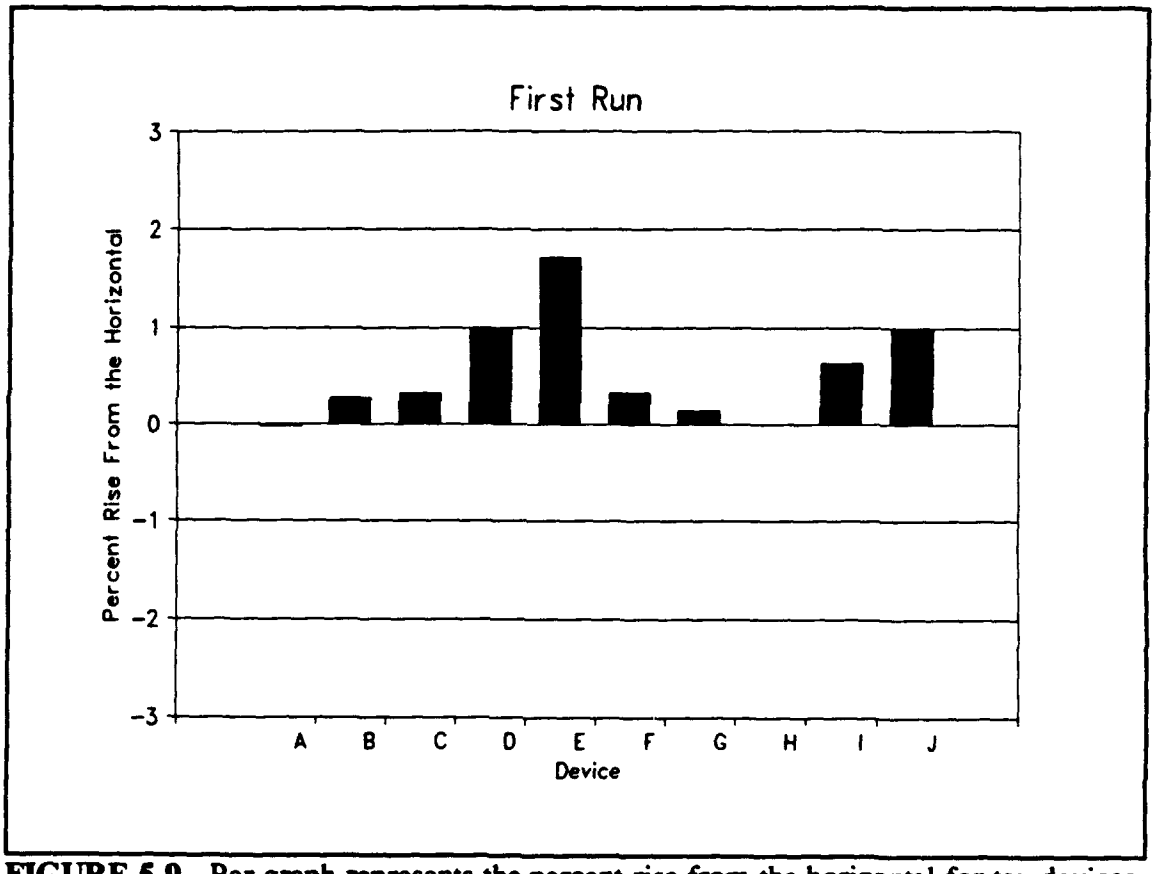

FIGURE 5-9. Bar graph represents the percent rise from the horizontal for ten devices. The data is from the first run with the Cf^{252} source.

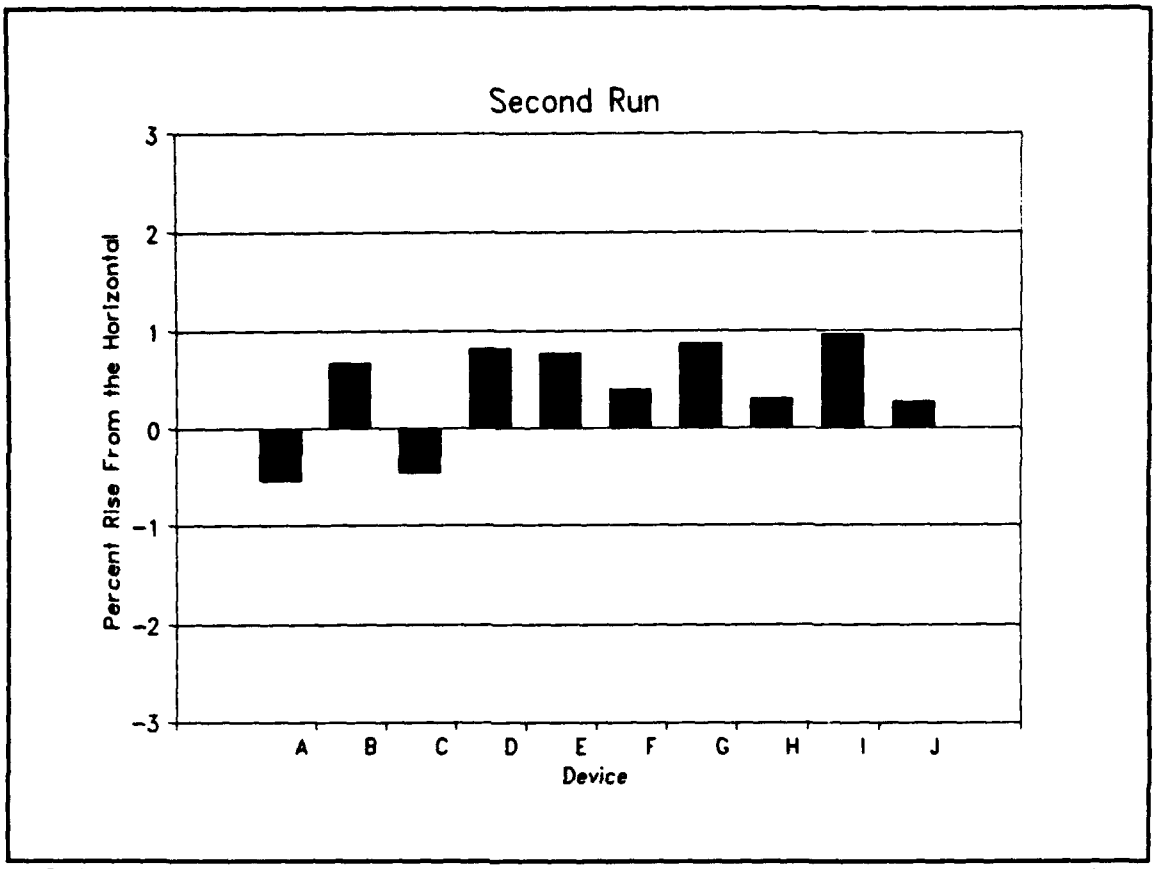

FIGURE 5-10. Bar graph represents the percent rise from the horizontal for ten devices. The data is from the second run with the Cf^{252} source.

sensitivity of the reader. The increase in bubbles can also be partially accounted for by inherent reader characteristics, which are discussed in Section 5.5.

The second group of ten dosimeters were irradiated once using the Pu-Be source. For this test, the concept of the "percent rise above the horizontal" was again used to analyze the acquired data. Figure 5-11 graphically provides the percent rise above the horizontal for the ten detectors irradiated by the Pu-Be source. The results of this test were similar to those obtained using the Cf^{252} source. The relative percent increases in the counts are very small, with all values below one percent. This data further indicates that the bubble growth has only a negligible effect upon the reader's ability to count

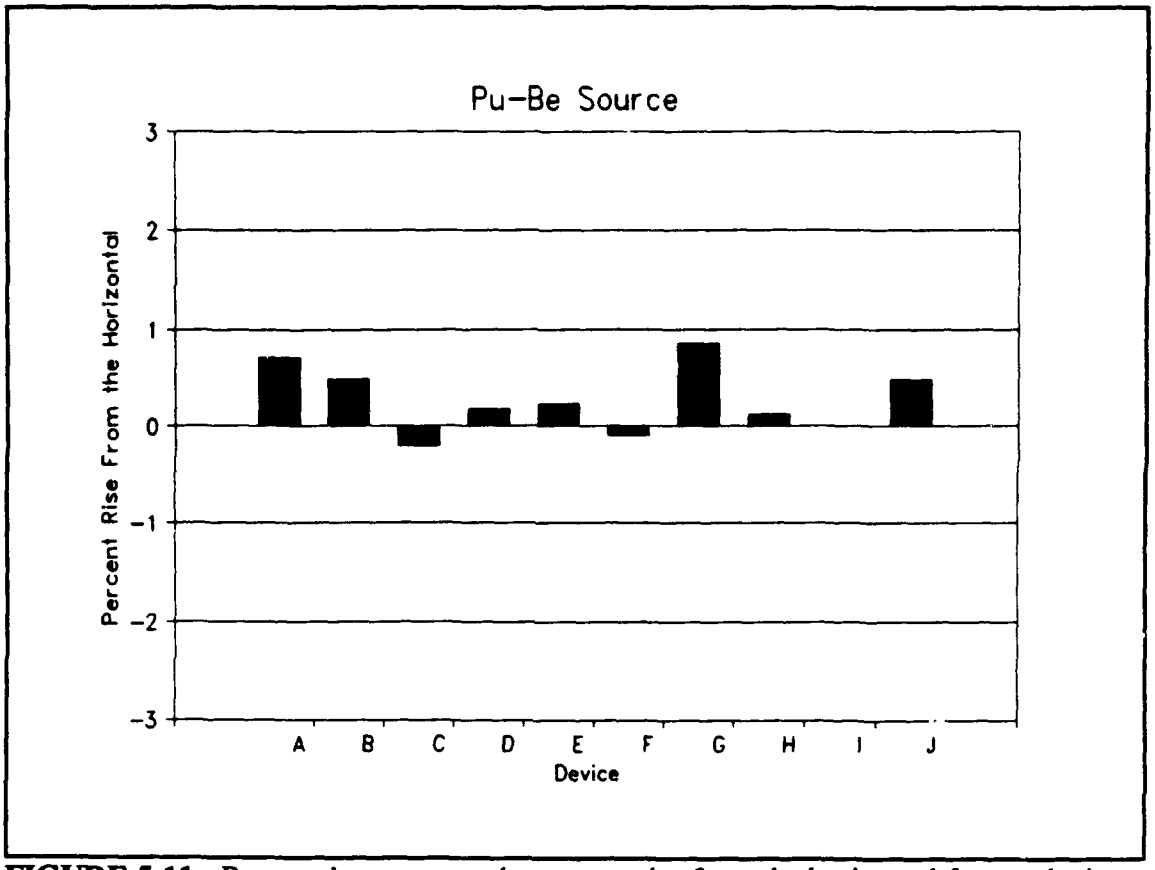

FIGURE 5-11. Bar graph represents the percent rise from the horizontal for ten devices. The data is from the test with the Pu-Be source.

accurately the number of bubbles initially present after irradiation. Furthermore, it is important to note that the higher energy of the Pu-Be neutron source did not noticeably affect the bubble growth process.

The third set of four dosimeters was irradiated using the Cf^{252} source and was evaluated over a very long period of time following the irradiation. Similar to the previous groups of dosimeters, the data was analyzed by determining the percent rise from the horizontal for each of the four devices. From Fig. 5-12 it is evident that the devices had a very negligible increase in response for the time period (1880 minutes) considered. The percent rise for device G is the largest and is less than 0.003 percent.

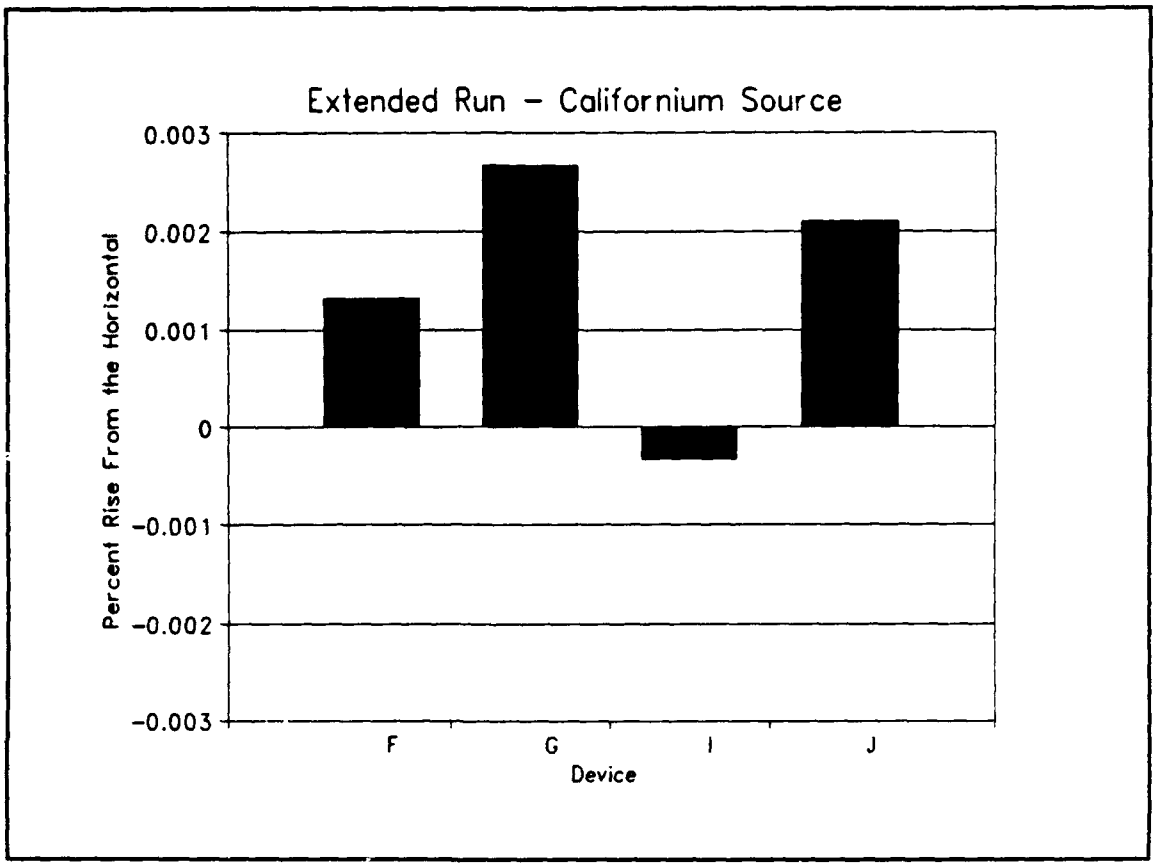

FIGURE 5-12. Bar graph represents the percents rise from the horizontal for four devices. The data is from the extended run with the Cf^{252} source.

From this data, it can be concluded that, over large periods of time, the response does not significantly change. When the results of this test are compared with the results of the first and second group of detectors irradiated, some interesting conclusions can be drawn.

The change in the bubble counts during the first twelve minutes after irradiation were much more dramatic than the change in counts for the extended run. This makes sense when considering the definition of "percent rise from the horizontal" and the drastic difference in time intervals over which the changes were observed. It can be concluded that although the bubble counts did slightly increase over the first twelve minutes after

irradiation, the rate of increase did not remain constant, but rather decreased rapidly with time. This observation remains consistent with the bubble growth histories provided in Fig. 5-7. The initial increase in response during the first twelve minutes after irradiation is fairly negligible when compared with the total change in response for the much longer extended run. Furthermore, the increase in response due to bubble growth was found to be much less than that due to the statistical fluctuations discussed in Section 5.1. As a result of these tests, it appears that the bubble growth characteristics of the BD-100R bubble detectors have a very minimal effect upon the BTI BDR-Series II optical reader's ability to count accurately the response. Additionally, the BD-100R bubble detectors can be read confidently immediately after irradiation.

5.3 LINEARITY STUDY

One of the most important characteristics of an accurate radiation detector is that its measurements have a linear relationship with the received dose or fluence. For example, if a device with a sensitivity of 50 bubbles/mrem is exposed to a source with a dose rate of 1 mrem/minute, the response counted must be consistent with the dose the device received. For a two minute exposure, the device should have approximately 100 bubbles, while for a four minute exposure, the device should register twice as many bubbles. A device linearity test verifies whether the detector sensitivity (bubbles/mrem) remains constant with a changing dose. The next test investigated the linear characteristics of the BD-100R bubble detector by exposing it to different neutron doses.

EXPERIMENTAL SET-UP

The linearity study was conducted utilizing ten different high sensitivity (46-50 bubbles/mrem) BD-100R devices. The devices were each irradiated for the different time periods of two, three, four, and six minutes using the Cf^{252} source previously described. These irradiation periods were chosen because they would provide bubble counts ranging from 200-600 bubbles, measurements lying well within the dynamic range of the optical reader. The actual experimental set-up for the linearity study was identical to that outlined in Fig. 5-1. All irradiations were performed at standard atmospheric pressure and constant room temperature (22°C).

DISCUSSION OF RESULTS

In this study, ten different BD-100R devices were each exposed to the Cf^{252} source for four different irradiation time periods. Figure 5-13 provides a graphical display of the data acquired for device G, one of the ten devices. In this figure, the number of bubbles for each of the four runs is plotted with respect to the length of irradiation in minutes. The best fit line through the data was determined by performing a linear regression. It is important to note how well the best fit line approximates the linear behavior of the data.

A linear regression was also performed on the data for each of the other nine devices. The linearity of each device's behavior was ascertained by calculating a correlation factor. This statistic ranges between zero and one, with one being optimal, and provides an indication of how closely the accumulated data matches the curve-fitting model used.

Figure 5-14 shows the correlation factors for each of the ten devices used in the linearity study. From the results provided in Fig. 5-14, it can be concluded that the BD-100R devices behave linearly with varying dose.

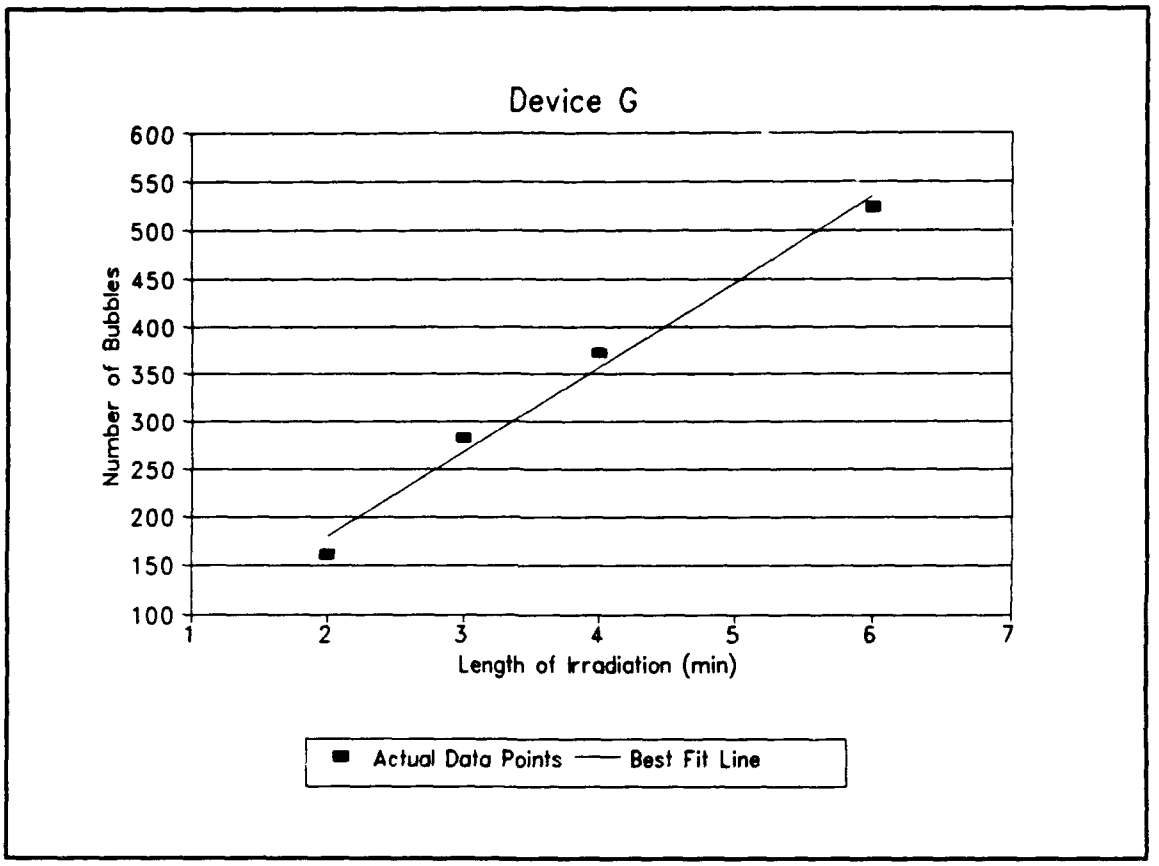

FIGURE 5-13. The response for device G is plotted with respect to the length of irradiation. Linearity is demonstrated for device G.

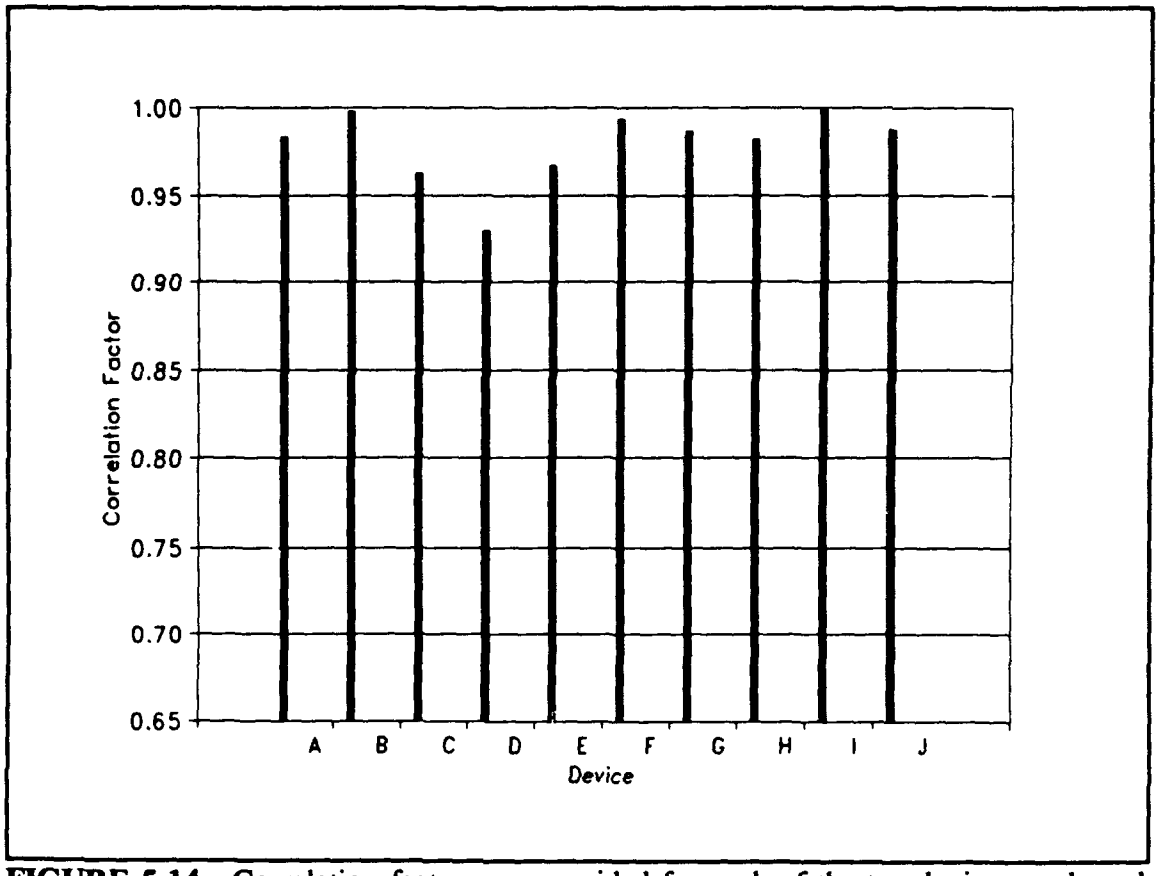

FIGURE 5-14. Correlation factors are provided for each of the ten devices evaluated in the linearity study. A correlation factor of 1.0 indicates perfect linearity.

5.4 TEMPERATURE RESPONSE STUDY

The critical amount of energy, E_c, necessary to form a bubble within a device depends upon the temperature of the superheated liquid droplet. This phenomenon was described in great detail in Chapters II, III, and IV and is clearly demonstrated in Fig 3-1. As a consequence, the response of a bubble detector is usually temperature sensitive and non-linearly increases with increasing temperature. Prior studies[6.34] have verified that both the Apfel detector and earlier models of the BD-100R do adhere to the temperature

dependence characteristics of bubble detectors.

BTI has conducted extensive research into ways of redesigning the BD-100R so that its temperature dependence is either eliminated or limited to a certain temperature region. Unlike the temperature compensation techniques offered in Chapter IV, the new BD-100R is mechanically compensated. A compensating gel which expands and contracts with changing temperatures is placed within the device immediately above the rigid gel matrix which contains the superheated liquid droplets. Increasing temperatures cause the compensating gel to expand and exert a pressure upon the gel matrix. As a result, the increased pressure counter-balances the effects of increased temperature upon E_c. This study evaluated the temperature characteristics of the new compensated BD-100R by measuring the response of the device at many different temperatures.

EXPERIMENTAL SET-UP

Ten different high sensitivity (36-62 bubbles/mrem) BD-100R detectors were each irradiated for five minutes at nine different temperatures ranging from (9.5°C to 46.1°C). The irradiations were performed with the devices held at the different temperatures by placing them in a Fisher Scientific low temperature incubator. The Cf^{252} source was positioned immediately above the center of the incubator so that each device would receive an equal dose. Three hours of wait time were allowed between each run so that both the incubator and BD-100R detectors could come into thermal equilibrium.

DISCUSSION OF RESULTS

The results of the BD-100R's temperature compensation evaluation are presented in Fig. 5-15. In this figure, the relative responses of both the uncompensated BD-100R and

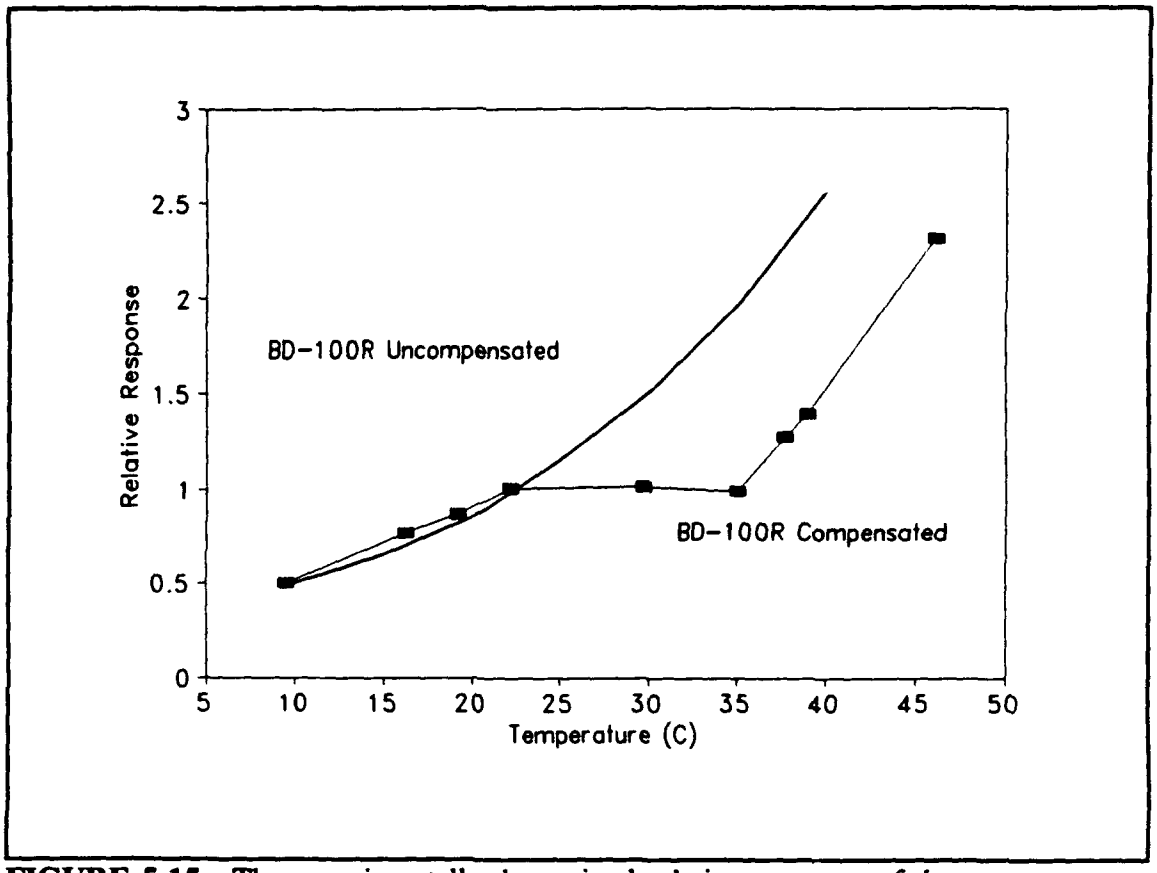

FIGURE 5-15. The experimentally determined relative response of the temperature compensated BD-100R is compared to that of the uncompensated BD-100R.

compensated BD-100R are presented. The manufacturer provided the data for the uncompensated BD-100R. The relative response for the compensated BD-100R was obtained by considering the responses of all ten devices. This was accomplished by adding the responses of all ten devices at each temperature and dividing the sum by the average of the combined responses for the flat region. As a result, the relative response

provided in Fig. 5-15 accounts for the responses of all ten devices and provides a better indication of the overall temperature characteristics of the compensated BD-100R device.

From Fig. 5-15, it is evident that the compensated BD-100R is vastly superior in performance to the earlier uncompensated version. The data obtained did for the most part verify the performance specifications provided by the manufacturer. The measured flat response was only a few degrees centigrade short of that predicted by the manufacturer. From this test, it can be concluded that the compensated BD-100R detector does have a region of constant response with respect to temperature for a relatively large temperature band (22.4°C to 34.4°C). However, the solution developed by BTI is still mechanical in nature and as a result, is subject to possible mechanical failure.

5.5 READER EVALUATION

The human eye counts accurately up to about fifty bubbles in a single BD-100R device. However, in order to achieve statistically valid measurements of a neutron source, more than fifty bubbles are required. Furthermore, virtually all of the testing presented in this report involved bubble counts significantly larger than fifty. Consequently, if a detector is to be exposed to significant doses, it is imperative that an accurate and dependable optical reader be available to measure the response. All of the bubble counting performed for the purposes of this report involved the use of the BTI BDR-Series II optical reader. Although the performance of the Series I device has already been fully evaluated[34], little has been published about the characteristics of this

new reader.

The optical reader, whose schematic is provided in Fig. 5-2, is composed of two cameras which simultaneously take picturers of different sections of the bubble detector. The cameras are linked to a computer assembly which analyzes the photos by examining the individual pixels which make up the images. Using an algorithm, the computer is able to count the number of bubbles by differentiating between shadows and other bubbles. The computer provides different threshold settings which can be manipulated to affect the sensitivity of the optical reader.

Initially, there were several unknowns associated with the operation of the optical reader. For example, it was not clear which threshold setting should be used for certain quantities of bubbles. Furthermore, the dynamic range and error associated with device's readings were also unknown. Consequently, these parameters were studied in order to gain an understanding of the reader's operational capabilities.

EXPERIMENTAL SET-UP

A group of tests were designed to determine the optimum threshold setting, the reader's dynamic range, and the error associated with the reader's counts. In the first series of tests, three previously irradiated BD-100R devices, each containing different numbers of bubbles, were evaluated at varying reader thresholds. Two of the devices contained a small enough number of bubbles (i.e. 47 bubbles and 87 bubbles), that the actual number of bubbles could be visually verified. This confirmation was done by visually counting the bubbles in the devices using the displayed pictures provided by the

reader's camera. The third device however, contained too many bubbles, approximately 140, and could not be visually verified. The three devices were each read at separate threshold settings ranging from (1 to 80). Furthermore, thirty independent readings were taken for each device at each of the detector thresholds evaluated.

The second series of tests utilized ten different high sensitivity (36-64 bubbles/mrem) BD-100R devices. The devices were each irradiated for the different time periods of two, four, six, eight, nine, and eleven minutes using the Cf^{252} source previously described. These irradiation periods were chosen so that the full dynamic range of the reader (i.e. maximum number of bubbles that can accurately be counted) could be determined and evaluated. The experimental set-up was identical to that outlined in the linearity study and in Fig. 5-1. All irradiations were performed at standard atmospheric pressure and constant room temperature (22°C).

DISCUSSION OF RESULTS

The goals of the first series of tests were to determine the optimum threshold setting for different numbers of bubbles and to quantify the error associated with the reader's counts. Figure 5-16 shows the number of bubbles counted at the different reader threshold settings for the device containing 47 bubbles. The number of bubbles plotted represents the average number of bubbles counted for the different threshold settings. It is important to note that between the threshold settings of 55 and 65, a plateau of consistent response existed. Furthermore, in this plateau, the reader was accurately able to determine the true number of bubbles. However, the data plotted in Fig. 5-16 only

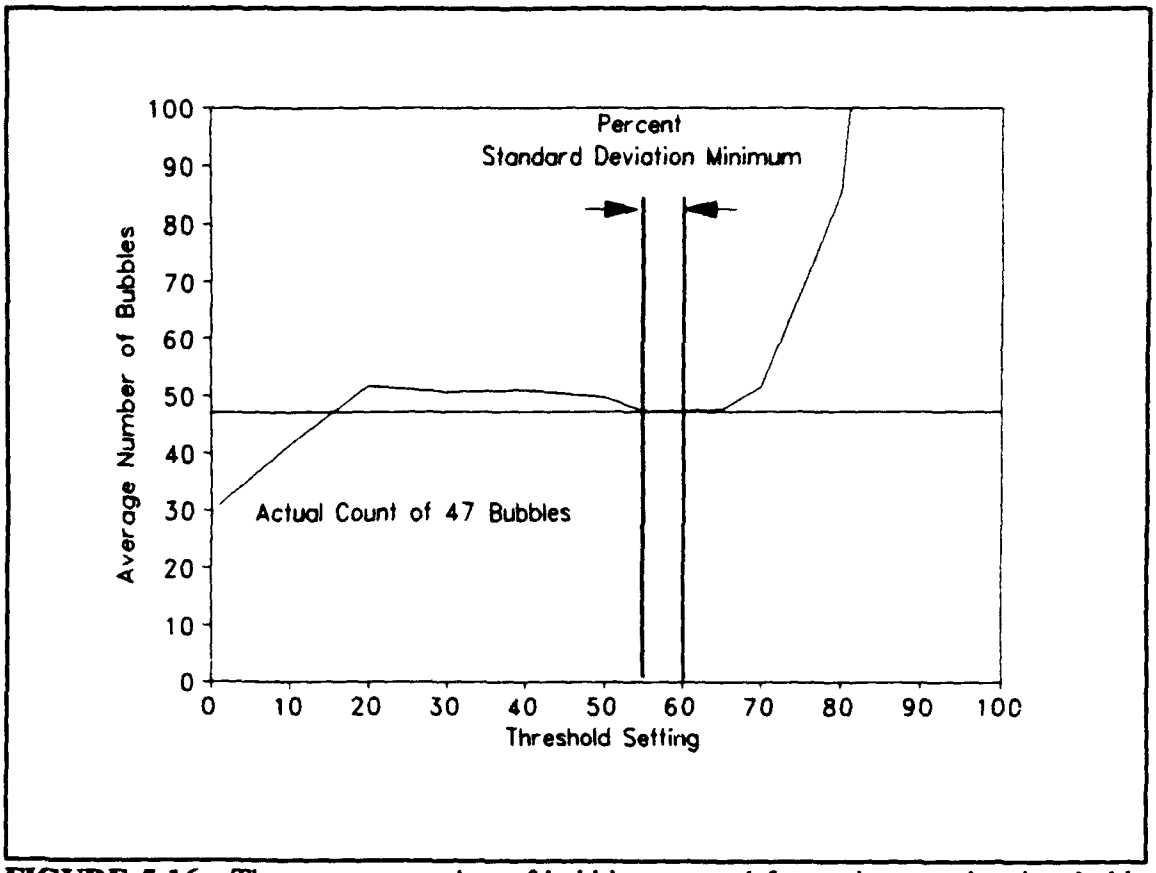

FIGURE 5-16. The average number of bubbles counted for various reader threshold settings. The detector had exactly 47 bubbles.

represents the average of thirty independent readings taken at each threshold setting. The amount of deviation present in the data was also analyzed and these results are shown in Fig. 5-17. The percent standard deviation achieved a minimum value between the threshold settings of 55 and 60. For these same threshold settings, the reader, as shown in Fig. 5-16, was found to be the most accurate.

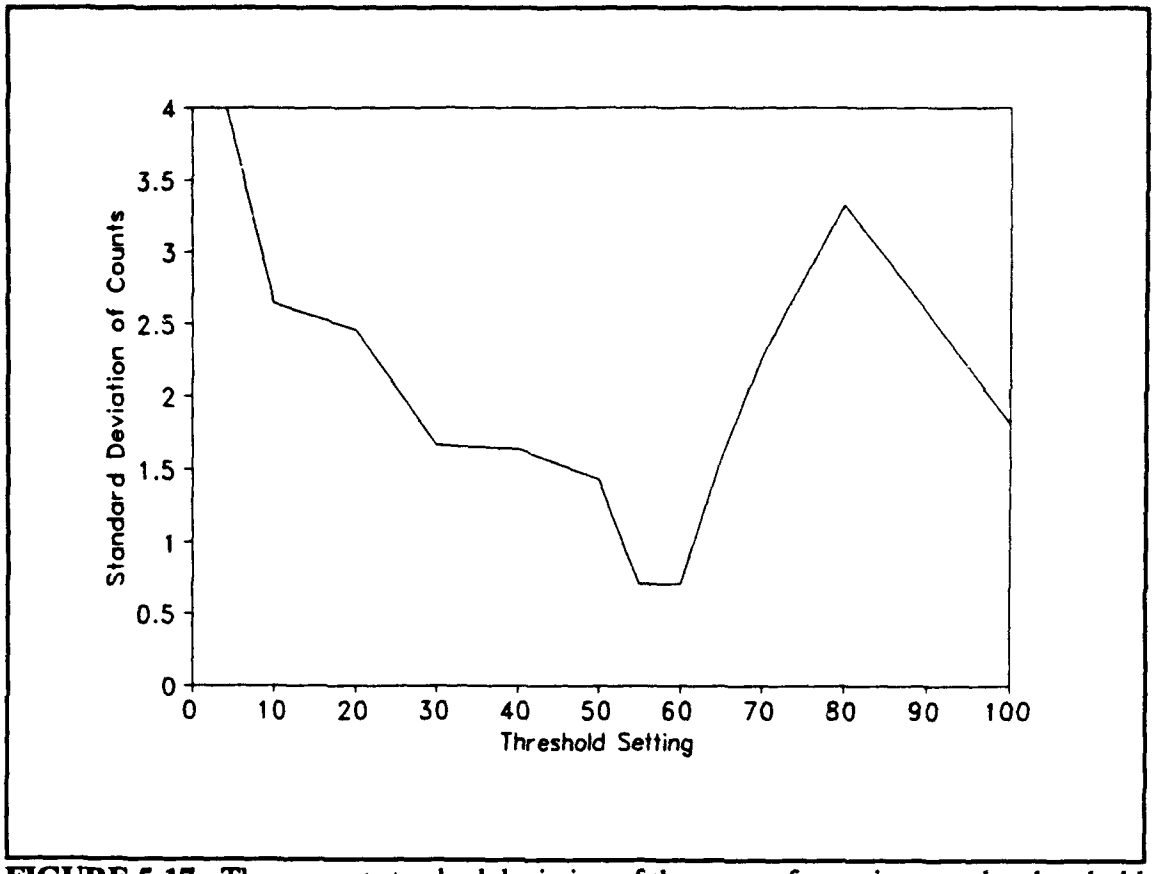

FIGURE 5-17. The percent standard deviation of the counts for various reader threshold settings. The detector had exactly 47 bubbles.

Figure 5-18, similar to Fig. 5-16, shows the average number of bubbles counted at each of the different threshold settings for the device containing 87 bubbles. In this plot, a plateau of consistent response exists between the threshold settings of 50 and 55. Subsequently, the reader was accurately able to detect the true number of bubbles over this region of threshold settings. In Fig. 5-19, the percent standard deviation of the counts at each threshold setting is presented. The unique relationship between detector accuracy and the minimum standard deviation in the counts was observed once again.

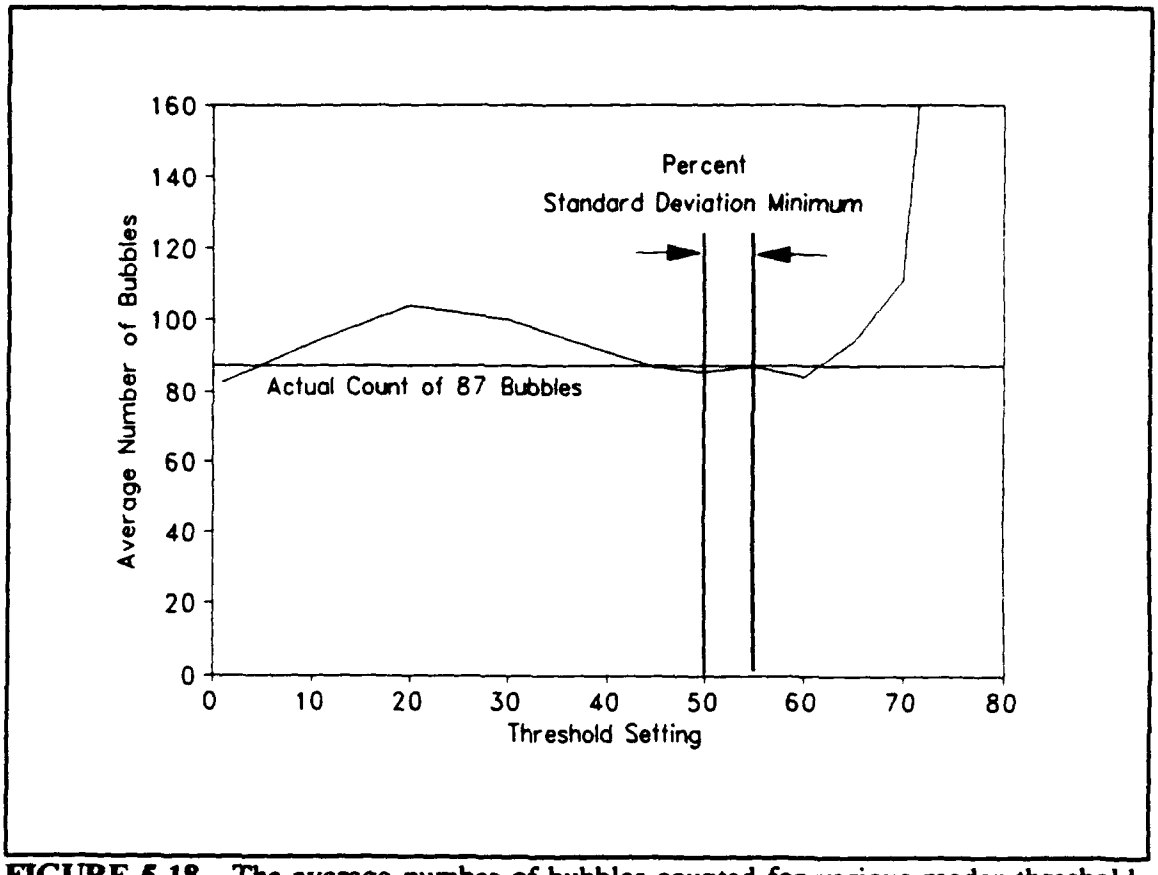

FIGURE 5-18. The average number of bubbles counted for various reader threshold settings. The detector had exactly 87 bubbles.

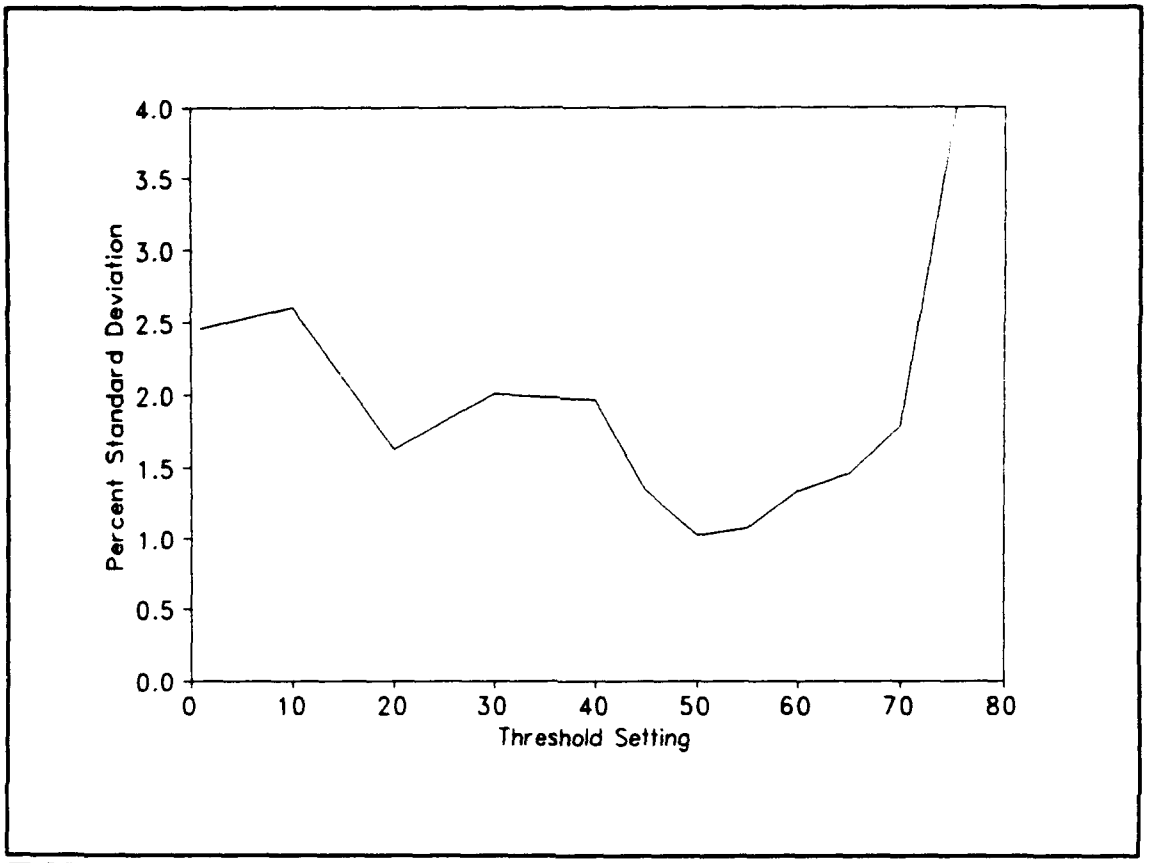

FIGURE 5-19. The percent standard deviation of the counts for various reader threshold settings. The detector had exactly 87 bubbles.

Figure 5-20 shows the average counts acquired for the device containing approximately 140 bubbles. Although the true number of bubbles was unknown and could not be compared to detector performance, a plateau of consistent response did develop between the threshold settings of 60 and 63. This plateau did correspond to a bubble count of approximately 140 bubbles, indicating precise reader measurements. Similar to the previous tests, the plot of the percent standard deviation of the counts, Fig. 5-21, developed a region of minimum standard deviation between the settings of 60 and 63, which corresponded to the bubble count plateau shown in Fig. 5-20.

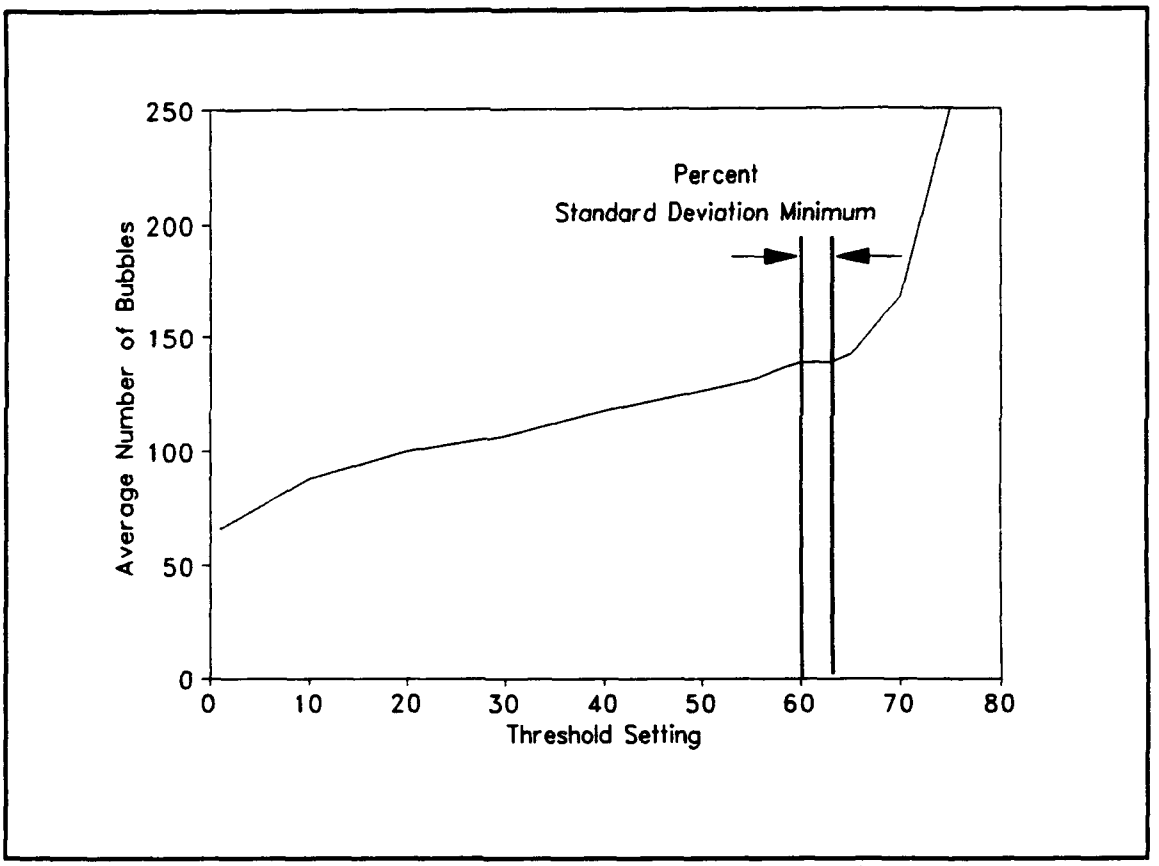

FIGURE 5-20. The average number of bubbles counted for various reader threshold settings. The detector had approximately 140 bubbles.

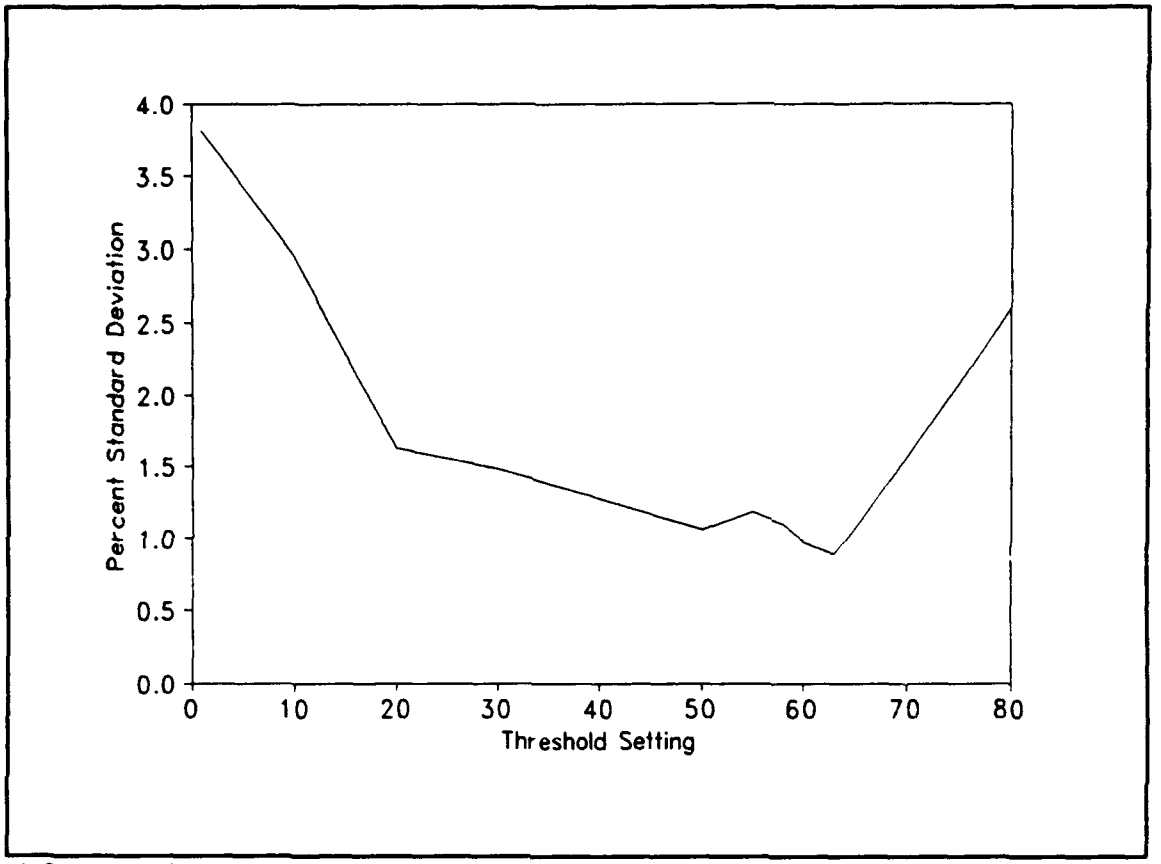

FIGURE 5-21. The percent standard deviation of the counts for various reader threshold settings. The detector had approximately 140 bubbles.

As a result of the first series of tests, several conclusions can be drawn about the operating characteristics of the optical reader. First of all, different threshold settings are required for different numbers of bubbles. The results of the three tests indicate that separate threshold regions do exist, where the reader accuracy is the highest. Next, the region of maximum accuracy corresponds directly to the zone in which the smallest percent standard deviation in the counts exists. Essentially, the detector becomes more accurate as the deviation in the counts decreases.

The second series of tests attempted to quantify the dynamic operating region of the reader by determining its upper bounds. This was accomplished by repeating the

linearity study and including longer periods of irradiation. The dynamic limit of the reader could easily be determined by evaluating the number of bubbles at which the detector would no longer provide linear readings. Figure 5-22 provides the results of the second linearity test. In this plot, the average counts of the ten different detectors are

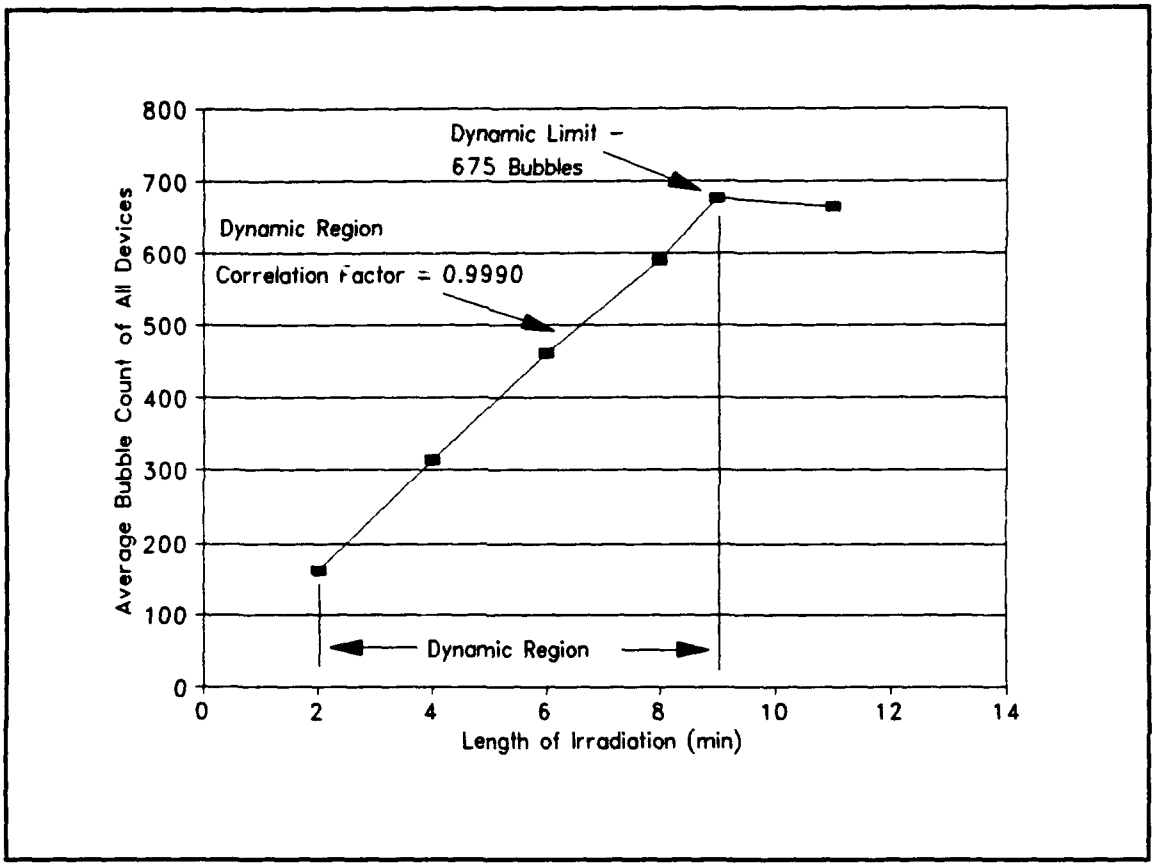

FIGURE 5-22. The dynamic limit of the optical reader was shown to be 675 bubbles for ten different detectors.

plotted with respect to the length of irradiation. After a period of irradiation of nine minutes, the devices no longer behaved linearly. For this test, an irradiation time of nine minutes corresponded to an average bubble count of 675 bubbles. Before the devices contained 675 bubbles, the reader provided consistently linear results, as demonstrated by a correlation factor of 0.999. Figure 5-23 emphasizes the linear behavior of the

devices in the dynamic region by showing the correlation factor for each device.

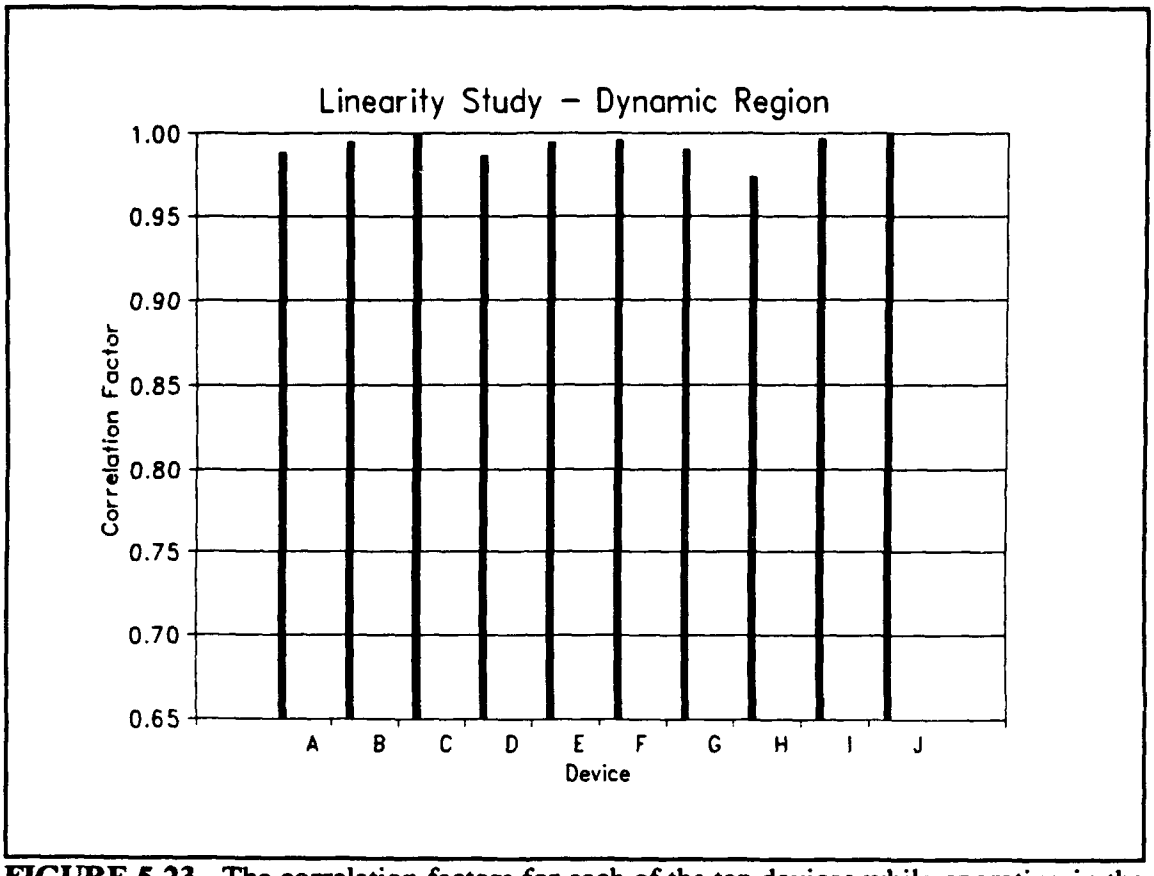

FIGURE 5-23. The correlation factors for each of the ten devices while operating in the dynamic region of the optical reader.

CHAPTER VI

CONCLUSIONS AND RECOMMENDATIONS FOR FUTURE WORK

Some overall project conclusions are presented and discussed. Areas that require future work are outlined. The 1993-1994 Trident Scholar program is addressed.

6.1 CONCLUSIONS

At the outset of this project, several problem areas were identified relating to the practical operation of neutron bubble detectors. These areas included the strong temperature dependence associated with the responses of the Apfel and BD-100R devices, the concept of bubble growth and how it relates to accurate bubble counting, and also the low sensitivities inherently associated with the devices. The Trident Scholar report was begun as a feasibility study which would study the full scope and possible solutions to these problems.

The temperature dependence problem was viewed as perhaps the most damaging disadvantage associated with the bubble detectors. Consequently, considerable theoretical work was undertaken to solve this problem and redesign the devices so that they would provide regions of consistent response with changing temperature. As a result of this work, a protocol was established for determining specifically whether a superheated liquid would provide a flat response over a specific temperature band. Furthermore, several alternate compounds were identified which would theoretically provide a flat response. Although the temperature compensated BD-100R was experimentally shown to provide

a plateau of consistent response, the concept of changing the droplet material is more favorable. Changing the droplet material solves the root of the problem, and the compensation does not rely upon mechanical methods which are subject to failure. Another advantage to varying the droplet materials is that, by doing so, the devices can be designed to meet the specific temperature requirements of the user.

A series of experiments were conducted at the United States Naval Academy's neutron generation facility to test the suitability of the devices to measure neutrons. The experiments conducted include the repeatability study, the bubble growth study, the linearity study, the study of the new temperature compensated BD-100R detector, and the reader evaluation study. The results of these tests were very favorable, indicating that the BD-100R device is a very capable neutron detection device. Linearity and repeatability were both clearly demonstrated. Furthermore, the bubble growth study demonstrated that although the bubbles do continue to grow after their initial formation, the growth has a negligible effect upon the optical reader's ability to measure accurately the devices. A probing evaluation of the optical reader provided the necessary data needed to maximize the reader's accuracy.

Although there are several other areas that must be further investigated, preliminary studies indicated that the bubble detector, specifically the BD-100R, is a valid neutron detector and has the potential to be used as a detector for nuclear treaty verification applications.

6.2 FUTURE WORK

As stated in Section 6.1, there are several other topics concerning detector operation that must be explored before a final decision can be reached concerning the suitability of the BD-100R for use by on-site inspection teams. Encouraged by the results provided in this report, the Defense Nuclear Agency has agreed to sponsor another Trident Scholar project for the 1993-1994 academic year. The new scholar will evaluate some of the recommendations made in this report and examine some new topics.

One of the primary tasks of the new project will be to have commercial vendors manufacture, if feasible, new bubble detectors. These detectors will incorporate the materials identified in this report as having potentially superior temperature response characteristics. Furthermore, these devices will be fully tested to validate previous predictions made concerning their temperature response characteristics and to evaluate their ability to measure neutron radiation effectively. Preliminary discussions with the commercial vendors, specifically Apfel Enterprises and BTI, have indicated that the new devices can be made.

Perhaps the most important task, however, is to develop operational procedures for making field measurements to determine the presence or absence of nuclear re-entry vehicles contained within a weapon. Once the procedures have been determined, they will be evaluated using a laboratory mockup of a warhead capable of simulating a variety of configurations.

Some other areas of investigation will include a complete evaluation of the BD-100R's gamma sensitivity. Earlier models of the device were found to be gamma

insensitive, however recent changes in the gel and device manufacturing could have altered this insensitivity. Finally, devices with increased neutron sensitivity will be ordered from the vendors in order to evaluate their characteristics. Device sensitivity is an important topic because it directly affects the number of bubbles that a device will register for a given neutron fluence. It is favorable to have the number of bubbles received for a given dose be as high as possible so as to maximize the statistical certainty associated with the counts.

APPENDIX

Critical Bubble Data for Alternate Compounds

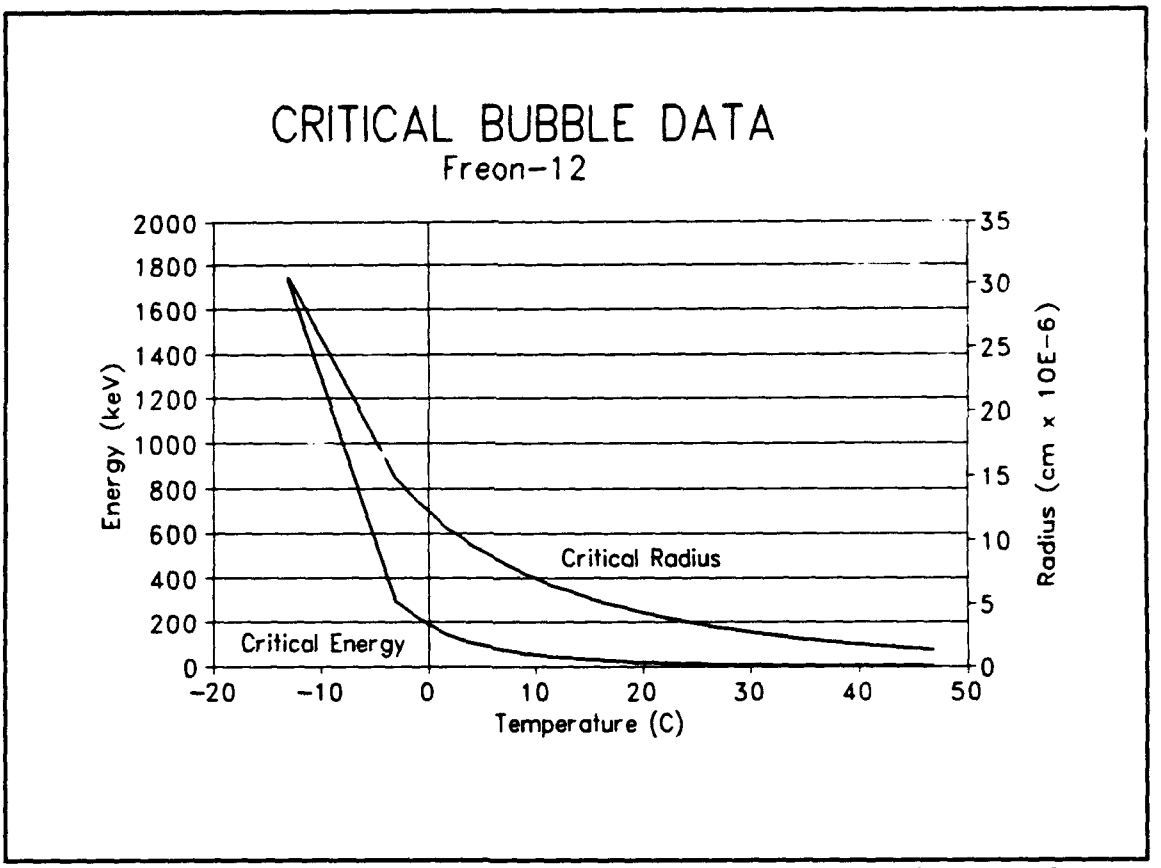

FIGURE A-1. Critical energy and bubble radius for Freon-12 as a function of temperature at 1 atmosphere.

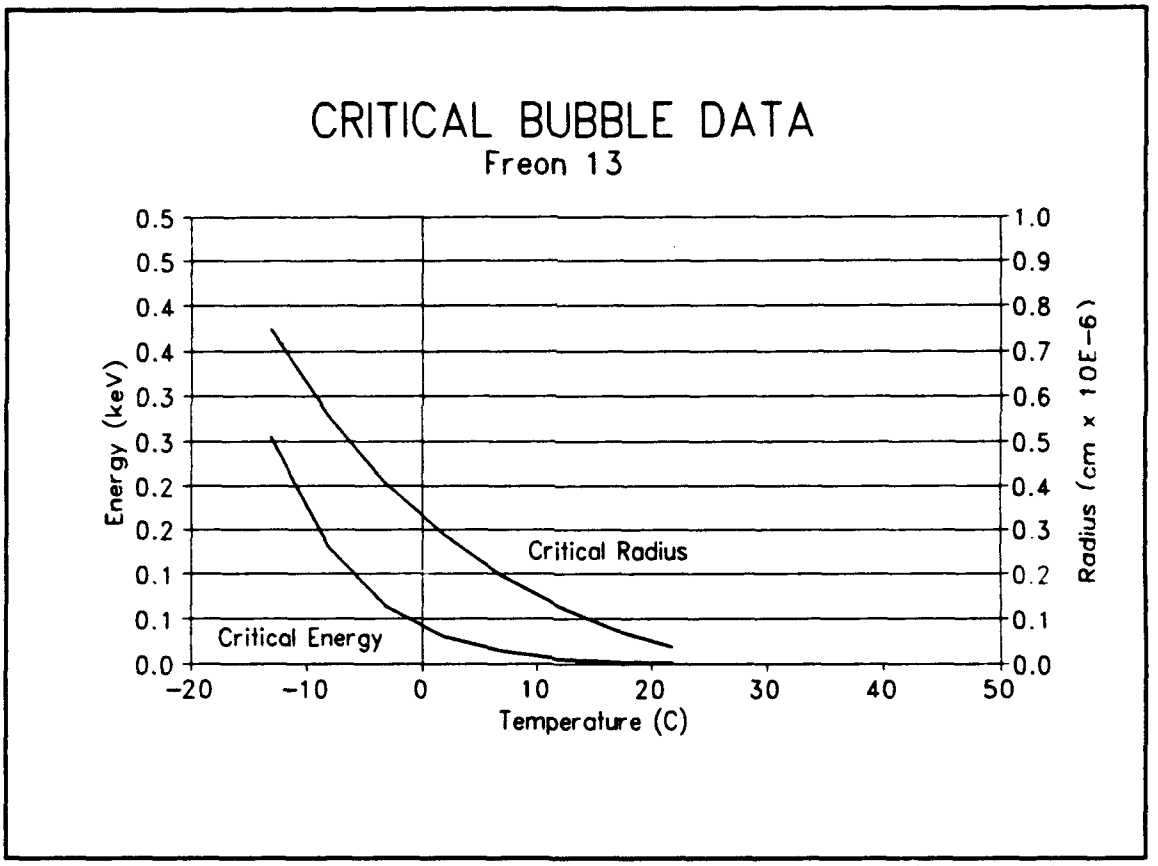

FIGURE A-2. Critical energy and bubble radius for Freon-13 as a function of temperature at 1 atmosphere.

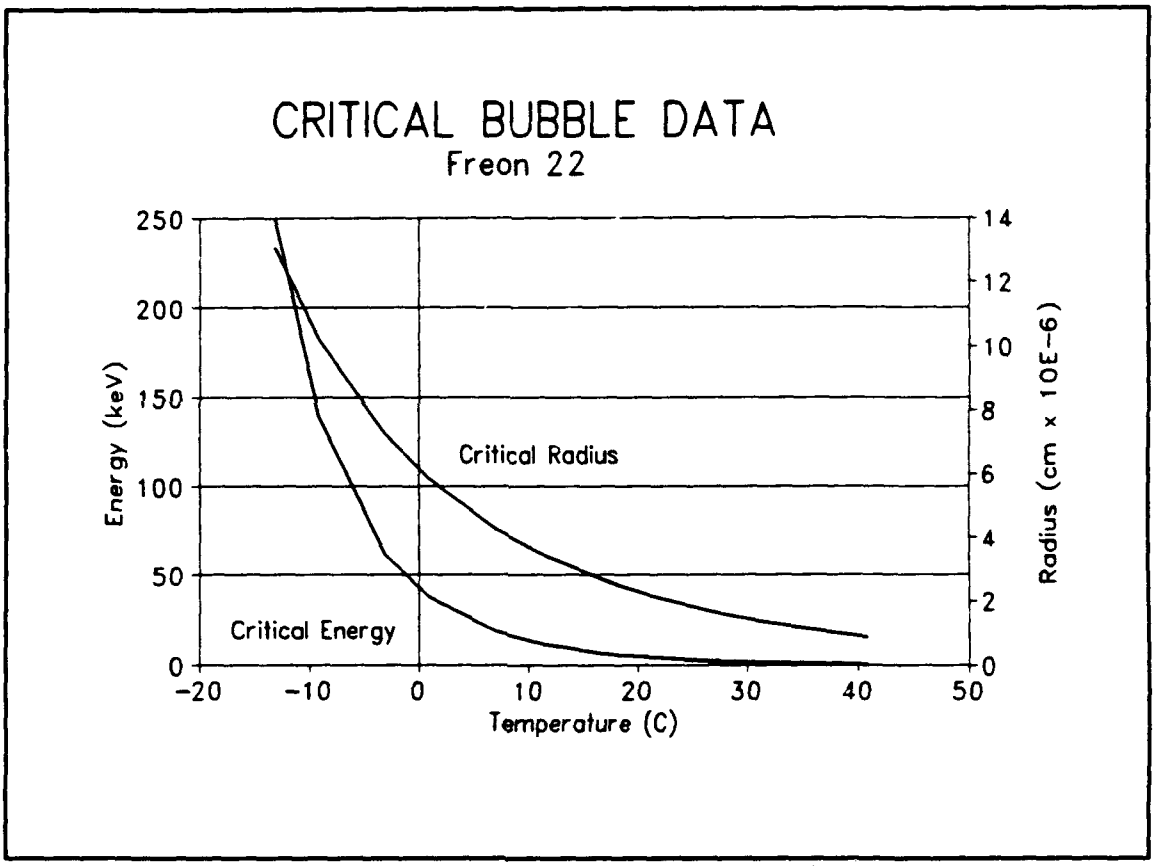

FIGURE A-3. Critical energy and bubble radius for Freon-22 as a function of temperature at 1 atmosphere.

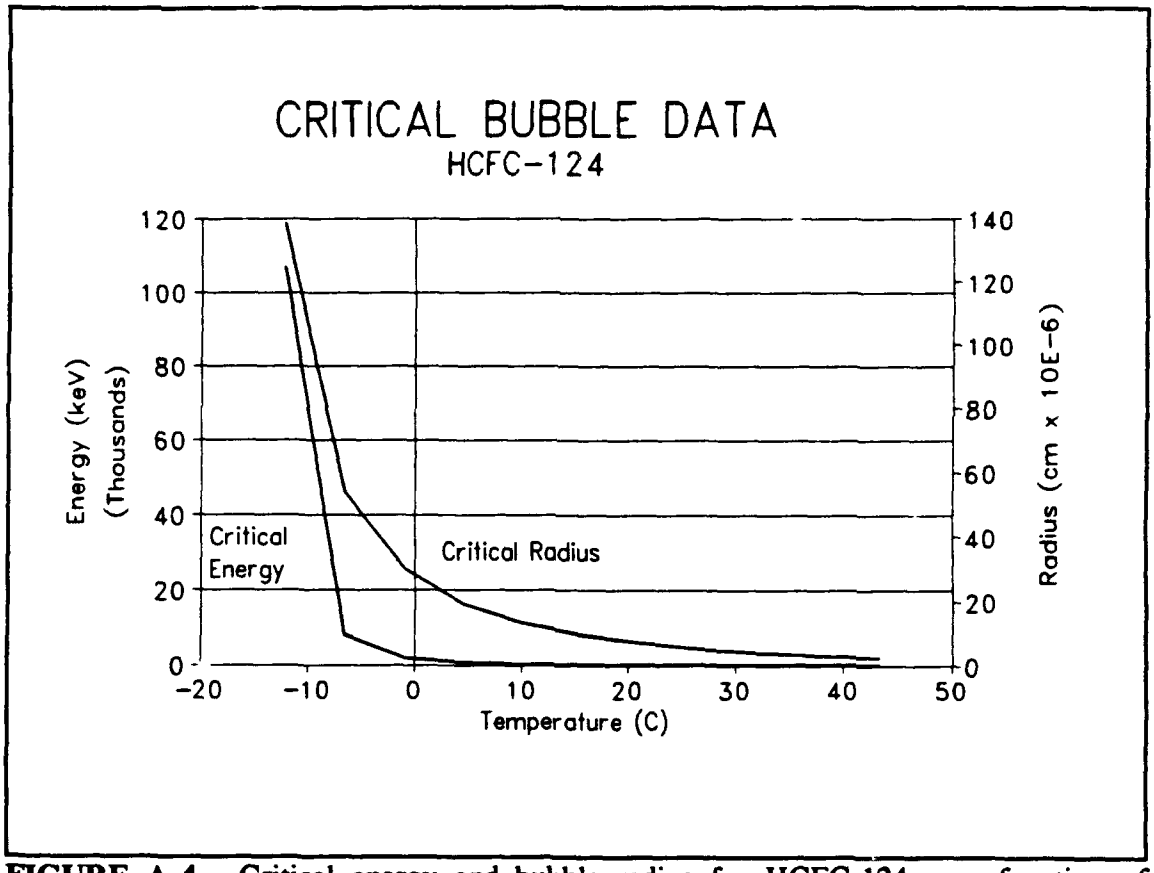

FIGURE A-4. Critical energy and bubble radius for HCFC-124 as a function of temperature at 1 atmosphere.

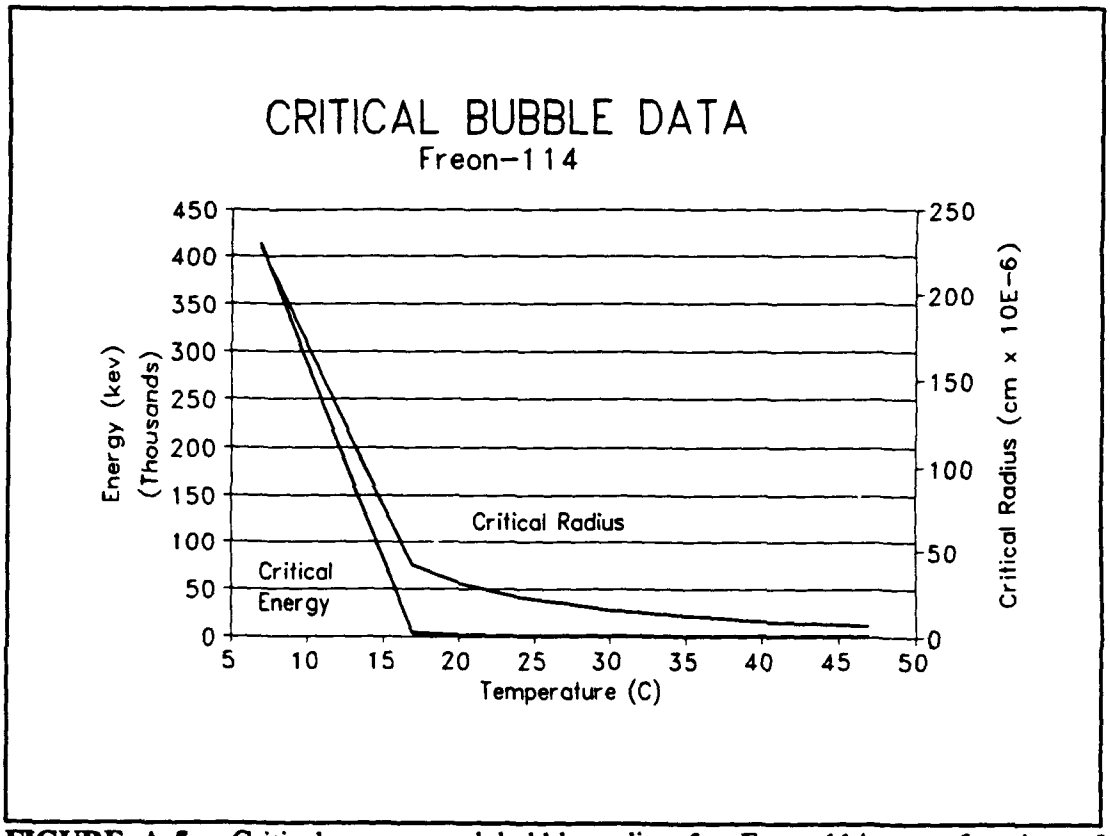

FIGURE A-5. Critical energy and bubble radius for Freon-114 as a function of temperature at 1 atmosphere.

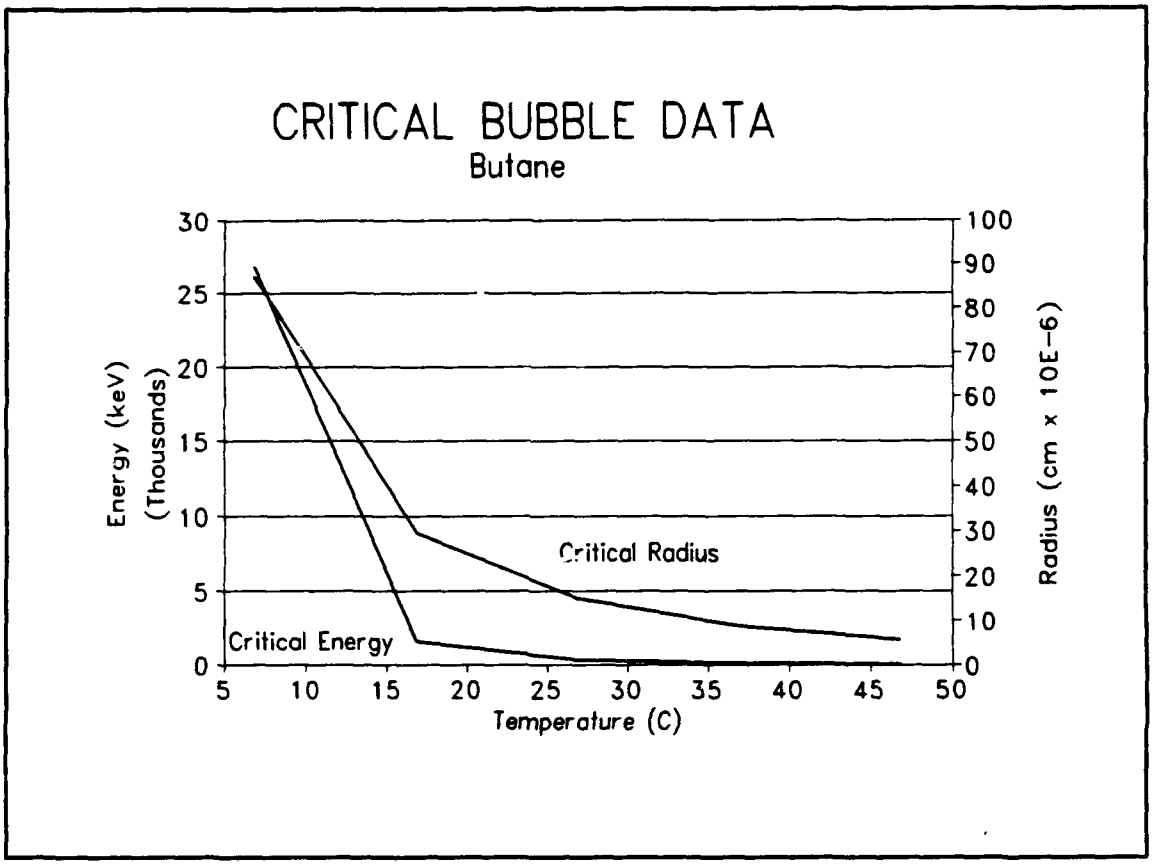

FIGURE A-6. Critical energy and bubble radius for butane as a function of temperature at 1 atmosphere.

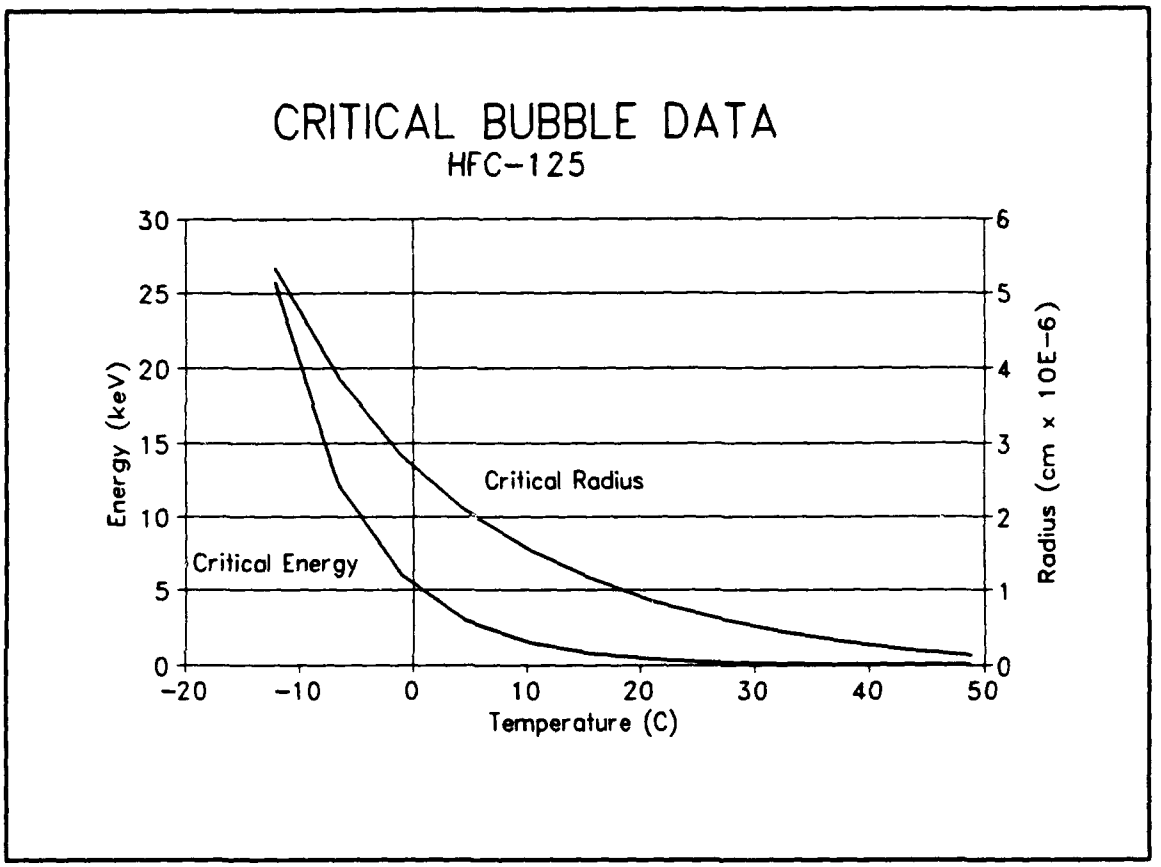

FIGURE A-7. Critical energy and bubble radius for HFC-125 as a function of temperature at 1 atmosphere.

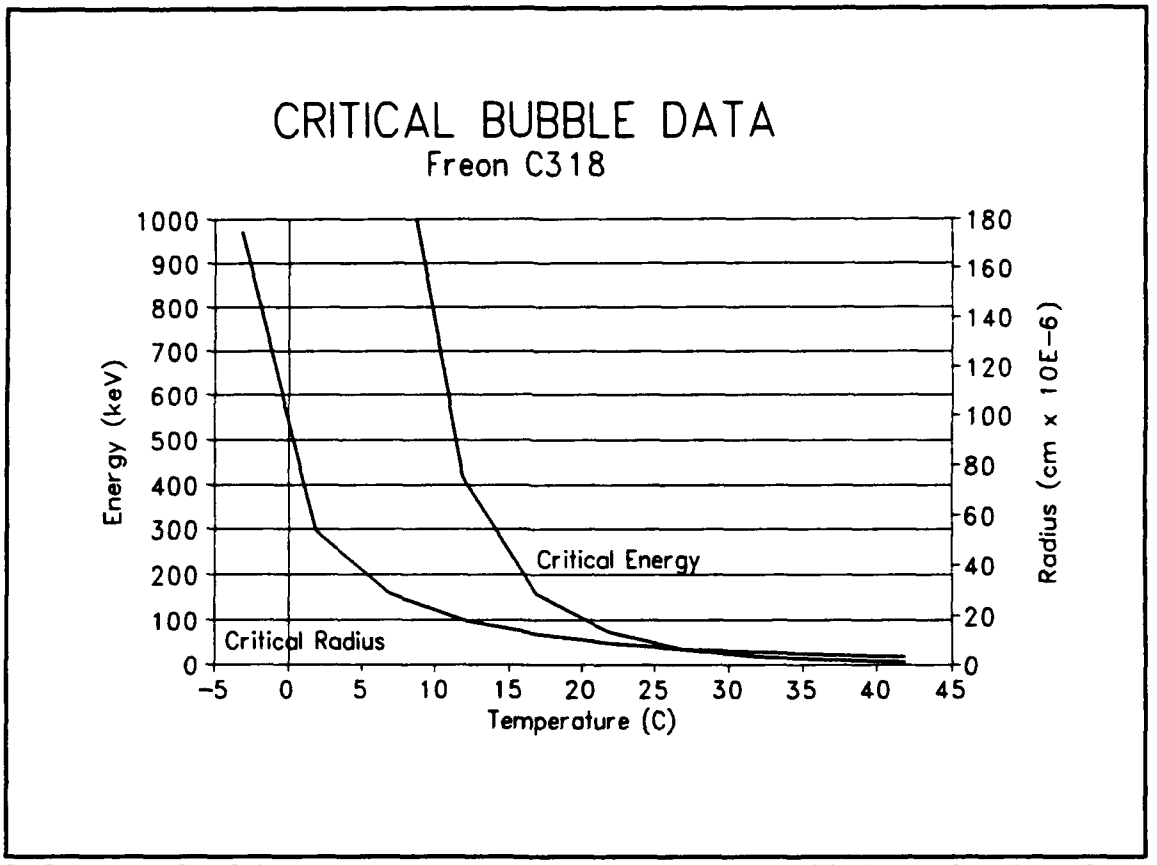

FIGURE A-8. Critical energy and bubble radius for Freon-C318 as a function of temperature at 1 atmosphere.

REFERENCES

1. Personal communication with Mr. Ed Hamilton, Center for Verification Research, March 1992 through May 1993.

2. Personal communication with Lt. Col. Bernard Simelton, Defense Nuclear Agency, March 1992 through May 1993.

3. S. Fetter, T.B. Cochran, L. Grodzins, H.L. Lynch, and M.S. Zucker, "Gamma-Ray Measurement of a Soviet Cruise-Missile Warhead," *Science*, **248**, 828-834 (1989).

4. R.A. August, G.W. Phillips, S.E. King, and J.H. Cutching, "Neutron Signatures," *Conference Record of the 1992 NSS and MIC*, 1992.

5. Naval Research Laboratory, "A High Efficiency Fast Neutron Detector," *NRL Memorandum Report 6518*, Washington, DC, 1989.

6. M.J. Harper, "A Theoretical Model of a Superheated Liquid Droplet Neutron Detector," Ph.D. Dissertation, University of Maryland, Department of Chemical and Nuclear Engineering (1991).

7. D.A. Glaser, "Some Effects of Ionizing Radiation of the Formation of Bubbles in Liquids," *Phys. Rev.*, **87**, 665 (1952).

8. G. Riel and N. Rao, "Superheated Drop, 'Bubble', Neutron Dosimeter Performance in a Work Environment," *Conference Record of the 1990 IEEE Nuclear Science Symposium*, Arlington, V.A., 1990.

9. R.E. Apfel, U.S. Patent No. 4,143,274 (6 March 1979).

10. R.E. Apfel, U.S. Patent No. 4,350,607 (21 September 1982).

11. H. Ing and H.C. Birnboim, U.S. Patent No. 4,613,758 (23 September 1986).

12. C.S. Sims, R.E. Swaja, and D.E. Jones, "Summary Statements from the Second Conference on Radiation Protection Dosimetry," *Health Phys.*, **57**(3), 461-463 (1989).

13. J.A. Douglas, "The Applications of TL Materials in Neutron Dosimetry," Environmental and Medical Sciences Division, United Kingdom Atomic Energy Authority, Harwell, England, 1978.

14. R.E. Apfel, "The Superheated Drop Detector," *Nucl. Instr. and Meth.*, **162**, 603-608 (1979).

15. H. Ing and H.C. Birnboim, "A Bubble-Damage Polymer Detector for Neutrons," *Nucl. Tracks and Radiat. Meas.*, **8**, 285-288 (1984).

16. F. Seitz, "On the Theory of the Bubble Chamber," *Phys. Fluids*, **1**, 2-13 (1958).

17 Ch. Peyrou, "Bubble Chamber Principles," Bubble and Spark Chambers, Vol. 1, Academic Press, New York, 1967.

18. C.R. Bell, "Radiation Induced Nucleation of the Vapor Phase," PhD Dissertation, Massachusetts Institute of Technology, 1970.

19. A. Norman and P. Spiegler, "Radiation Nucleation of Bubbles in Water," *Nucl. Sci. Instr.*, **27**, 935-937 (1956).

20. M.M. El-Nagdy and M.J. Harris, *J. Brit. Nucl. Eng. Soc.*, **10**, 131 (1971).

21. L.W. Dietrich and T.J. Connolly, *Nucl. Sci. Eng.*, **50**, 273 (1973).

22. C.R. Bell, N.P. Oberle, W. Rohsenow, N. Todreas, and C. Tso, "Radiation-Induced Boiling in Superheated Water and Organic Liquids," *Nucl. Sci. Eng.*, **53**, 458-465 (1974).

23. R.E. Apfel, Y-C. Lo, and S.C. Roy, "Superheated Drop Detector: A Potential Tool in Neutron Research," *Nucl. Instr. and Meth.*, **A255**, 199-26 (1987).

24. M.J. Harper, "Calculation of Recoil Ion Effective Track Lengths in Neutron Radiation-Induced Nucleation," *Nucl. Sci. and Eng.*, 1992.

25. Personal Conversation with DuPont Laboratories, September 1992.

26. Reynolds, W.C., Thermodynamic Properties in SI, Department of Mechanical Engineering at Stanford University, Stanford, CA, 1979.

27. Computer Program, "Refprop," obtained from the National Institute of Standards and Technology, September 1992.

28. P. Spiegler, J. Hopenfeld, and A. Norman, "Operating Conditions of Bubble Chamber Liquids," *Rev. Sci. Instr.*, **34**, 308 (1963)

29. R.B. Schwartz, "Neutron Personal Dosimetry," *Natl. Bur. Stand. (U.S.) Spec. Publ. 250-12*, Washington, DC, 1987.

30. R.J. Howerton, R.E. Dye, P.C. Giles, J.R. Kimlinger, S.T. Perkins, and E.F. Plechaty, 'Omega" A CRAY 1 Executive Code for LLNL Nuclear Data Libraries," *Lawrence Livermore National Laboratory Report UCRL-50400*, Livermore, CA, 1983.

31. D.I. Garber and R.R. Kinsey, Neutron Cross Sections, Volume II, Curves, *Brookhaven National Laboratory Report BNL-325*, Upton, NY, 1976.

32. J.F. Ziegler and J.M. Manoyan, Computer Code "Transport of Ions in Matter (TRIM)," IBM Research, Yorktown, NY, 1990.

33. Knoll, G.F., Radiation Detection and Measurement, John Wiley and Sons, New York, NY, 1989.

34. E.J. Reilly, "Evaluation of Bubble Dosimeter Response to Neutron Radiation," *Trident Scholar Report No. 159*, United States Naval Academy, Annapolis, MD, (1989).